HIGH-PERFORMANCE CO OXIDATION CATALYSTS ENGINEERED FOR CO_2 LASERS

By

STEVEN DWAYNE GARDNER

A DISSERTATION PRESENTED TO THE GRADUATE SCHOOL
OF THE UNIVERSITY OF FLORIDA IN PARTIAL FULFILLMENT
OF THE REQUIREMENTS FOR THE DEGREE OF
DOCTOR OF PHILOSOPHY

UNIVERSITY OF FLORIDA

1990

ACKNOWLEDGMENTS

I wish to express my sincere thanks to Professor Gar B. Hoflund whose instruction and guidance made this research possible. We have shared countless discussions through which his knowledge and optimism have served to motivate me both personally and professionally. I would also like to acknowledge the efforts of David R. Schryer, Billy T. Upchurch, Erik J. Kielin and Jacqueline Schryer at NASA Langley Research Center who provided the catalytic activity measurements. As exemplified during several NASA-sponsored workshops, their contributions have had an enormous impact on the quality of this entire research project. Support of this research under NASA grant NAG-I-794 is also gratefully acknowledged. Finally, I wish to thank my wife, Carmen, for her encouragement and forbearance during the seemingly endless years of graduate study. Throughout the exhausting hours of research, she has been a constant reminder of what is most important in my life.

TABLE OF CONTENTS

Abstract of Dissertation Presented to the Graduate School of the University of Florida in Partial Fulfillment of the Requirements for the Degree of Doctor of Philosophy

HIGH-PERFORMANCE CO OXIDATION CATALYSTS ENGINEERED FOR CO_2 LASERS

By

STEVEN DWAYNE GARDNER

December, 1990

Chairman: Gar B. Hoflund
Major Department: Chemical Engineering

The low-temperature CO oxidation activity of numerous materials has been evaluated in order to develop efficient catalysts for use in CO_2 lasers. The materials were screened for activity in small, stoichiometric concentrations of CO and O_2 at temperatures near 55 °C. An Au/MnO_x catalyst was synthesized which exhibited exceptional CO oxidation activity while maintaining negligible performance decay over a period of at least 70 days. The data suggest that Au/MnO_x has potential applications in air purification and CO gas sensing as well.

Extensive surface characterization data from Pt/SnO_x and Au/MnO_x catalysts are reported which relate surface composition and chemical state information to corresponding CO oxidation activity data. Ion scattering spectroscopy (ISS), Auger electron spectroscopy (AES), angle-resolved

Auger electron spectroscopy (ARAES) and X-ray photoelectron spectroscopy (XPS) were utilized to observe the behavior of these surfaces as a function of numerous pretreatments which alter their catalytic activity. The results suggest that $Pt(OH)_2$ and Pt/Sn alloy formation may play a key role in the CO oxidation mechanism on Pt/SnO_x surfaces. A Pt_3Sn alloy was subsequently characterized before and after H_2 reduction to study its surface characteristics.

Surface characterization of Au/MnO_x and MnO_x was performed in order to elucidate the CO oxidation mechanism. The spectral data yield evidence that the enhanced CO oxidation activity of Au/MnO_x is related to Mn present primarily as Mn_3O_4 with substantial amounts of water or hydroxyl groups. The spectra are consistent with very small Au particles which may exist in an oxidized state. The behavior of Au/MnO_x and MnO_x toward an inert pretreatment suggests the possibility of a $Au-MnO_x$ interaction.

CHAPTER 1
INTRODUCTION

This research is a collection of studies whose main objective is to develop low-temperature CO oxidation catalysts which can be effectively utilized in CO_2 lasers. The studies themselves represent systematic efforts to synthesize and evaluate new catalysts for this application and to gain fundamental information about the low-temperature CO oxidation mechanism. It will become apparent during the course of the investigations, however, that the results have potential applications beyond CO_2 lasers.

In order to provide an understanding of the basis for this research, this introductory section highlights important aspects of CO_2 laser operation and identifies the need for low-temperature CO oxidation catalysts. This is followed by a review which summarizes previous, related research on CO_2 lasers utilizing CO oxidation catalysis. Afterwards the individual studies themselves are presented. The research concludes with a summary of the overall results with recommendations for future research.

CO_2 Lasers in Remote Sensing Applications

The advent of pulsed lasers has made it possible to utilize pulsed laser energy in a radar fashion (laser radar

or lidar) with applications in altimetry, ranging, pollution detection, atmospheric chemistry, and weather monitoring [1-5]. Recently, the National Aeronautics and Space Administration (NASA) has undertaken a project to develop a laser atmospheric wind sounder (LAWS) which will incorporate a CO_2 Doppler lidar [6]. The LAWS system will operate from a satellite platform in earth orbit and measure global wind velocities for a period of up to three years. It is anticipated that the data obtained from LAWS will enhance the understanding of atmospheric dynamics and aid in weather prediction. The same techniques may be employed to detect dangerous wind shear near airports. A CO_2 lidar was chosen because the technology is mature and the corresponding CO_2 laser radiation is safe to the eye. However, as described below, there are significant problems which need to be solved before CO_2 lidars can be operated in space or other remote locations.

* Carbon dioxide lasers are commonly operated in an open-cycle mode. That is, fresh CO_2 laser gas flows continuously through the laser from an external storage tank and is subsequently exhausted to the environment. Unattended operation for an extended period of time, therefore, requires large, massive reservoirs of CO_2 laser gas. Consequently, this method of operation is undesirable for CO_2 lidars which will be deployed in remote locations such as

earth orbit. An additional complication arises for CO_2 lidars which must transmit signals long distances through the atmosphere. The atmosphere contains a significant concentration of CO_2 (approximately 300 parts per million) and H_2O both of which absorb CO_2 laser radiation. As a result, the CO_2 lidar beam may experience considerable attenuation as it propagates through the atmosphere [4,6]. A solution is to use a CO_2 laser gas which contains a CO_2 isotope such as $C^{18}O_2$. Relative to a common-isotope CO_2 ($C^{16}O_2$) laser which operates at a wavelength of 10.6 micrometers, a laser containing $C^{18}O_2$ emits radiation at 9.1 micrometers which interacts less with atmospheric constituents. However, $C^{18}O_2$ is much more expensive than CO_2 and therefore open-cycle laser configurations which use $C^{18}O_2$ are not economical.

* An alternative to open-cycle CO_2 laser operation is known as closed-cycle operation [7]. A CO_2 laser operating in a closed-cycle mode is initially charged with a CO_2 gas mixture and subsequently sealed. This configuration is advantageous because it eliminates the need for an external CO_2 storage tank and the CO_2 gas mixture itself is conserved. Unfortunately, there is a serious problem with CO_2 lasers which precludes closed-cycle operation. During the lasing process, CO_2 in the laser gas is dissociated into stoichiometric amounts of CO and O_2. The gradual loss of

CO_2 steadily decreases the power output of the laser. Perhaps most critical, however, is the increase in O_2 concentration which can lead to arcing and ultimately to laser failure. An overall solution is to incorporate a CO oxidation catalyst into the working confines of the CO_2 laser to recombine the CO and O_2 into CO_2. Successful closed-cycle operation is achieved by continuously recirculating the laser gas across a suitable catalyst bed. The resulting configuration is compact and portable and permits the CO_2 laser to be utilized in remote locations for an extended period of time.

The requirements for an effective CO_2 laser catalyst are rather stringent [7,8]. An appropriate catalyst must exhibit exceptional CO oxidation activity under the conditions which correspond to steady-state CO_2 laser operation. That is, the catalyst must maintain activity at temperatures near or below 50 °C in a gas mixture which contains small, stoichiometric concentrations of CO and O_2 and as much as 50% CO_2. In addition, the use of $C^{18}O_2$ requires that the catalyst preserve the integrity of the isotopic laser gas mixture. The catalyst should also be resistant to dusting which could damage the delicate optics within the laser.

CO_2 Lasers and Low-Temperature CO Oxidation Catalysis

Few catalysts have been researched and targeted specifically for use in CO_2 lasers. Ordinarily, CO oxidation catalysts are screened for activity using test gases which consist of small concentrations of CO in air (excess O_2). As a result, the performance of most CO oxidation catalysts remains to be evaluated in the CO_2 laser environment. Excess O_2 facilitates CO oxidation and therefore numerous catalysts perform well under these conditions even at low temperatures (less than 100 °C) [9-17]. However, CO oxidation in stoichiometric concentrations of CO and O_2 is much more difficult. Consequently, under these conditions only a limited number of catalysts are available which exhibit significant low-temperature CO oxidation activity. The following paragraphs summarize previous research directed towards testing and evaluating low-temperature CO catalysts in CO_2 laser environments.

Hopcalite (a mixed-oxide catalyst consisting of approximately 60% MnO_2 and 40% CuO with trace amounts of other oxides) has been tested in a sealed CO_2 laser with limited success [18]. Appreciable CO oxidation activity was realized only when excess CO (approximately 0.5%) was introduced into the CO_2 laser gas mixture. This is due largely to the fact that the CO oxidation rate over hopcalite is approximately first-order with respect to CO

concentration [11,12,19]. Contrary to the CO_2 laser's low tolerance for O_2, a small excess in CO concentration is not harmful to the CO_2 laser performance. The hopcalite catalyst was able to sustain laser performance for a period of up to 10^5 pulses with no indication of failure. In order to satisfy the requirements for LAWS, the laser must be capable of at least 10^9 pulses [6]. Therefore, more extensive testing is needed to verify the performance of hopcalite. However, considering the activity decay which has previously been observed for hopcalite catalysts [19], it is doubtful that hopcalite will provide a sufficient lifetime for the laser.

It has been shown that a heated Pt wire may be used to recombine CO and O_2 in atmospheres similar to those in sealed CO_2 lasers [20,21]. Activity measurements between 700 and 1300 °C indicated significant recombination rates which were independent of the CO and O_2 partial pressures. Nevertheless, this overall approach to CO and O_2 recombination is undesirable in that it is fragile and requires additional energy input to heat the Pt catalyst. In addition, the power dissipated in the laser may cause thermal expansion of the laser components resulting in decreased performance. It is much more advantageous to utilize a catalyst which is effective near the steady-state

temperatures of the CO_2 laser, particularly for space applications where there are weight and power constraints.

Catalysts consisting of Pt and/or Pd supported on SnO_x (Pt/SnO_x, Pd/SnO_x, $Pt-Pd/SnO_x$) have received considerable attention with respect to CO oxidation in CO_2 lasers [7,8,22-26]. As a result, several interesting observations have been made regarding their performance characteristics. It has been demonstrated that optimum Pt/SnO_x performance results from Pt concentrations between 15 and 20 wt% [27]. Further enhancements in activity are realized by pretreating the Pt/SnO_x surfaces with CO or H_2 at elevated temperatures (near 125 to 225 °C) [26]. It has also been determined that relative to Pt/SnO_x and Pd/SnO_x alone, bimetallic catalysts consisting of $Pt-Pd/SnO_x$ yield better performance [27,28]. The performance of a 2 wt% Pt/SnO_x catalyst has been verified during actual closed-cycle CO_2 laser operation. Utilizing an external catalyst bed containing 150 grams of 2 wt% Pt/SnO_x at 100 °C, the CO_2 laser maintained 96% of its maximum power output for at least 28 hours with no indication of failure [29].

Although Pt/SnO_x and Pd/SnO_x appear to be promising catalysts for the CO_2 laser application, they are not yet totally compatible with long-term laser operation in space. Isotopic reaction studies [30] have indicated that about 15% of the total amount of O_2 which participates in CO

oxidation over Pt/SnO_x originates from the Pt/SnO_x surface itself. This is likely to be the case for Pd/SnO_x and $Pt-Pd/SnO_x$ as well. Since these SnO_x-based surfaces ordinarily contain $^{16}O_2$, the isotopic integrity of a $C^{18}O_2$ laser gas mixture would be destroyed. However, a procedure has been developed to label Pt/SnO_x with $^{18}O_2$ yielding $Pt/Sn^{18}O_x$ [30]. A preliminary test (lasting 17 days) has indicated that $C^{18}O$ oxidation over the $^{18}O_2$-labelled Pt/SnO_x catalyst yields essentially 100% $C^{18}O_2$ within experimental error. Nevertheless, the tests need to be performed over longer periods to ensure isotopic compatibility. The long-term performance characteristics of Pt/SnO_x, Pd/SnO_x and $Pt-Pd/SnO_x$ represent another area for concern. In the presence of stoichiometric CO and O_2 near ambient temperatures, all of these SnO_x-based catalysts exhibit significant decay in CO oxidation activity over extended time [27,28]. Consequently, their performance is currently unacceptable in long-term CO_2 laser applications such as LAWS.

A study has recently evaluated the performance of a sealed CO_2 laser containing a Au catalyst [31]. The internal wall of the laser's discharge tube was coated with a thin, discontinuous Au film to recombine the products of CO_2 dissociation. The activity of the Au film appears to result from the presence of atomic oxygen in the laser

discharge. However, the presence of a conductive Au film in the laser amplification volume can create serious problems under certain conditions. Care must be taken to ensure that the Au film is sufficiently discontinuous (Au islands) so as to avoid interference with the laser's electrical requirements. In addition, the Au surface area must be kept low to minimize stray reflection lasing which reduces power output. Therefore, the disadvantages associated with coating such a large surface with Au under conditions which minimize (but not eliminate) the drawbacks noted above render this approach highly cost-ineffective and inefficient.

Considering the previous research on CO oxidation catalysis in CO_2 lasers, much of the present research has been directed toward SnO_x-based materials such as Pt/SnO_x. Chapters 1 through 4 describe surface characterization studies of Pt/SnO_x and Pt-Sn alloy surfaces. These studies were performed to learn more about the low-temperature CO oxidation mechanism over Pt/SnO_x catalysts. Chapter 5 presents results of activity screening experiments designed to identify new low-temperature CO oxidation catalysts for the CO_2 laser application. Finally, Chapters 6 and 7 report activity and surface characterization data for a Au/MnO_x catalyst whose exceptional activity was identified in the former screening experiments.

CHAPTER 2
EVIDENCE OF ALLOY FORMATION DURING REDUCTION OF PLATINIZED TIN OXIDE SURFACES

Introduction

Platinized tin oxide surfaces (Pt/SnO_2 or Pt/SnO_x) have been proven to be efficient, low-temperature, CO oxidation catalysts which makes them useful in CO_2 laser applications [7,8,23]. However, relatively little is understood about the oxidation of CO over Pt supported on reducible oxides. In order to understand the mechanism, it is necessary to determine the surface composition, chemical states of the surface species, and types of interactions between the surface species. It also appears that surface hydrogen has a large influence on the catalytic behavior of these surfaces [26].

Alumina-supported Pt/Sn bimetallic catalysts are important in hydrocarbon reforming processes [32-34]. The addition of Sn generally leads to prolonged catalyst lifetime through an improved resistance toward coke formation. Furthermore, the reaction selectivity is enhanced toward aromatization which results in an increase in the reformate octane number.

It is important to understand the nature of the Pt/Sn interaction in both the CO oxidation catalysts and the reforming catalysts. This point has been controversial for many years with regard to Pt/Sn reforming catalysts. Many studies suggest that a Pt/Sn alloy is formed during reduction [35,36] while others suggest that tin is present as an oxide [37-42]. Recent studies by Davis and coworkers [43,44] are particularly convincing in demonstrating that an alloy forms during reduction using X-ray photoelectron spectroscopy (XPS) and in-situ X-ray diffraction. The diffraction patterns indicate that the composition of the alloy is PtSn, but other alloys such as Pt_3Sn may form at different metal loadings.

The purpose of the present study is to investigate the Pt/Sn interaction on a platinized tin oxide surface similar to those used in CO oxidation. Auger electron spectroscopy (AES), ion scattering spectroscopy (ISS), and XPS have been used to examine the platinized tin oxide surface before, during and after reduction by vacuum annealing and after exposure of the reduced surface to oxygen at room temperature.

Experimental

A tin oxide film was prepared by thermal hydrolysis of Sn^{4+} from a solution containing 3 M $SnCl_4$ and 1.5 M HCl [45]. The solution was sprayed onto a titanium foil which

had been heated and maintained at 500 °C in air. The resulting tin oxide film was about 5000 angstroms thick and it contained significant amounts of hydrogen [46-50]. Platinum was deposited by impregnating the tin oxide film with a saturated chloroplatinic acid solution. The film was then rinsed with distilled water and calcined in air at 500 °C for one hour.

The sample was inserted into an ultrahigh vacuum (UHV) system (base pressure of 10^{-11} Torr) which is described in detail in the Appendix. The UHV system contained a double-pass cylindrical mirror analyzer (CMA) (Perkin-Elmer PHI Model 25-270AR) used for AES, ISS and XPS. The AES experiments were performed in the nonretarding mode using a 3-keV, 10-μA primary beam with a 0.2-mm spot diameter. The ISS spectra were collected in the nonretarding mode using a 147°-scattering angle and pulse counting detection [51]. A 1-keV, 100-nA $^4He^+$ primary beam was defocused over a 1-cm-diameter area to minimize sputter damage. The XPS spectra were collected in the retarding mode using a 25-eV pass energy and Mg Kα excitation. The sample was heated radiantly using a tungsten filament and its temperature was measured with an optical pyrometer.

Results and Discussion

An AES spectrum and an ISS spectrum taken from the as-prepared surface are shown in Figure 2-1. The AES spectrum exhibits peaks due to Pt, Sn, O, Cl and C. The large Pt feature at 64 eV indicates that the surface contains a high concentration of Pt which is consistent with the ISS spectrum shown in Figure 2-1(b). Several features appear in the ISS spectrum. The Sn peak is a shoulder on the Pt peak and the peak at 0.6 E/E_o is due to contamination (probably Na). The secondary ions apparently desorb with a threshold at 0.12 E/E_o. This suggests that charging is occurring on this surface which shifts the elemental features to higher E/E_o than predicted by the binary collision model [52]. A very small O peak is at 0.49 E/E_o and the peak at 0.28 E/E_o may be due to C. A crude estimate of the elemental cross sections [53] and surface composition suggests that the outermost layer of atoms contains about 60 at% Pt.

Next the sample was annealed under vacuum in increments of 50 °C from 250 to 450 °C for 30 minutes at each temperature. The ISS spectra taken after annealing at 300 and 450 °C are shown in Figures 2-2(a) and 2-2(b), respectively. Several changes have occurred after annealing the as-prepared sample at 300 °C. The Sn shoulder has become a more prominent peak and its size has increased relative to the Pt peak. Charging is no longer apparent on this

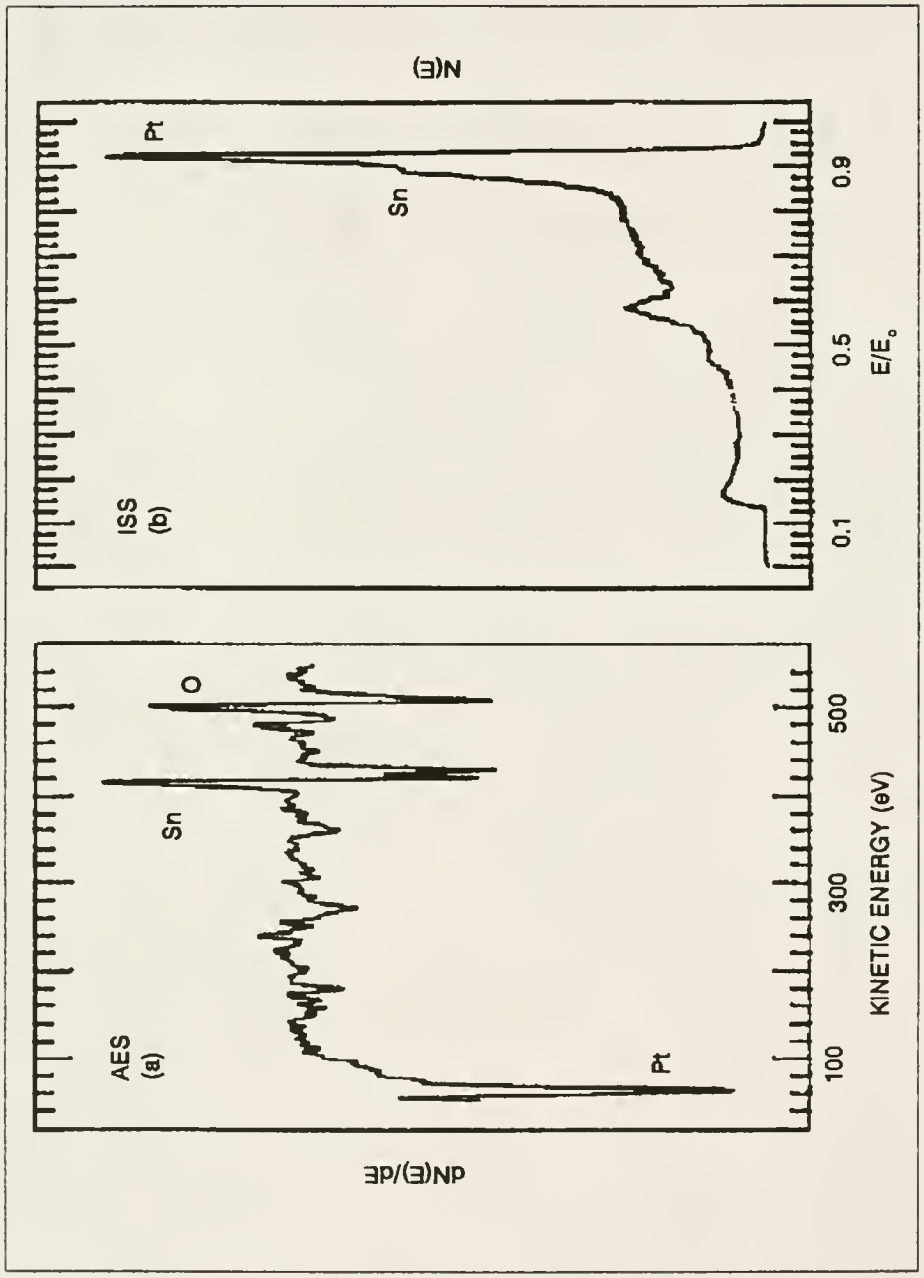

Figure 2-1. The (a) AES and (b) ISS spectra taken from the as-prepared sample after insertion into the vacuum system and pumpdown.

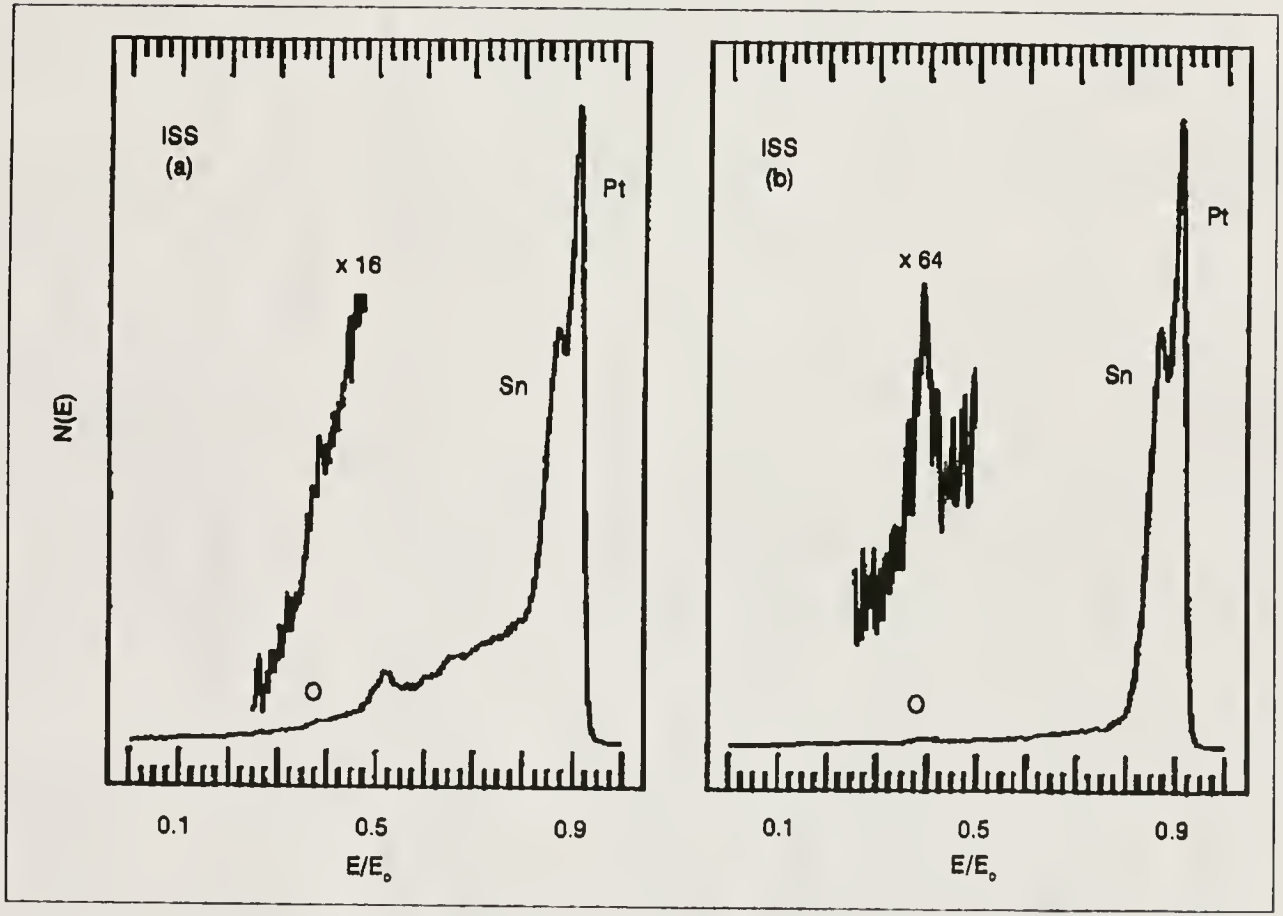

Figure 2-2. The ISS spectra taken after annealing the the sample in vacuum at (a) 300 °C and (b) 450 °C.

surface so the peak positions are approximately those predicted by the elastic binary scattering equation. Both the contamination peak at 0.52 E/E_o and the O peak at 0.39 E/E_o are reduced in intensity, and the C peak is no longer apparent. Furthermore, the background intensity is significantly decreased from that observed in Figure 2-1(b). A possible explanation is discussed below.

The trends observed in annealing to 300 °C are continued by annealing to higher temperatures. Figure 2-2(b) shows that the surface formed after annealing at 450 °C is very different from the as-prepared surface. In comparing Figures 2-2(a) and 2-2(b), the Sn peak is increased with respect to the Pt and is even more well defined. The contaminant peak is no longer present and the O peak apparently is further decreased in intensity. Also, the inelastically scattered ions composing the background are greatly decreased in intensity. Several similarities are observed between the ISS spectrum shown in Figure 2-2(b) and the spectra taken from Pt_3Sn surfaces in previous studies [see Reference 54, Figure 5(b)]. Both surfaces produce comparable inelastic backgrounds and display similar Pt, Sn and O features with regard to peak shapes and relative peak heights. The small inelastic background is characteristic of spectra taken from metallic surfaces where the electron mobility is sufficiently high to rapidly

neutralize inelastically scattered ions. The fact that the ISS spectrum taken from a reduced platinized tin oxide surface closely resembles an ISS spectrum taken from a Pt/Sn alloy surface (rather than an ISS spectrum taken from a nonreduced platinized tin oxide surface) supports the assertion that a Pt/Sn alloy forms during reduction of the platinized tin oxide surface.

The AES spectrum shown in Figure 2-3(a) and the Sn 3d XPS spectrum shown in Figure 2-3(b) were also taken from the sample after annealing at 450 °C. Comparing Figures 2-1(a) and 2-3(a) shows that the Pt-to-Sn peak height ratio essentially remains constant at a value of 1.12 during the annealing. However, the Sn-to-O peak height ratio increases from 1.10 to 1.37 during annealing by either migration of O below the near-surface region or desorption of O from the surface. These facts suggest an increased interaction between Sn and Pt in the near-surface region. The Sn 3d XPS spectrum shown in Figure 2-3(b) has a dominant peak at a binding energy of 486.4 eV. This feature is due to Sn present as an oxide, but it is difficult to determine the precise nature of this oxide from the Sn 3d features as discussed previously [32]. The arrows in Figure 2-3(b) indicate shoulders which are apparent at an approximate binding energy of 484.5 eV. This binding energy suggests that

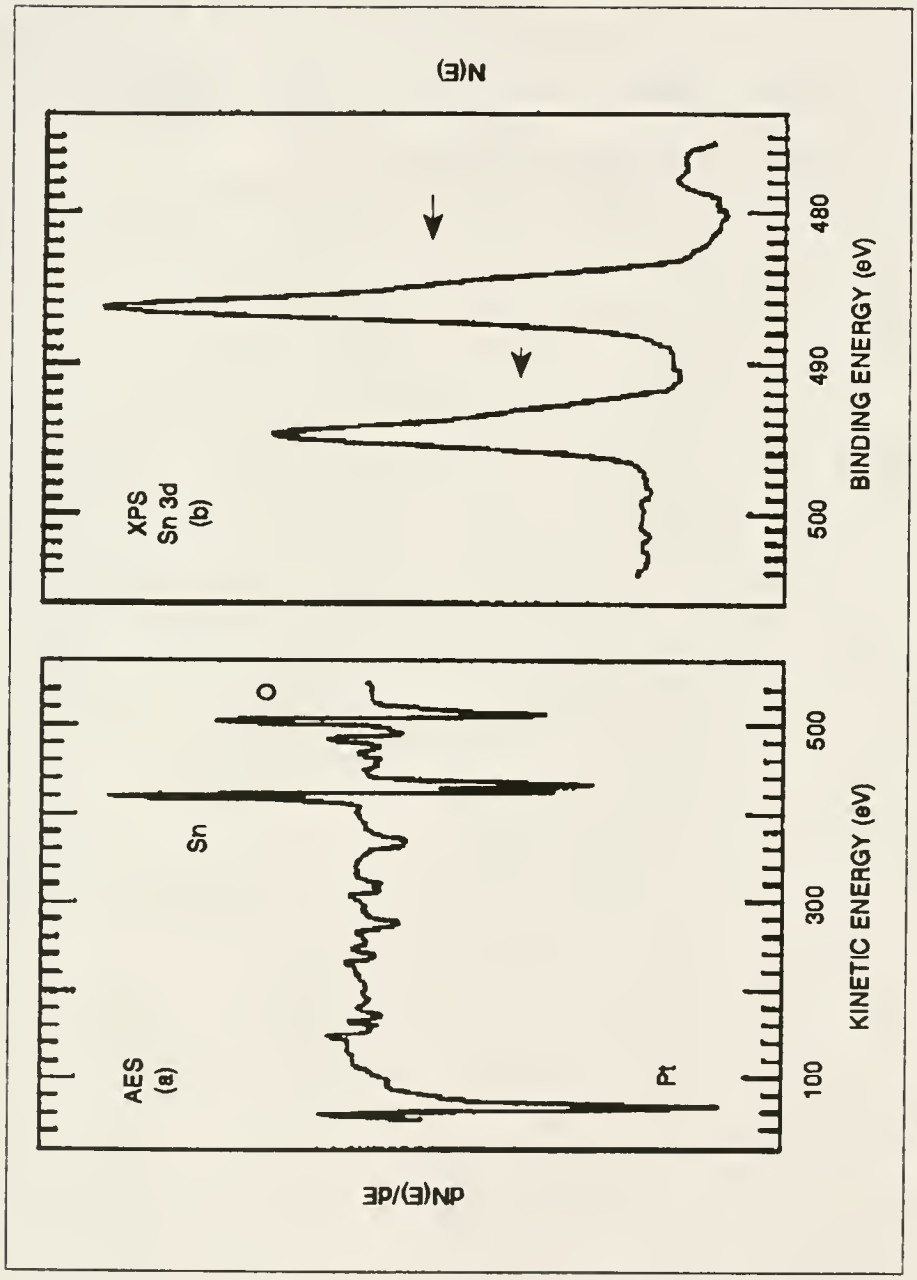

Figure 2-3. The (a) AES spectrum and (b) XPS spectrum taken after annealing the sample under vacuum at 450 °C.

Sn is also present in metallic or alloyed form. Only the oxidic feature at 486.4 eV is present before annealing the sample so tin oxide is reduced to metallic or alloyed Sn during the vacuum annealing, which is a reductive process. A study by Paffett and Windham [55] provides evidence that the form of the Sn is alloyed rather than metallic. They deposited metallic Sn on a Pt(111) surface and showed that an alloy forms during annealing at or above 150 °C. The 450 °C annealing temperature used in the present study then should result in alloy formation. Thus, the ISS, AES and XPS results are all consistent with the assertion that a Pt/Sn alloy is formed during the reduction of platinized tin oxide.

Similar annealing treatments have been carried out on tin oxide films which did not contain Pt [45,48,50,56]. In these studies vacuum annealing to 450 °C or above did not result in reduction of the tin oxide to metallic Sn. Water of hydration or hydroxyl groups are removed from the surface by vacuum annealing and a portion of the SnO_2 is reduced to SnO, but metallic Sn does not form. In fact, a tin oxide surface which has been reduced by argon-ion sputtering is actually enriched in O by vacuum annealing through migration of bulk O to the surface [56]. These observations demonstrate the important role which Pt plays in

reducing the Sn to metallic form which then alloys with the Pt.

Next, the oxidative behavior of the surface was examined by exposing the sample to 10^{-7} Torr of oxygen for 1 hour at room temperature. The ISS and XPS spectra taken from this surface are shown in Figures 2-4(a) and 2-4(b), respectively. The expanded O feature in the ISS spectrum indicates that the amount of O in the outermost surface layer of atoms increases by about 30% during the oxygen exposure. By comparison of Figures 2-2(b) and 2-4(a), it can be seen that the oxygen exposure has increased the height of the Sn peak with respect to the height of the Pt peak. This behavior is characteristic of Pt/Sn alloys as described in previous studies [54,57]. The differences between the ISS spectra shown if Figures 2-2(b) and 2-4(a) are quite similar to those obtained by exposing a Pt_3Sn alloy surface to low-pressure oxygen at room temperature [see Reference 57, Figures 5(a) and 5(b)]. Also, there is a very slight reduction in the size of the shoulders on the XPS Sn 3d peaks. The extent of this reduction is so small that it is necessary to hold an expanded version of Figure 2-3(b) over Figure 2-4(b) in order to observe the decrease in the size of the shoulders. The nonreactive behavior of this surface toward oxygen as detected by XPS is also characteristic of Pt/Sn alloy surfaces [57,58]. Using XPS,

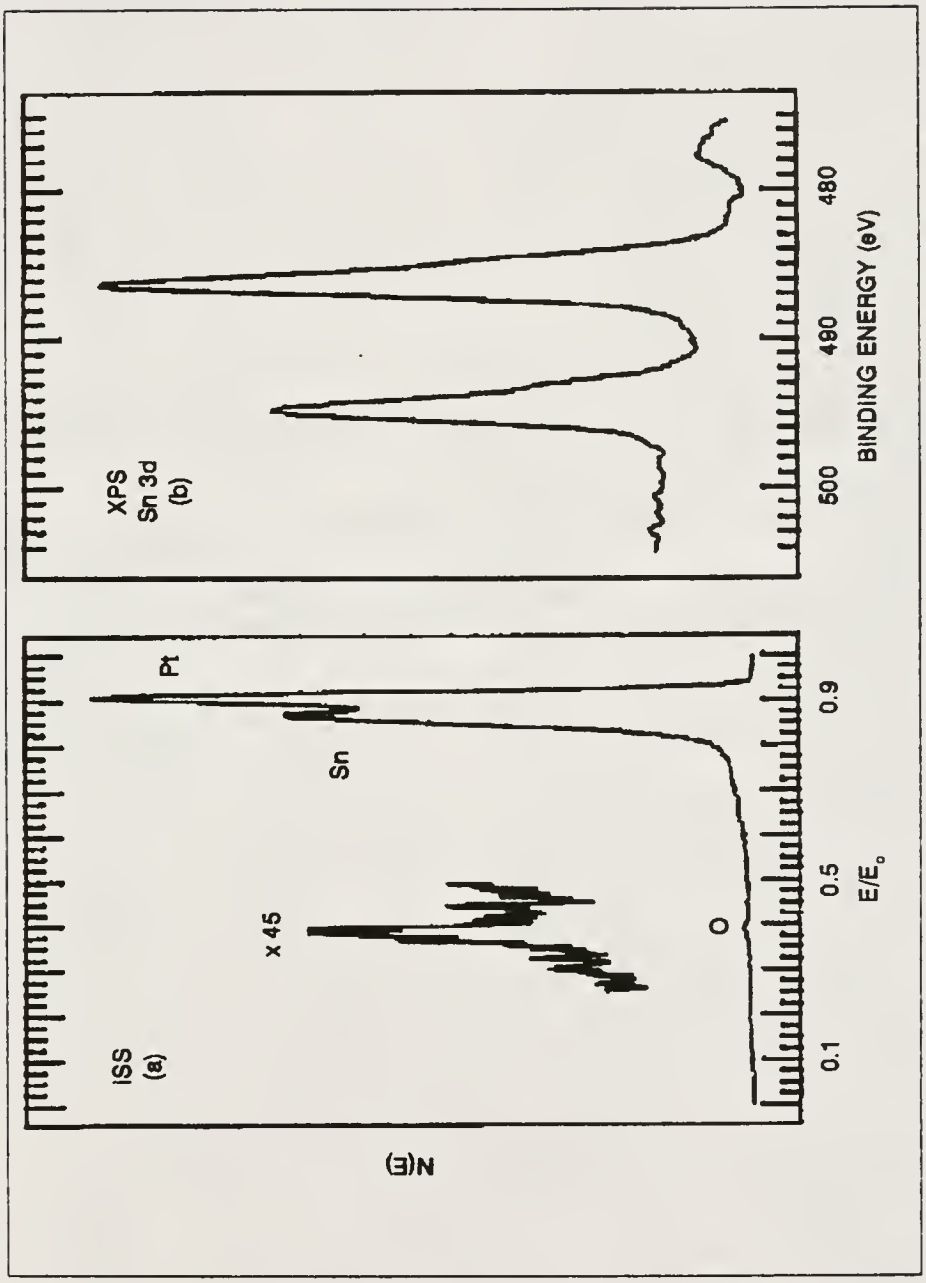

Figure 2-4. The (a) ISS and (b) XPS spectra taken after exposing the 450 °C-reduced surface to 10^{-7} Torr of oxygen for 1 hour at room temperature.

Cheung [58] found that Sn alloyed with Pt exhibits greater resistance toward oxidation than metallic Sn. It appears that the Pt/Sn alloy bond causes the Sn to be less susceptible to oxidation. Therefore, this finding also supports the assertion that the shoulders observed in the XPS Sn 3d spectra are due to alloyed Sn rather than elemental Sn, but quantification of the rates of oxygen adsorption on a Pt/Sn alloy and polycrystalline Sn has not yet been carried out.

It is interesting to compare the oxidative and reductive properties of platinized titania (Pt/TiO_2) with those of platinized tin oxide presented in this study since both titania and tin oxide are reducible, conductive oxides. A recent study by Hoflund and co-workers [59] of platinized titania shows that the outermost layer always exhibits a large ISS peak due to O. Reduction of this surface results in encapsulation of the Pt by TiO, and oxygen exposure forms TiO_2 which migrates back off the Pt. This behavior is quite different than that for the platinized tin oxide surface for which the O lies underneath the Sn and Pt. It is interesting to note that oxygen exposure of a polycrystalline Sn surface results in incorporation of O beneath an outermost layer of Sn atoms [60]. One possible explanation for the dramatically different behavior of platinized tin oxide and platinized titania is that tin oxide is more readily reduced to metal than titania in the presence of

Pt. Reduction of a platinized tin oxide surface by annealing under vacuum then results in the formation of a Pt/Sn alloy rather than encapsulation of the Pt by reduced oxidic support species as observed on platinized titania.

Summary

The Pt/Sn interaction at a platinized tin oxide catalyst surface has been examined using ISS, AES and XPS after reduction of the surface by vacuum annealing and exposure of the reduced surface to oxygen. After reduction XPS shows that metallic or alloyed Sn is formed, AES shows an increase in the Sn-to-O peak height ratio and the ISS spectrum becomes similar to that taken from a Pt/Sn alloy surface. Furthermore, exposure to oxygen at room temperature induces changes similar to those found for a Pt_3Sn alloy surface. These facts all support the assertion that a Pt/Sn alloy is formed during reduction.

CHAPTER 3
SURFACE CHARACTERIZATION STUDY OF THE REDUCTION OF AN AIR-EXPOSED Pt_3Sn ALLOY

Introduction

Platinum/tin systems are important catalytic materials for hydrocarbon reforming [33-40,61-66] and low-temperature CO oxidation [7,8,22,23]. The presence of Sn alters the catalytic behavior of Pt so it is important to understand the nature of the Pt-Sn interaction. In the previous chapter it was shown that a Pt/Sn alloy forms when a platinized tin oxide film is reduced by annealing in vacuum. This result suggests the importance of characterizing Pt/Sn alloy surfaces since these surfaces may be responsible for the unique catalytic properties of Pt/Sn systems. Early studies by Bouwman and co-workers [67-70] show that the surface compositions of PtSn and Pt_3Sn samples are readily altered by ion sputtering, annealing in vacuum, exposure to oxygen or exposure to hydrogen. More recent studies by Hoflund and co-workers [54,57,71,72] have focused primarily on the surface enrichment in Sn of Pt_3Sn alloy surfaces caused by annealing in vacuum or oxygen exposure. These studies utilized angle-resolved Auger electron spectroscopy (ARAES) [73], high-energy-resolution Auger electron

spectroscopy (HRAES) [74], scanning Auger microscopy (SAM), ion scattering spectroscopy (ISS) and angle-resolved X-ray photoelectron spectroscopy (ARXPS).

Relatively little work has been done on the reduction of oxidized Pt/Sn alloy surfaces. The purpose of the present study is to examine an air-exposed Pt_3Sn alloy surface before and after reducing the surface by annealing hydrogen. Results from ISS, ARAES and XPS are presented.

Experimental

Details of the method used to prepare the Pt_3Sn sample appear in a related study [71]. The sample was stored in argon until use. It was inserted into the UHV system (see Appendix) and sputter-cleaned until all C and O contamination was removed. Then the sample was exposed to air and reinserted into the vacuum system. After the oxidized sample was characterized, it was moved into a preparation chamber attached to the UHV system and reduced under 1 Torr of hydrogen at 300 °C for 1 hour. The heating was carried out using a special heating system [75] which did not expose any hot spots to the hydrogen which would cause dissociation to atomic hydrogen. Thus, the effects of the reduction are due only to exposure to molecular hydrogen. The sample temperature was measured using an optical pyrometer. After reduction the sample was moved back into

the UHV system without air exposure for further characterization.

The ARAES, ISS and XPS experiments were performed using a Perkin-Elmer PHI Model 25-270AR double-pass cylindrical mirror analyzer (CMA) containing an internal electron gun and movable aperture as the charged particle energy analyzer. The ARAES experiments were performed in the nonretarding mode using a 3-keV, 10-μA primary beam from an external, glancing incidence electron gun. The electron beam incidence angle was approximately 20° off the alloy surface plane. Rotation of the 90°-slotted aperture allowed for selection of emission angles of 75° to obtain more bulk-sensitive spectra and 20° to obtain more surface-sensitive spectra. The ISS spectra were also collected in the nonretarding mode using a 147°-scattering angle and pulse counting detection [51]. Sputter damage was minimized through the use of a 1-keV, 100-nA $^4He^+$ primary beam defocused over an area of about 1 cm^2. Both survey and high-resolution XPS spectra were collected with Mg Kα excitation in the retarding mode using 50- and 25-eV pass energies, respectively.

Results and Discussion

An ISS spectrum taken after sample cleaning and air exposure is shown if Figure 3-1(a). This spectrum contains a predominant peak due to Sn and very small peaks due to Pt

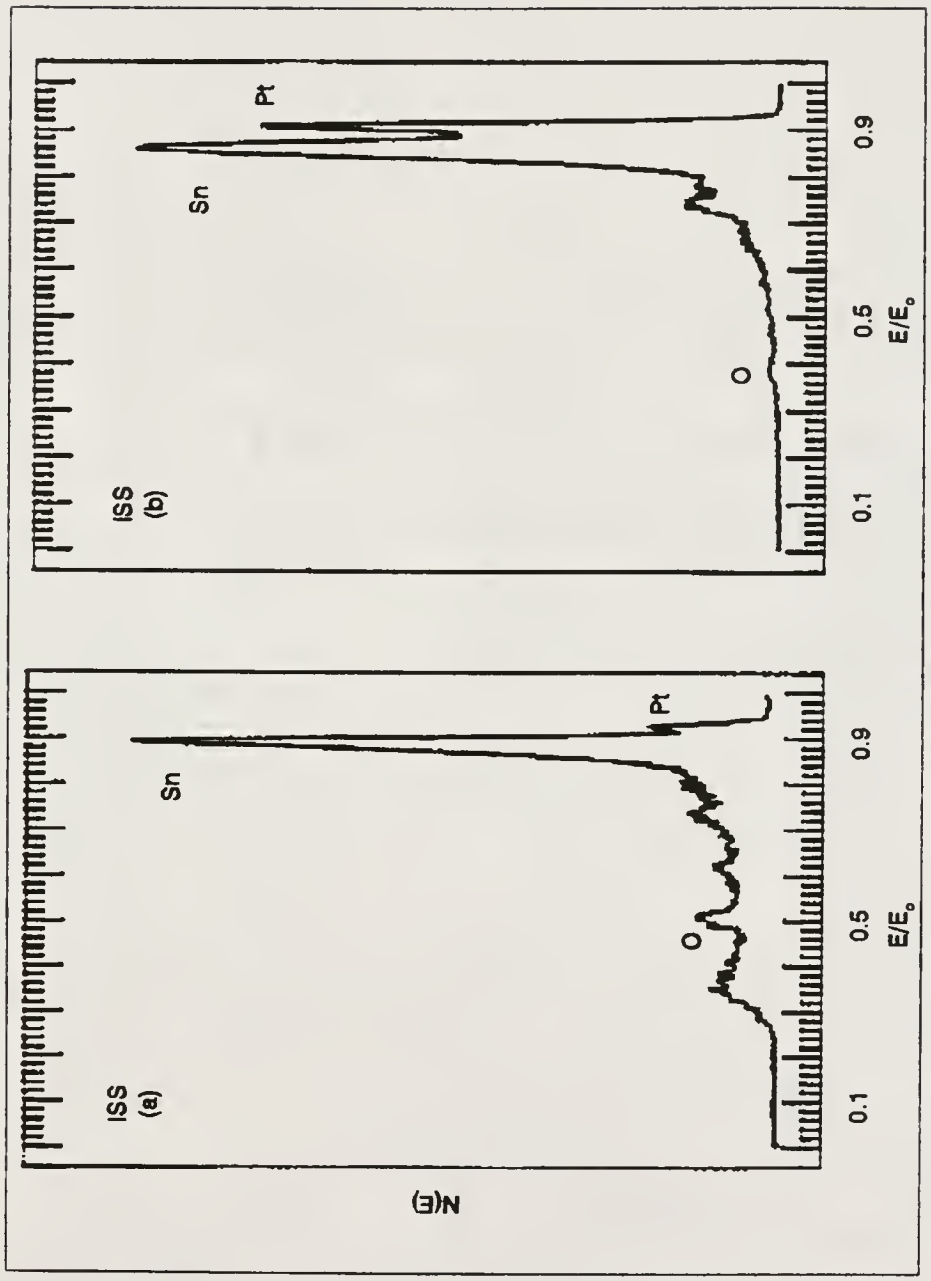

Figure 3-1. The ISS spectra taken from the polycrystalline Pt_3Sn sample after (a) sputter cleaning and exposing to air and (b) reducing the air-exposed sample under 1 Torr of hydrogen for 1 hour at 300 ^{o}C.

and O. The O peak is shifted from its appropriate E/E$_o$ value of 0.4 to 0.5, the background is fairly large and no ions are detected below an E/E$_o$ of 0.26. These facts indicate that the surface is oxidic in nature and that charging is occurring. This ISS spectrum is quite similar to that taken from an oxygen-exposed Sn surface [60].

Annealing in hydrogen dramatically alters the composition of the outermost layer of surface atoms as seen in the ISS spectrum of Figure 3-1(b). The Pt peak has grown in size nearly to that of the Sn peak, the O peak is significantly decreased in size, the O peak appears at its predicted E/E$_o$ value of 0.4 indicating that charging is no longer a problem and the inelastic background is reduced indicating that the outermost surface layer is more metallic in nature. Figures 3-1(a) and 3-1(b) were collected using the same instrument settings and are scaled accurately with respect to each other. Thus, the Sn peak height does not change significantly during the reduction. The ISS cross section of O is much smaller than that of Pt [53]. This suggests that the decrease in the number of O atoms may roughly correspond to the increase in the number of Pt atoms in the outermost surface layer. It is probable that the O atoms are removed from the surface layer through water formation during the reduction. Although speculative, it is possible that the Pt which migrates to

the surface fills the vacancies left by the O. The chemical interaction between the Pt and hydrogen provides a driving force for the Pt migration as discussed by Bouwman and co-workers [67] much like the chemical interaction between the Sn and O provides a driving force for Sn migration to the surface during an oxygen exposure [54,57,72,73]. These studies also demonstrate that annealing a Pt/Sn alloy surface in vacuum rather than hydrogen enriches the near-surface region in Sn and not in Pt. A hydrogen environment is necessary to enrich the near-surface region in Pt.

Figure 3-2(a) shows a bulk-sensitive AES spectrum and Figure 3-3(a) shows a surface-sensitive AES spectrum taken from the cleaned and air-exposed sample. There are Sn, C and O peaks appearing in these spectra but no peaks due to Pt appear. This fact provides clear evidence that a fairly thick (>30 angstroms) layer of tin oxide forms over the Pt-rich region during the air exposure. The same conclusion has been reached in a previous study by Hoflund and Asbury [72] using angle-resolved XPS. The O/Sn peak-height ratios in Figures 3-2(a) and 3-3(a) are 0.61 and 0.58, respectively. These comparable values indicate that the composition of the tin oxide layer is fairly uniform with depth. The ratios are also typical of those obtained from tin oxide surfaces [50]. The C peak is probably due to

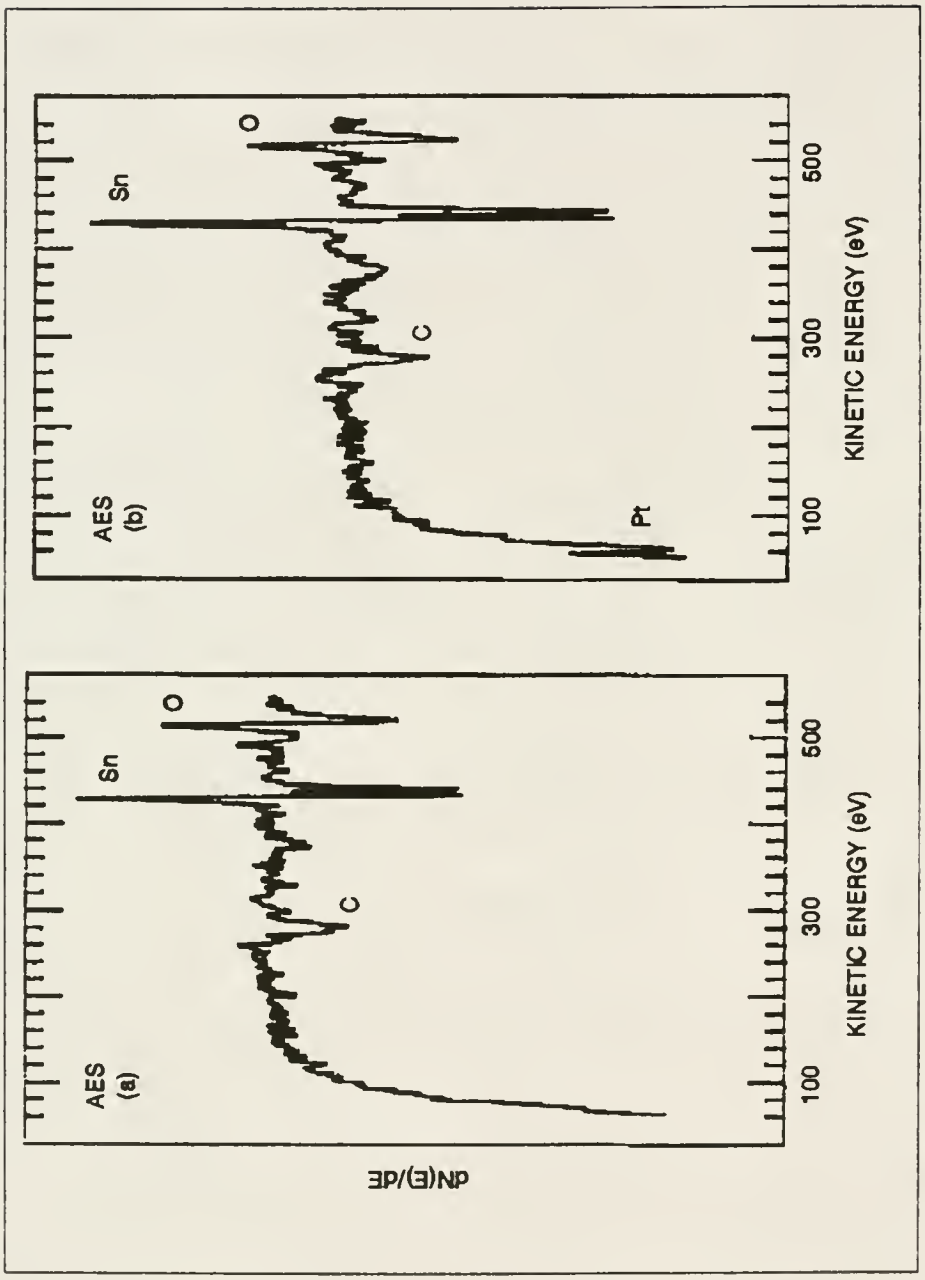

Figure 3-2. Bulk-sensitive AES spectra taken from the (a) air-exposed and (b) reduced Pt_3Sn surfaces.

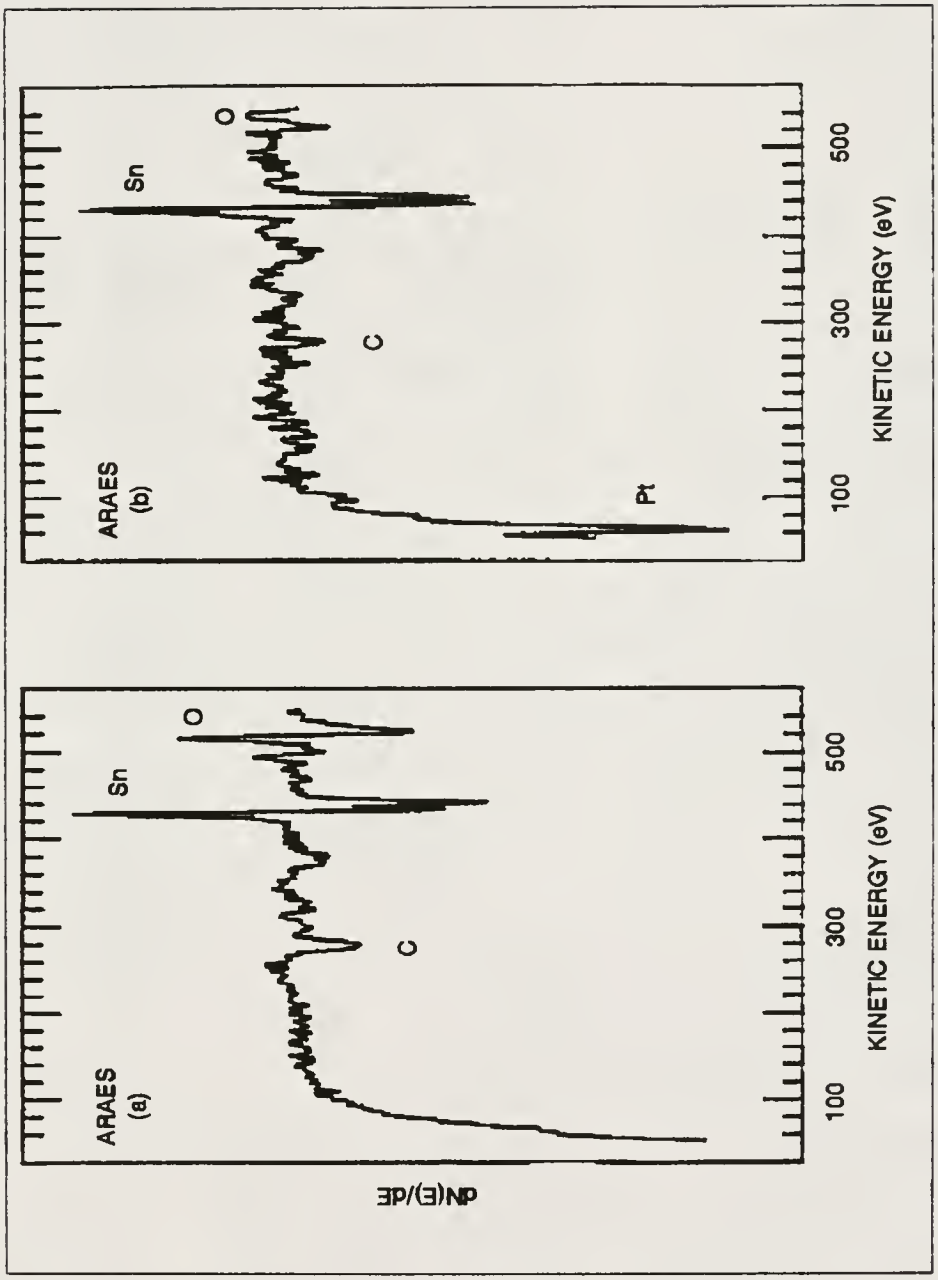

Figure 3-3. Surface-sensitive ARAES spectra taken from the (a) air-exposed and (b) reduced Pt_3Sn surfaces.

adsorption of hydrocarbons during the air exposure and always appears after exposing these samples to air.

Figures 3-2(b) and 3-3(b) show the bulk-sensitive and surface-sensitive AES spectra, respectively, taken after the reduction. Two changes due to the reduction are observed by comparing the bulk-sensitive AES spectra shown in Figures 3-2(a) and 3-2(b). The O/Sn ratio is substantially reduced and Pt migrates to the near-surface region during the reduction. Both of these facts are consistent with the ISS spectrum shown in Figure 3-1(b) even though the bulk-sensitive AES probes more deeply beneath the surface than ISS. Comparing the surface-sensitive spectrum shown in Figure 3-3(b) and the bulk-sensitive spectrum shown in Figure 3-2(b), it is seen that more Pt and less O are contained in the near-surface region than at greater depths. This observation supports the assertion that Pt replaces O which has been removed during the reduction. It is also possible to qualitatively describe the depth composition profiles of the Pt and O from these spectra. Initially, the O had a fairly uniform concentration through the oxidic region (of greater depth than that probed by the bulk-sensitive AES). After the reduction the O concentration is low at the surface and increases at greater depths. The Pt is more concentrated at the surface and less so at greater depths. It is seen that the increase in Pt and decrease in

O in the near-surface region is large by comparing the surface-sensitive spectra shown in Figures 3-3(a) and 3-3(b).

The XPS survey spectra taken before and after the reduction are shown in Figures 3-4(a) and 3-4(b), respectively. Peaks due to Sn, O, Pt, C, and Ta are observed in the spectra. The Ta peak appears because a Ta strip was used to hold the sample on the mounting block. As observed by the presence of the large Pt 4f peaks in Figure 3-4(a), XPS probes more deeply than bulk-sensitive AES. This Pt signal originates from a Sn-depleted region which lies beneath the tin oxide layer [57,72]. After the reduction the Pt peaks are increased in size and the height of the O 1s peak is decreased. These results are consistent with both the ISS and AES spectra even though XPS probes more deeply than the other two techniques.

High-resolution XPS spectra of the Sn 3d, Pt 4f and O 1s features before (A(a), B(a) and C(a), respectively) and after reduction (A(b), B(b) and C(b), respectively) are shown in Figure 3-5. The Sn 3d peaks shown in A(a) have a binding energy of 486.4 eV which corresponds to that of oxidic Sn (SnO, SnO_2 or Sn hydroxides) [32,50]. However, these peaks are broad and contain a shoulder at about 485.0 eV which is due either to alloyed or to metallic tin lying beneath the oxide layer [72]. After the reduction most of

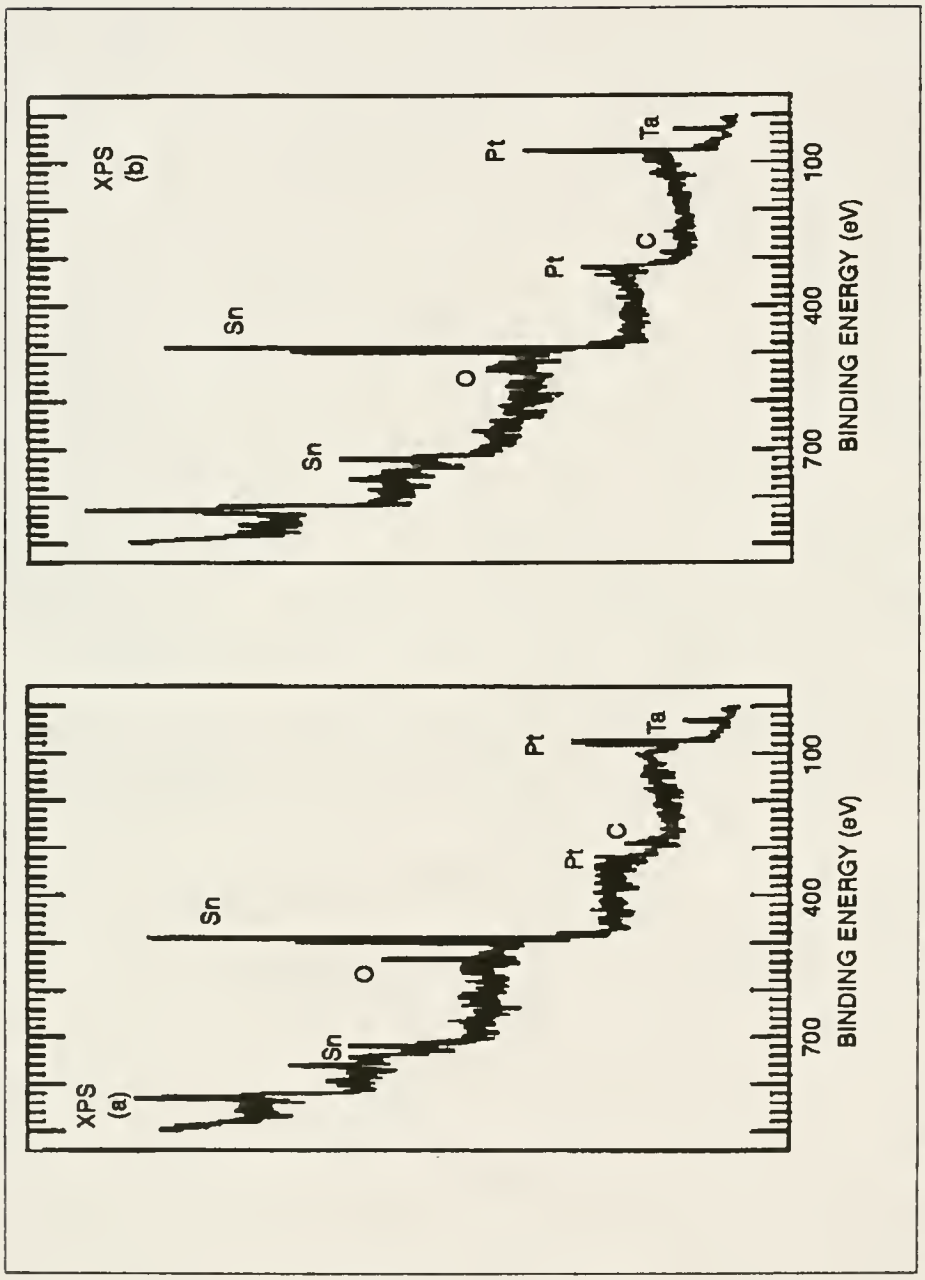

Figure 3-4. The XPS survey spectra taken from the (a) air-exposed and (b) reduced Pt_3Sn surfaces.

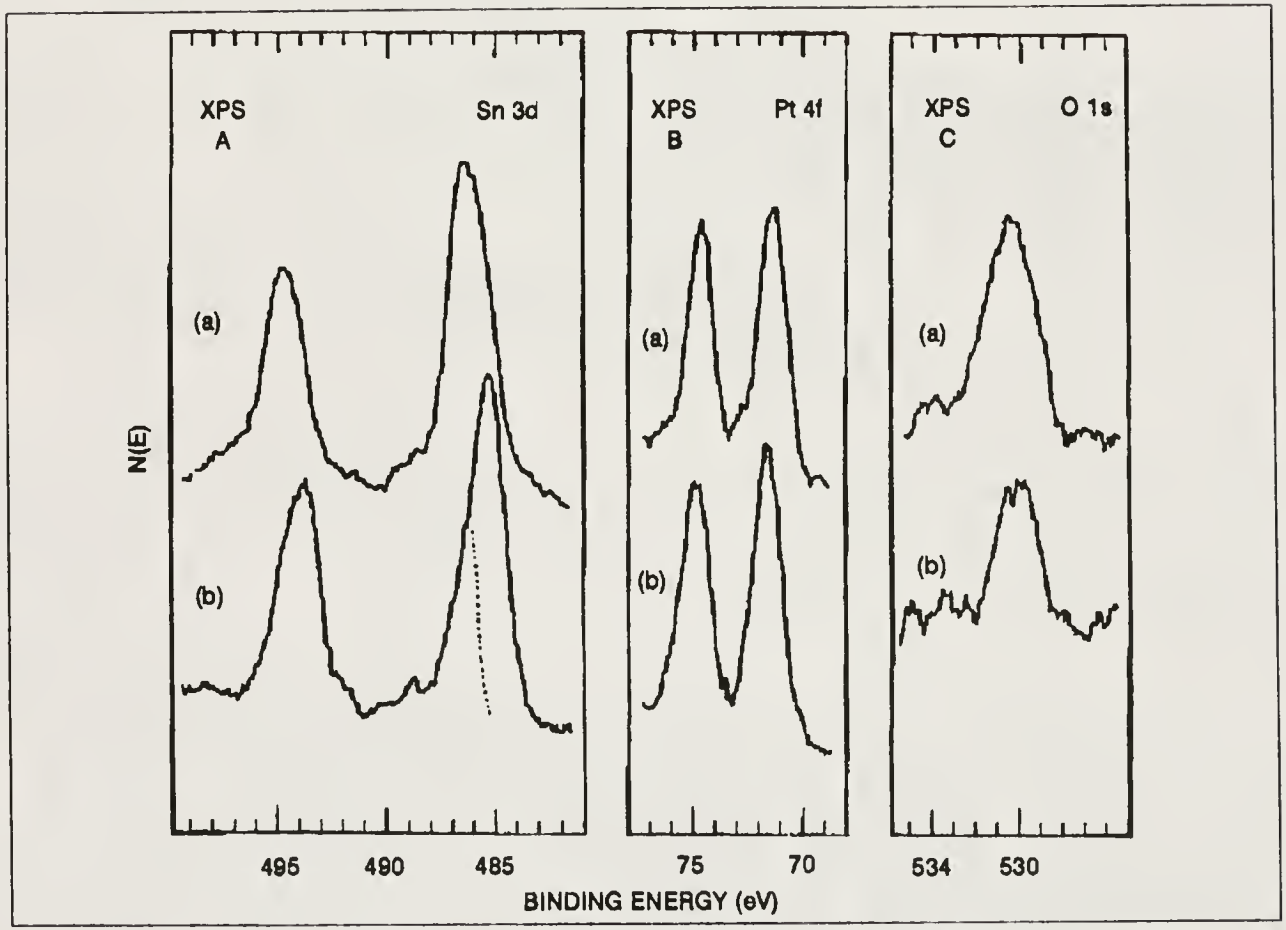

Figure 3-5. High-resolution XPS spectra taken from the (a) air-exposed and (b) reduced Pt_3Sn surfaces showing the (A) Sn 3d peaks, (B) Pt 4f peaks and (C) O 1s peak. The shoulder emphasized by the dotted line in A(b) is oxidic Sn.

the Sn is in the form of alloyed or metallic Sn as evidenced by the peak position of about 485.3 eV. This value is larger than the Sn 3d binding energy of 484.6 eV for metallic Sn. Since a detailed deconvolution of these peaks has not been attempted in this study, a rigorous assignment of binding energies to species is not made. Further work on this topic is in progress. A higher binding energy shoulder at approximately 486.4 eV (shown as a dotted line) is also present after the reduction. This is consistent with the AES spectra shown in Figures 3-2(b) and 3-3(b), which show that most of the O lies beneath the surface.

The Pt 4f peaks shown in Figure 3-5B(a) lie at a binding energy of 71.5 eV which is about 0.6 eV larger than that of metallic Pt. The width and shapes of these peaks suggest that only one chemical form of Pt contributes to this spectrum. As discussed above, this Pt is probably an Sn-depleted alloy, but the reason for the binding energy difference from metallic Pt is not currently understood. After reduction the Pt 4f binding energy is 71.7 eV. Again, it appears that only one chemical form of Pt is present. One possibility is that the Sn-depleted Pt alloy has a binding energy of 71.5 eV and that this binding energy increases to 71.7 eV as the Sn concentration increases after reduction of the alloy. Two studies [55,58]

suggest that the Sn and Pt peaks obtained from an alloy are shifted to higher binding energy. This and other possibilities are being investigated.

Figure 3-5C(a) shows the XPS O 1s peak taken from the air-exposed alloy surface and Figure 3-5C(b) shows the O 1s peak taken from the reduced alloy surface. The width and shape of the peak in Figure 3-5C(a) indicates that two forms of O are present on the air-exposed sample: an oxidic form with a binding energy at 530.5 eV and hydroxyl groups with a binding energy at about 531.5 eV. The reduction process removes the hydroxyl groups leaving only the oxidic form beneath the surface.

Summary

An air-exposed, polycrystalline Pt_3Sn surface has been examined using ISS, ARAES and XPS before and after reduction by heating at 300 °C under 1 Torr of hydrogen for 1 hour. Before reduction the surface was covered with a fairly thick (about 40 angstroms), uniform layer of tin oxide and hydroxide. Beneath this layer was a Pt-rich region. The ISS data shows that the outermost atomic layer contains mostly Sn and O with only a very small amount of Pt present.

Reduction results in loss of O and enrichment in Pt of the near-surface region. The ISS data shows (1) that the outermost atomic layer is strongly enriched in Pt through

migration of Pt to the surface, (2) that the outermost atomic layer becomes more metallic and (3) that O is removed from the outermost atomic layer during the reduction. The ARAES data suggest that the Pt migrates to the surface from the Pt-rich region by moving through vacancies left by the O which reacted with the hydrogen and desorbed, thus strongly enriching the outermost layer in Pt. The XPS data shows that most of the tin oxide is reduced to metallic form and probably is present as alloyed Sn. The reduction results in loss of hydroxyl groups but a subsurface, oxidic form remains under the reductive conditions used. It is likely that reduction under the conditions used in this study but for longer periods would result in complete removal of the O leaving a Pt-rich alloy at the surface.

CHAPTER 4
EFFECT OF PRETREATMENT ON A PLATINIZED TIN OXIDE CATALYST USED FOR LOW-TEMPERATURE CO OXIDATION

Introduction

It has been observed that the performance of platinized tin oxide catalysts used for low-temperature CO oxidation can be enhanced through reductive pretreatments prior to reaction [26]. For the pretreatment and reaction conditions used (see Figure 4-1), the unpretreated catalyst exhibits the lowest long-term activity. Pretreatment in CO at 100 °C greatly enhances the long-term activity, and a further enhancement occurs following CO pretreatment at 125 °C. Utilizing higher pretreatment temperatures up to 225 °C yields no change in the catalytic activity compared to the pretreatment at 125 °C. In order to understand how platinized tin oxide catalysts function in converting CO and O_2 to CO_2 at low temperatures, it is necessary to characterize the composition and chemical states of the species present at these surfaces. This has been accomplished in this study using several surface characterization techniques, including ion scattering spectroscopy (ISS), X-ray photoelectron spectroscopy (XPS) and Auger electron spectroscopy (AES) to examine the surface of

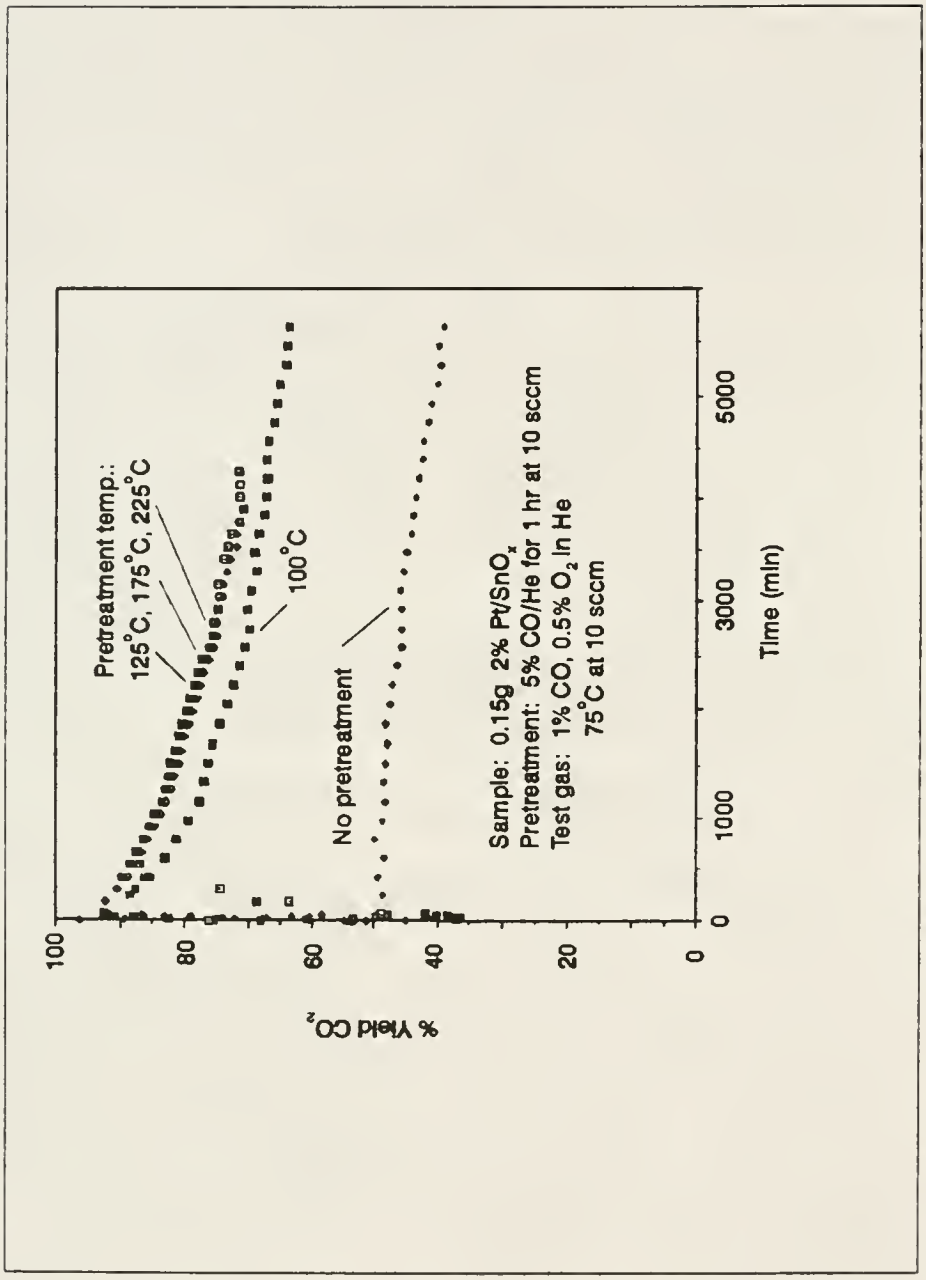

Figure 4-1. Catalytic activity of the Engelhard Pt/SnO_x catalyst for CO oxidation as a function of time and pretreatment temperature.

platinized tin oxide before and after pretreatment in CO as a function of the pretreatment temperature. It is anticipated that these studies will lead to a better understanding of this catalytic process and eventually to the development of improved catalysts for this application.

Experimental

The platinized tin oxide catalyst was acquired from Engelhard Industries in powdered form. It has an average particle size of 1 μm and a BET surface area of 6.9 m^2/gram. For the characterization studies, the powder was pressed into thin disks approximately 1 cm^2 in diameter. These were inserted directly into the ultrahigh vacuum (UHV) system (see Appendix) for pretreatment and characterization. Pretreatments were performed by moving the sample into a preparation chamber (base pressure of 10^{-7} Torr), introducing CO at a pressure of 40 Torr and heating the sample at the prescribed temperature for 1 hour. Then the sample was allowed to cool while the preparation chamber was pumped down to 10^{-7} Torr before moving the sample into the main analytical chamber (base pressure of 10^{-11} Torr) for analysis by ISS, XPS and AES. The samples were heated at 75, 100, 125 and 175 °C in the preparation chamber using a custom sample heater [75], which did not expose the reducing gas to hot spots that would have dissociated the CO. Two different as-prepared samples were analyzed

without prereduction and the results were found to be reproducible. A new sample was prepared and introduced into the analysis chamber for each reduction temperature studied.

The ISS, XPS and AES data were taken using a double-pass cylindrical mirror analyzer (CMA) (Perkin-Elmer PHI Model 25-270AR) as the charged-particle energy analyzer. The ISS spectra were collected in the nonretarding mode using a 147°-scattering angle and pulse counting detection [51]. A 1-keV, 100-nA $^4He^+$ primary ion beam was defocused over a 1-cm-diameter area and spectra were collected as quickly as possible (typically 90 s) to minimize damage from sputtering. The AES experiments were performed in the nonretarding mode using a 3-keV, 10-μA primary electron beam with a 0.2-mm spot diameter. The XPS experiments were performed in the retarding mode using Mg Kα excitation. Survey XPS spectra were collected using a 50-eV pass energy whereas a 25-eV pass energy was utilized for obtaining elemental lineshape information.

Results and Discussion

An XPS survey spectrum taken from the as-received Engelhard platinized tin oxide catalyst is shown in Figure 4-2. The peaks of significant size are due only to O and Sn, and no peaks due to C or other typical contaminants appear. In fact, this spectrum is essentially identical to

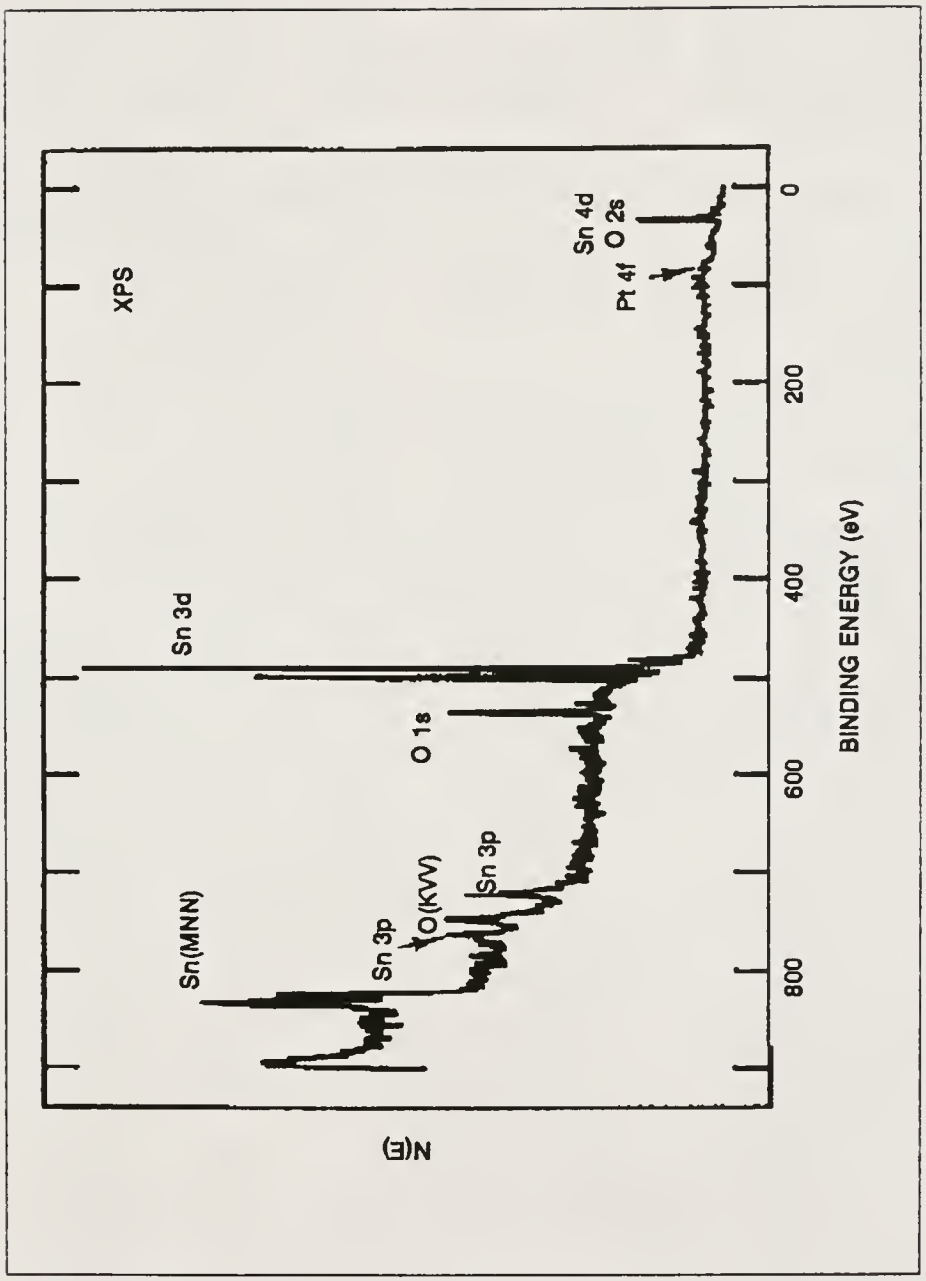

Figure 4-2. The XPS survey spectrum taken from the as-received Engelhard Pt/SnO_x catalyst.

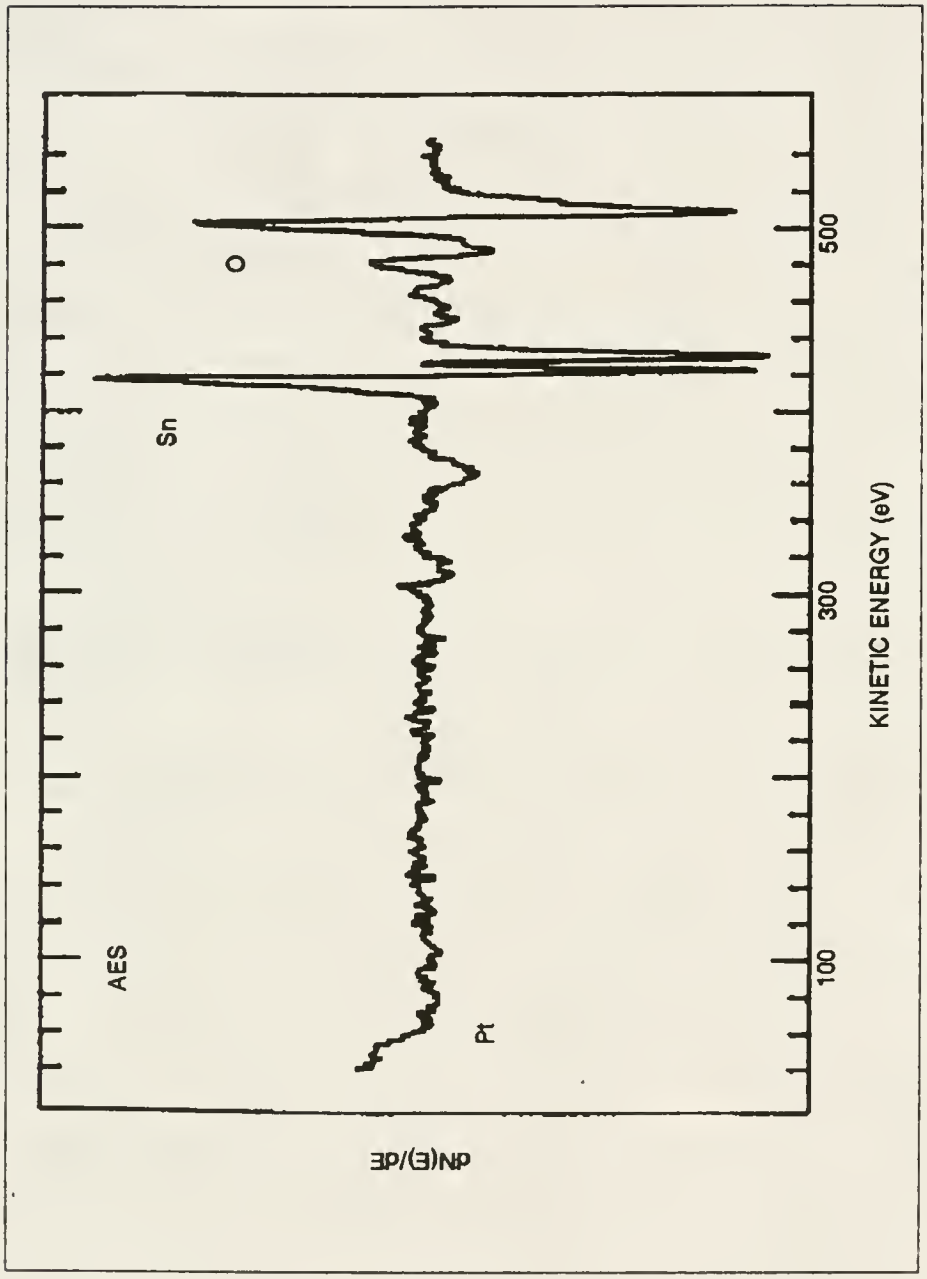

Figure 4-3. The AES spectrum taken from the as-received Engelhard Pt/SnO_x catalyst.

an XPS spectrum obtained from a very clean tin oxide surface. It is most interesting that the predominant Pt 4f peaks are so small that they cannot be discerned readily in this spectrum. A corresponding AES spectrum taken from the same surface is shown in Figure 4-3. Again, the predominant features are due to Sn and O, and this spectrum is similar to one obtained from a clean tin oxide surface. However, a feature due to Pt appears at a binding energy near 64 eV. It can be described as an edge rather than a typically shaped AES peak. Similar Pt features have been observed in a study of the electro-chemisorption of Pt on tin oxide [76]. This feature is more prominent than the Pt XPS peaks in Figure 4-2. In agreement with the XPS data, no contaminant peaks are apparent in this AES spectrum. As the catalyst is reduced at various temperatures, very small changes are observed in the XPS and AES spectra corresponding to Figures 4-2 and 4-3, but taken from the reduced surfaces. Therefore, these survey spectra are not shown.

Ion scattering spectroscopy is a particularly useful technique for examining catalytic surfaces because it is very highly surface sensitive (outermost one or two atomic layers). The ISS spectra taken before (a) and after (b-e) reduction are shown in Figure 4-4. The spectrum shown in (a) consists of peaks due to O, Sn and Pt, and the high inelastic background is characteristic of ISS spectra taken

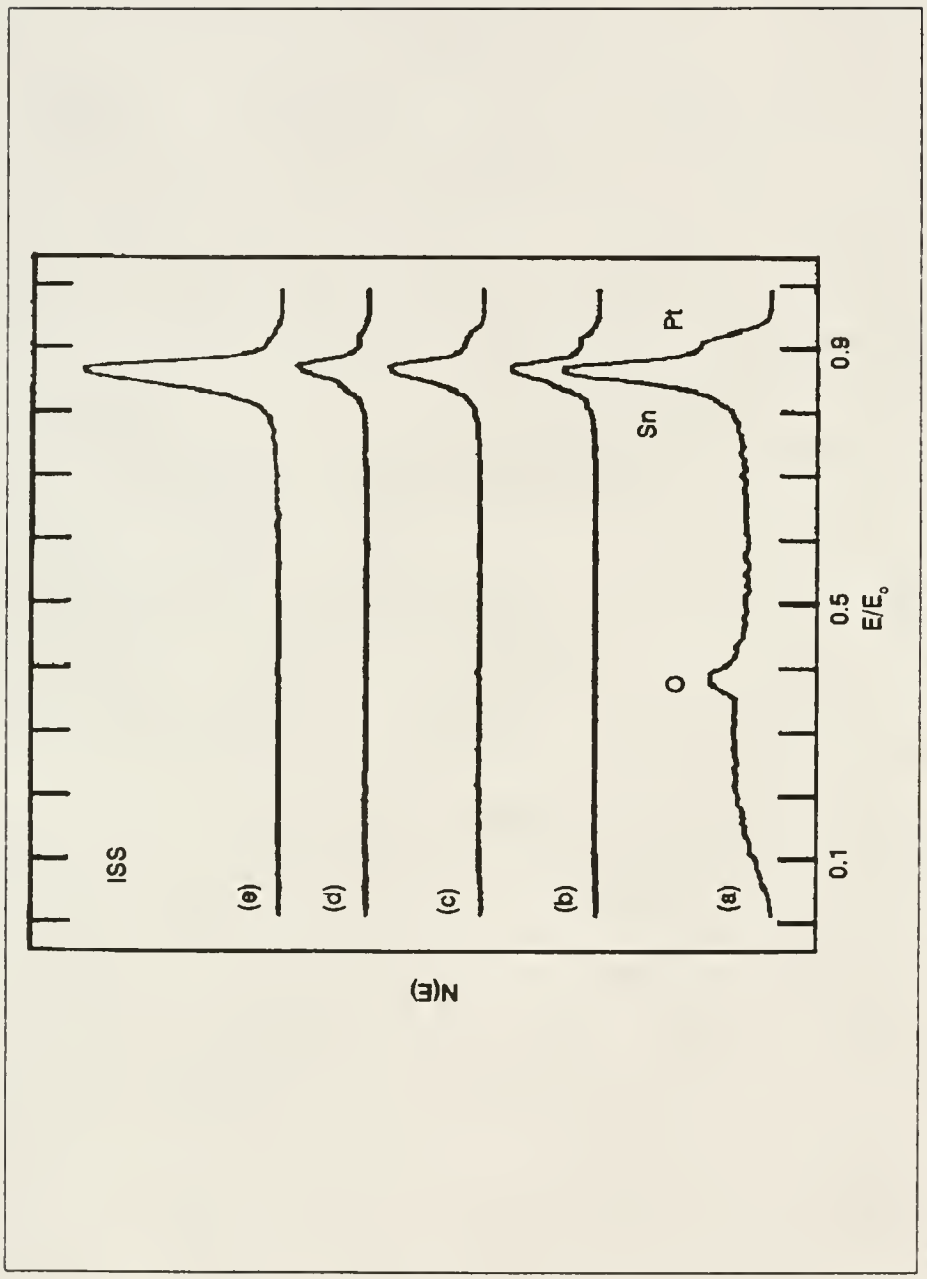

Figure 4-4. The ISS spectra taken from (a) an unpretreated sample and samples reduced at (b) 75, (c) 100, (d) 125 and (e) 175 °C in 40 Torr of CO for 1 hour.

from nonmetallic surfaces. In such a case, inelastically scattered ions are not efficiently neutralized since the electron mobility at a non-metallic surface is so low that these ions contribute to the background signal. A previous study by Asbury and Hoflund [60] showed that O penetrates beneath the surface during room-temperature oxygen exposure of polycrystalline Sn. This suggests that the fairly large O peak in (a) is due to O associated with the Pt and/or perhaps with hydroxyl groups attached to Sn that may lie above the surface [50].

The ISS spectra shown if Figure 4-4(b-e) were obtained from samples reduced in 40 Torr of CO for 1 hour at 75, 100, 125 and 175 °C respectively. All four spectra have two characteristics in common. Firstly, the pretreatments have resulted in negligible inelastic backgrounds, which is indicative of the formation of surfaces with a metallic nature. Secondly, the O peak is no longer discernible after the reductions, which is also consistent with the observation that the surfaces appear to be metallic. The reductive pretreatment results in an increase in the Sn/Pt ratio, and the extent of this increase is greater at higher reduction temperatures. As shown in chapter 1, an increase in the ISS Sn/Pt ratio during reduction of platinized tin oxide surfaces has been found to be indicative of alloy formation. All of the ISS spectra shown in Figure 4-4 were

taken using the same instrument settings, but the maximum peak heights vary considerably. Although the variation is not understood, it could be due to changes in ion neutralization probability, surface morphological changes or changes in the concentration of surface hydrogen, which have been shown to alter the ISS signal strength [77,78].

The Sn 3d XPS spectra and Sn MNN AES spectra taken before and after reduction are shown in Figures 4-5 and 4-6, respectively. Before pretreatment (air-exposed sample) the Sn $3d_{5/2}$ lineshape and peak position (486.4 eV) indicate that Sn is present in the +2 or +4 oxidation states most likely as SnO, $Sn(OH)_2$, SnO_2 or $Sn(OH)_4$ and that metallic Sn is absent. As discussed by Hoflund and coworkers [32], it is not possible to distinguish between these species based on the XPS Sn 3d peaks, but more specific information can be gained about these species using electron energy-loss spectroscopy (ELS) [48,56], valence band XPS [48,50], electron-stimulated desorption (ESD) [49,50] or secondary ion mass spectrometry (SIMS) [46,47,79]. The metallic XPS Sn $3d_{5/2}$ peak appears at an energy of 484.6 eV [80]. When a small amount of metallic Sn and a relatively large amount of tin oxides or hydroxides are present, a slight broadening appears on the low-binding-energy sides of the oxidic XPS Sn 3d features. This is the case for the 175 °C-reduced sample as shown in

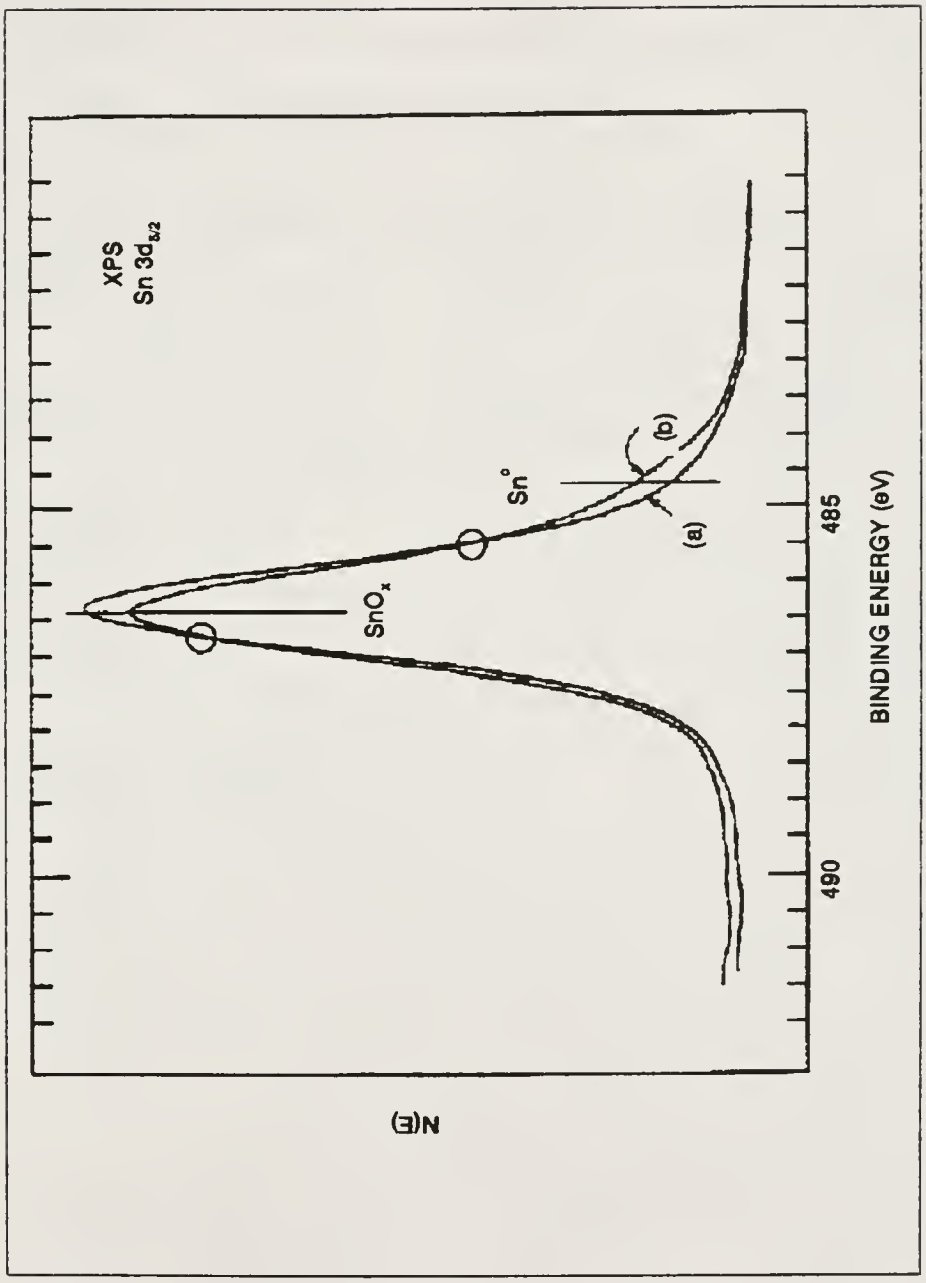

Figure 4-5. The XPS Sn 3d peaks obtained from (a) an unpretreated sample and (b) a sample reduced at 175 °C in 40 Torr of CO for 1 hour. The circled regions indicate crossing points.

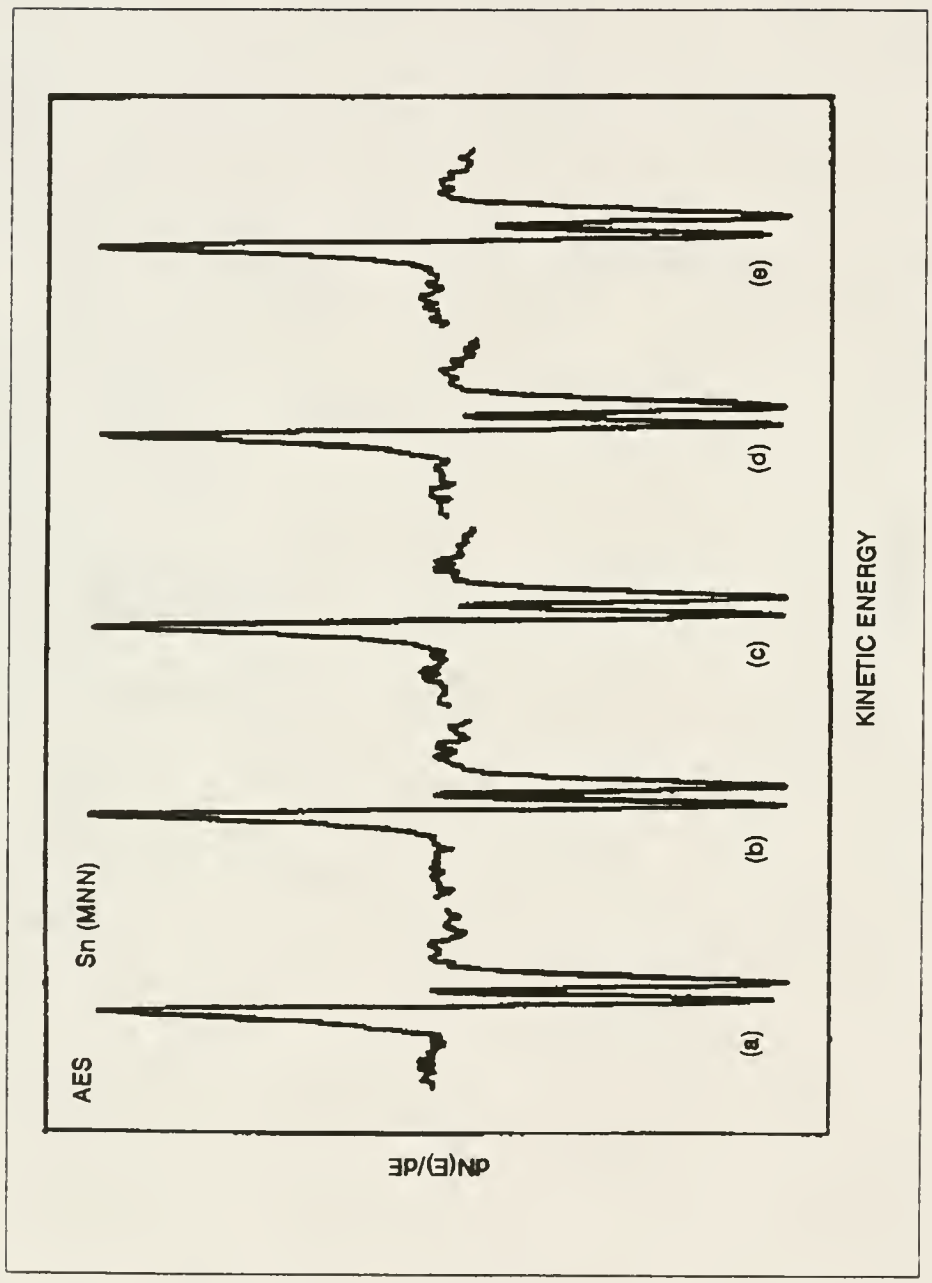

Figure 4-6. The AES Sn MNN peaks obtained from (a) an unpretreated sample and samples reduced at (b) 75, (c) 100, (d) 125 and (e) 175 °C in 40 Torr of CO for 1 hour.

Figure 4-5. Samples reduced at lower temperatures also yield this metallic shoulder, and the amount of metallic Sn produced generally increases as the annealing temperature increases with the most being produced at 175 °C. However, the amounts of metallic Sn produced at 75 and 100 °C appear similar. Similar observations can be made by considering the AES Sn MNN peaks shown in Figure 4-6. The high-kinetic-energy oxidic peak lies at 430 eV, while the high-kinetic-energy metallic peak lies at 423 eV. The peaks shown in Figure 4-6(a) are characteristic of oxidic Sn. When metallic Sn is present, the height of the splitting between the two primary peaks decreases. This is observed in spectra (b)-(e) taken from the reduced samples. In agreement with the XPS Sn 3d spectra, the extent of metallic Sn formation is greater at elevated reduction temperatures with the maximum amount of metallic Sn being produced at 175 °C. Further reduction, either for prolonged periods or at higher temperatures than used in this study, would undoubtedly result in the production of increased amounts of metallic Sn.

The XPS O 1s peaks are shown in Figure 4-7. These were taken before (a) and after (b) reduction at 175 °C. The peak shown in (a) exhibits a distinct asymmetry on the high-binding-energy side due to the presence of hydroxyl groups, which are responsible for a shoulder at

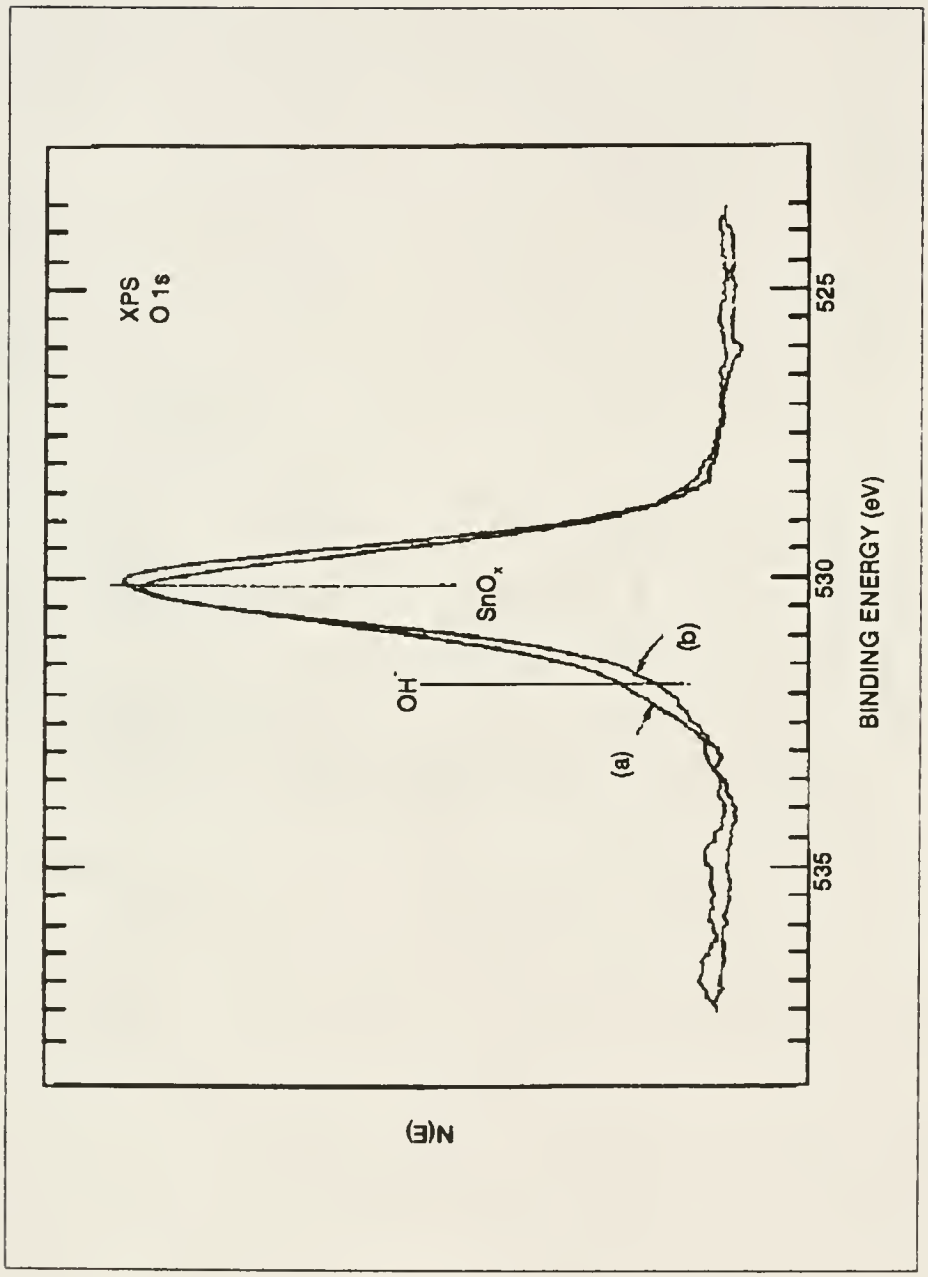

Figure 4-7. The XPS O 1s peaks obtained from (a) an unpretreated sample and (b) a sample reduced at 175 °C in 40 Torr of CO for 1 hour.

approximately 531.8 eV. It is also possible that the very small shoulder near 533.0 eV is due to adsorbed water. This assignment is consistent with results obtained in the study of hydrated polycrystalline tin oxide films by Tarlov and Evans [81]. Pretreatment at 75 °C slightly reduces the amounts of adsorbed water and hydroxyl groups present while pretreatment at 100 °C or above eliminates the adsorbed water and further reduces the concentration of hydroxyl groups. The 175 °C pretreatment results in the lowest surface hydroxyl group concentration. It is interesting to note that these hydroxyl species are strongly bonded to the surface and require annealing at 600 °C in vacuum for nearly complete removal [48,50,82].

The O content of the near-surface region is decreased by the pretreatment process. The AES and XPS O/Sn atomic ratios obtained at the various pretreatment temperatures are listed in Table 4-1. A decrease in the O/Sn ratio is caused by loss of adsorbed water, a decrease in hydroxyl group concentration, reduction of tin oxides and hydroxides to metallic Sn and reduction SnO_2 to SnO. However, the relative importance of these factors cannot be assessed completely from the types of data taken in this study. The amount of Pt present on these surfaces is so small that changes in the Pt oxidation state, which are discussed below, would not affect the O/Sn atomic ratios presented in

Table 4-1. The O/Sn atomic ratios versus pretreatment temperature.

Pretreatment	AES[a]	XPS[b]
Untreated	1.32	1.56
75 °C	1.08	1.45
100 °C	1.05	1.39
125 °C	1.04	1.33
175 °C	1.05	1.21

[a]Calculated using methods described in reference 128.
[b]Calculated using methods described in reference 80.

Table 4-1. The AES and XPS results in Table 4-1 are different with respect to both magnitude and trend. The AES data indicate that the near-surface region loses about 20% of its O regardless of the reduction temperature. The XPS O/Sn atomic ratios are considerably larger than the AES values and decrease monotonically as the pretreatment temperature increases. Either the XPS values differ from the AES values due to inaccuracies in the tabulated cross sections or the variation is due to the fact that AES and XPS probe different volumes of the near-surface region. If the difference were due only to inaccurate cross sections, then the XPS O/Sn ratios obtained from the reduced samples would not show such a large variation with reduction temperature. Thus, the variation is due to the fact that XPS probes more deeply than AES, which is consistent with mean-free-path arguments also. The kinetic energies of the XPS O 1s and Sn 3d electrons are 723 eV and approximately 770 eV, respectively, while the kinetic energies of the AES O and Sn electrons are near 510 eV and 430 eV, respectively. The corresponding mean free paths (τ) are about 6 angstroms for XPS and 4 angstroms for AES [83]. Since most of the XPS and AES electrons originate within a depth of approximately $3(\tau)$, XPS probes about 18 angstroms beneath the surface while AES probes at a depth of about 12 angstroms. Then, the data in Table 4-1 indicate that the near-surface region

probed by AES contains less O than the region probed by XPS for the untreated sample and samples reduced at 75-175 °C. Reduction at any of the temperatures used causes the AES O/Sn ratio to drop from 1.32 to about 1.06 whereas the XPS O/Sn ratio decreases monotonically as the reduction temperature increases. The essentially constant AES value probably results from competing processes, that is, O leaving the surface as CO_2 during the reduction and O migrating to the near-surface region from farther beneath the surface. This is consistent with the trend of the XPS data implying that subsurface reduction takes place to a greater extent at higher temperatures. A similar phenomenon has been observed previously for the reduction of a TiO_2 (001) surface [84].

The XPS Pt 4f peaks obtained from the unpretreated samples are shown in Figure 4-8(a), and the peak assignments used in this study are listed in Table 4-2. Most of these assignments were taken from a standard reference [80], but the 72.3 eV feature has been assigned as Pt-O-Sn in previous studies of platinized tin oxide surfaces [32,56]. The spectrum shown in Figure 4-8(a) indicates that very little metallic Pt is present and that the Pt species consist mostly of Pt-O-Sn, $Pt(OH)_2$ and Pt oxides. In fact, a spectrum very similar to this one has been taken

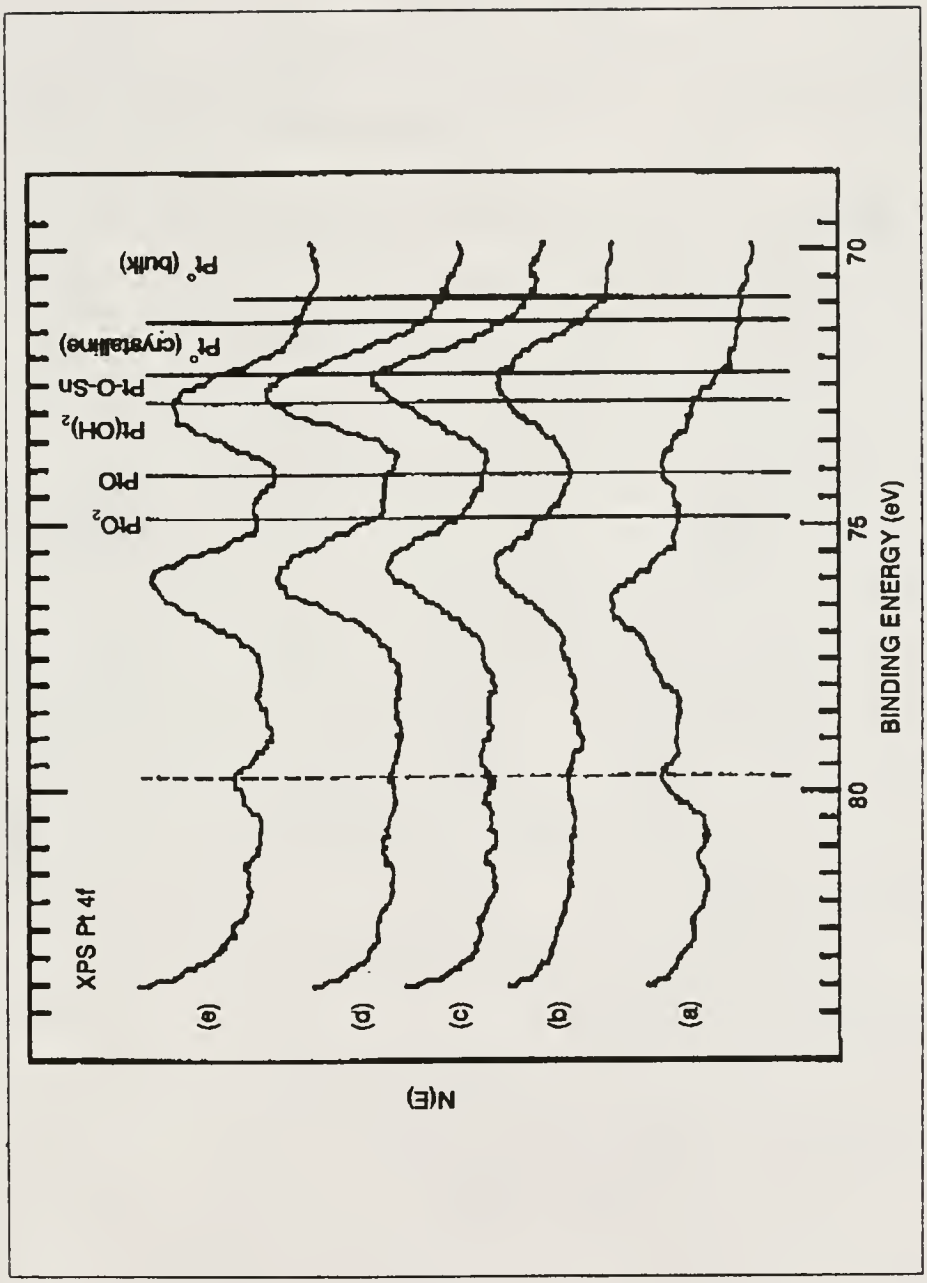

Figure 4-8. The XPS Pt 4f peaks obtained from (a) an unpretreated sample and samples reduced at (b) 75, (c) 100, (d) 125 and (e) 175 °C in 40 Torr of CO for 1 hour.

Table 4-2. The XPS Pt 4f peak assignments.

Species	Binding Energy (eV)
Pt° (bulk)[a]	70.9
Pt° (crystalline)[b]	71.3
Pt-O-Sn[b]	72.3
$Pt(OH)_2$[a]	72.8
PtO[a]	74.2
PtO_2[a]	74.9

[a]Assignments taken from Reference 80.
[b]Assignments taken from References 32 and 89.

from a co-deposited platinum/tin oxide film after calcining in air at 725 K for 1.5 hours [32].

The XPS Pt 4f spectra taken after pretreating at 75 and 100 °C are shown in Figures 4-8(b) and 4-8(c), respectively. These two spectra are quite similar in that very little metallic Pt is present and the predominant species consist of Pt-O-Sn and $Pt(OH)_2$. The metallic Pt apparently is in the form of small crystallites. A shoulder due to PtO_2 may also be present in both spectra, but this shoulder is smaller after the 100 °C reduction. The relative amounts of Pt-O-Sn and $Pt(OH)_2$ are similar in both spectra. Pretreating at a temperature 25 °C higher produces a significant change in the Pt species present, as shown in Figure 4-8(d). The predominant Pt species after the 125 °C reduction are $Pt(OH)_2$ and Pt-O-Sn in approximately equal amounts. Also, a small amount of metallic Pt is present after this pretreatment, and features due to Pt oxides do not appear.

Reduction at 175 °C produces a further and more pronounced shift in the Pt chemical state toward $Pt(OH)_2$ as shown in Figure 4-8(e). The Pt-O-Sn feature is now a shoulder on the $Pt(OH)_2$ peak, and the amount of metallic Pt present is decreased compared to the lower temperature reductions. The spectrum shown in Figure 4-8(a), taken from the unpretreated sample, exhibits a prominent feature

at 79.8 eV binding energy. Since the splitting between the Pt $4f_{7/2}$ and Pt $4f_{5/2}$ peaks is approximately 3.35 eV, this feature does not correspond to the Pt $4f_{5/2}$ peak of any of the species listed in Table 4-2. The 75 °C pretreatment reduces the size of this feature, and it does not appear after the 100 or 125 °C pretreatment. Therefore, it behaves like an oxidic feature and reappears in Figure 4-8(e).

It is interesting to compare the spectral information contained in Figure 4-8 with the kinetic information contained in Figure 4-1. The nonpretreated catalyst exhibits a low activity compare to any reduced catalyst. This correlates with the facts that the Pt is predominantly oxidic on the unpretreated catalyst and that significant changes in the Pt chemical state occur during the reductive pretreatments used in these studies. As the pretreatment temperature increases, more of the Pt is converted into $Pt(OH)_2$. This fact suggests that the $Pt(OH)_2$ plays an important role in the conversion of CO and O_2 into CO_2 at low temperatures. In this discussion a relationship is being drawn between the long-term catalytic behavior (past the first 500 minutes of reaction) and the chemical state of the Pt after the pretreatment but before the onset of reaction (time=0 in Figure 4-1). The initial catalytic behavior is quite complex [26], and changes may occur in the

Pt chemical state during this period. Consequently, characterization studies are in progress in which the state of the catalytic surface is being examined as the reaction is run for various periods of time. These studies should lead to an understanding of the chemical changes responsible for the unusual, initial catalytic behavior and the long-term decay in catalytic activity.

A small amount of metallic Pt forms during both the 125 and 175 °C pretreatment, and metallic Sn is also present as stated above. Paffett and Windham [55] have deposited layers of Sn on Pt(111) and found that alloy formation during annealing at or above 150 °C is strongly suggested by their data. Also, Fryberger and Semancik [85] have found that Pd deposited on SnO_2 (110) alloys with the Sn even at room temperature. It is anticipated that alloy formation occurs in the Engelhard catalyst under the pretreatment conditions used in this study. Since the amount of Pt present on this surface is small, it is likely that most of the metallic Sn is not alloyed while probably all of the Pt is alloyed.

Summary

A platinized tin oxide catalyst (commercially available from Engelhard Industries for low-temperature CO oxidation) has been examined using surface analytical techniques, including ISS, AES and XPS, before and after

pretreatment by annealing in 40 Torr of CO for 1 hour at 75, 100, 125 and 175 °C. The results have been correlated with catalytic activity data. The nonpretreated sample consists primarily of oxidic Sn (SnO_2, SnO and $Sn(OH)_x$) with a very small amount of Pt present as Pt-O-Sn, $Pt(OH)_2$, PtO and PtO_2 species. Reduction results in loss of both O and OH^- from the Sn and produces metallic Sn. The extent of these processes increases as the pretreatment temperature increases. The chemical state of the Pt changes with pretreatment temperature. At or below 100 °C, the predominant forms are Pt-O-Sn and $Pt(OH)_2$. As the reduction temperature increases, more $Pt(OH)_2$ forms. This fact suggests that $Pt(OH)_2$ plays an important role in the low-temperature catalytic oxidation of CO. The results demonstrate that the application of surface analytical techniques in studies of real catalysts can provide information that is useful in understanding catalytic behavior.

CHAPTER 5
CHARACTERIZATION STUDY OF SILICA-SUPPORTED PLATINIZED TIN OXIDE CATALYSTS USED FOR LOW-TEMPERATURE CO OXIDATION: EFFECT OF PRETREATMENT TEMPERATURE

Introduction

Research has indicated that platinized tin oxide (Pt/SnO_x) is an efficient CO oxidation catalyst at conditions which correspond to steady-state CO_2 laser operation [7,8,23,28]. As discussed in the previous chapter, the performance of Pt/SnO_x may be further enhanced following pretreatment in CO at elevated temperatures. However, for CO reduction temperatures above about 175 °C, a sharp, temporary decrease in activity is observed initially [26]. This induction period is believed to be the result of surface dehydration caused by combination of surface hydroxyl groups and desorption of water. No significant induction period results when Pt/SnO_x is humidified either after CO pretreatment or during the reaction itself and optimum pretreatment times exist which are consistent with the hypothesis involving surface dehydration. The data obtained thus far suggest that CO_2 is produced through decomposition of a bicarbonate species formed from adsorbed CO, a surface hydroxyl group and lattice oxygen [86].

Acknowledging the importance of surface hydroxyl groups, there has been considerable effort directed towards the development of a platinized tin oxide catalyst which is supported on a silica substrate ($Pt/SnO_x/SiO_2$) [27,87]. Hygroscopic silica may improve the performance of Pt/SnO_x surfaces by preventing extensive surface dehydration and consequent activity loss. Experiments have been conducted wherein the catalyst performance has been optimized with respect to several variables including pretreatment procedures [27]. Superior performance is realized by using a reductive pretreatment in 5% CO/He at 125 °C for 1 hour. As pretreatment temperatures approach 250 °C, there is a significant decrease in the observed activity. The optimized $Pt/SnO_x/SiO_2$ catalyst represents a significant improvement over commercially available Pt/SnO_x with respect to low-temperature CO oxidation activity and performance decay.

In order to understand these experimental observations, a characterization study has been carried out on silica-supported Pt/SnO_x before and after reduction in CO at 125 and 250 °C. This study utilized ion scattering spectroscopy (ISS) and X-ray photoelectron spectroscopy (XPS) to examine the concentrations and chemical states of species present at these surfaces and the changes which occur during reduction.

Experimental

The catalyst prepared for this study consisted of a thin layer of platinum and tin oxide dispersed on a silica gel substrate [27,87]. The silica gel was impregnated with tin oxide by evaporation of a stirred solution of tin metal powder and silica gel in concentrated nitric acid at 150 °C. Subsequently, Pt was precipitated from an aqueous solution of platinum tetraamine dihydroxide and formic acid with heating followed by drying at 150 °C. The final product was heated in air at 150 °C for 4 hours.

As-prepared, silica-supported Pt/SnO_2 samples were inserted into an ultrahigh vacuum (UHV) system (see Appendix) which has an ultimate pressure near 10^{-11} Torr. After initial surface characterization, the samples were transferred into a preparation chamber connected to the UHV system and reduced in 10 Torr of CO for 2 hours at 125 or 250 °C. Heating was accomplished using a platform heating element [75] which did not dissociate the reducing gas. Sample temperatures were measured using a thermocouple attached to the stainless-steel sample support block. After reduction each sample was returned to the UHV analytical chamber without air exposure for further characterization.

Energy analysis for the ISS and XPS experiments was accomplished using a Perkin-Elmer PHI Model 25-270AR double-pass cylindrical mirror analyzer (CMA). The CMA

contained an internal, movable aperture which varied the polar acceptance angle for incoming particles. The ISS spectra were collected in the nonretarding mode using a 147°-scattering angle, which was fixed by the experimental geometry, and pulse counting detection [51]. A 100-nA, 1-keV $^4He^+$ primary ion beam was defocused over a 1-cm^2 area to minimize sputter damage. Survey and high-resolution XPS spectra were recorded with Mg Kα excitation in the retarding mode using 50- and 25-eV pass energies respectively.

Results and Discussion

Survey XPS spectra taken from one silica-supported Pt/SnO_x catalyst sample before and after reduction in 10 Torr of CO at 125 °C appear in Figure 5-1, and XPS survey spectra taken from another sample before and after reduction at 250 °C appear in Figure 5-2. The two catalyst samples examined were similar in that both were randomly dispensed from the same catalyst batch. The spectra shown in Figures 5-1(a) and 5-2(a) were taken from the air-exposed surfaces. They exhibit predominant peaks due to Sn and O while peaks due to Pt are present but less discernible. Differences between Figures 5-1(a) and 5-2(a) with regard to the O/Sn ratio suggest that the as-prepared catalyst samples lack uniformity in average surface composition. Nevertheless, important information may still be obtained with respect to data taken from each catalyst

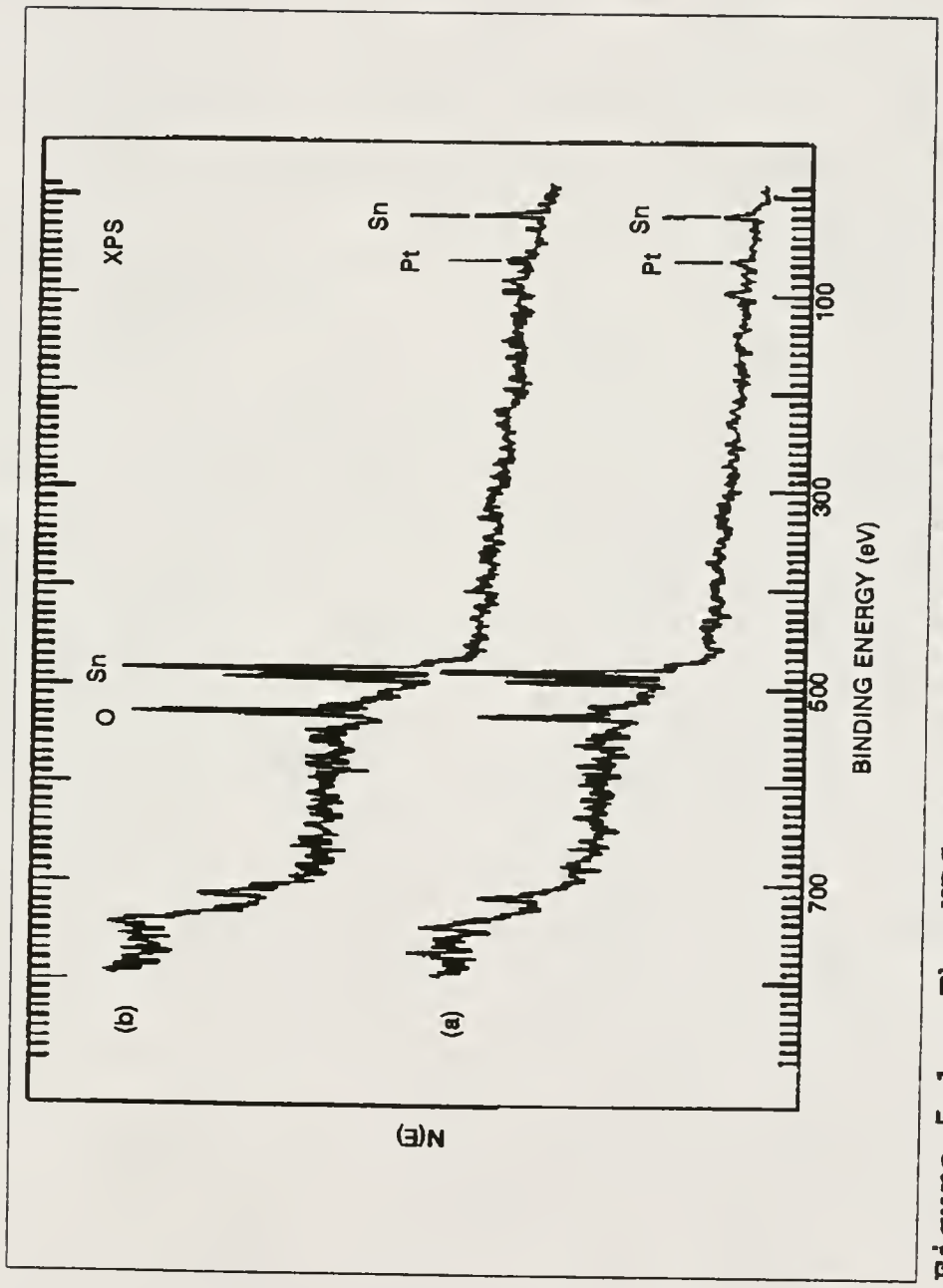

Figure 5-1. The XPS survey spectra taken from the silica-supported Pt/SnO_x surface (a) before and (b) after CO reduction at 125 °C.

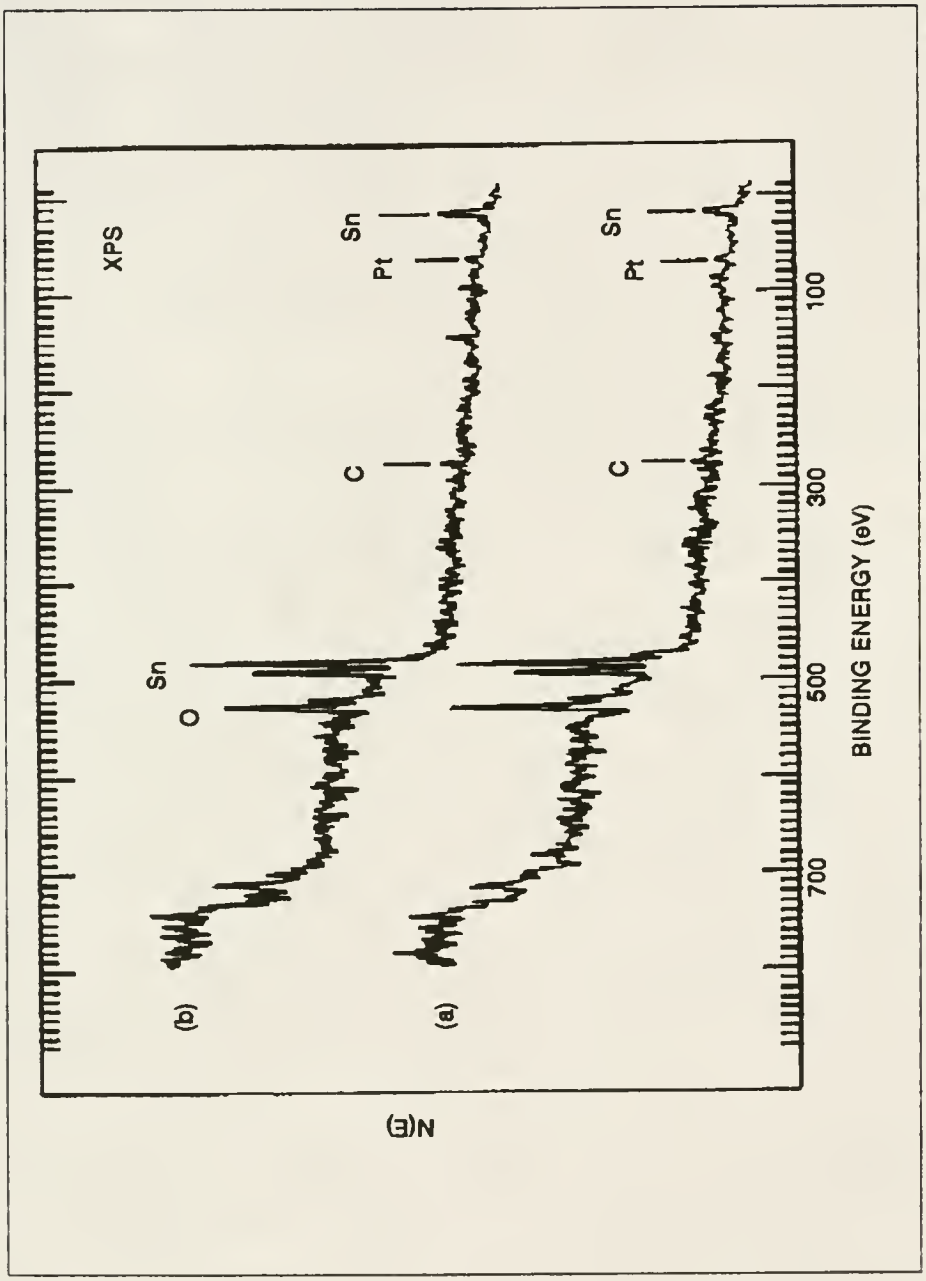

Figure 5-2. The XPS survey spectra taken from the silica-supported Pt/SnO_x surface (a) before and (b) after CO reduction at 250 °C.

sample before and after reduction. A thick tin oxide surface layer (> 50 angstroms) is indicated by the lack of Si XPS signals arising from the silica substrate. Only trace amounts of C and surface contaminants are detected. Reduction in CO results in changes in the Sn and O signals as shown in Figures 5-1(b) and 5-2(b). The spectra indicate that the surface region of the sample reduced at 125 °C becomes oxygen-enriched while depletion of surface O occurs in the sample reduced at 250 °C. A possible mechanism responsible for this result is discussed below.

An ISS spectrum taken from an air-exposed, silica-supported Pt/SnO_x surface before reduction is shown in Figure 5-3(a), and ISS spectra taken after reduction in CO at 125 and 250 °C appear in Figures 5-3(b) and 5-3(c), respectively. Figure 5-3(a) reveals distinct Pt and O features and a Sn peak which appears as a shoulder on the Pt peak. Peaks due to small amounts of contaminants such as C and Na are also present as are some peaks due to charging. Peaks due to charging shift in energy as the sample is rotated so they can be distinguished easily from elemental peaks, which appear at energies near those predicted by the elastic binary collision model [52,88]. After catalyst reduction at 125 °C, Figure 5-3(b) indicates that the surface composition has changed considerably. The Sn and Pt peaks have increased in size significantly, and the Sn peak

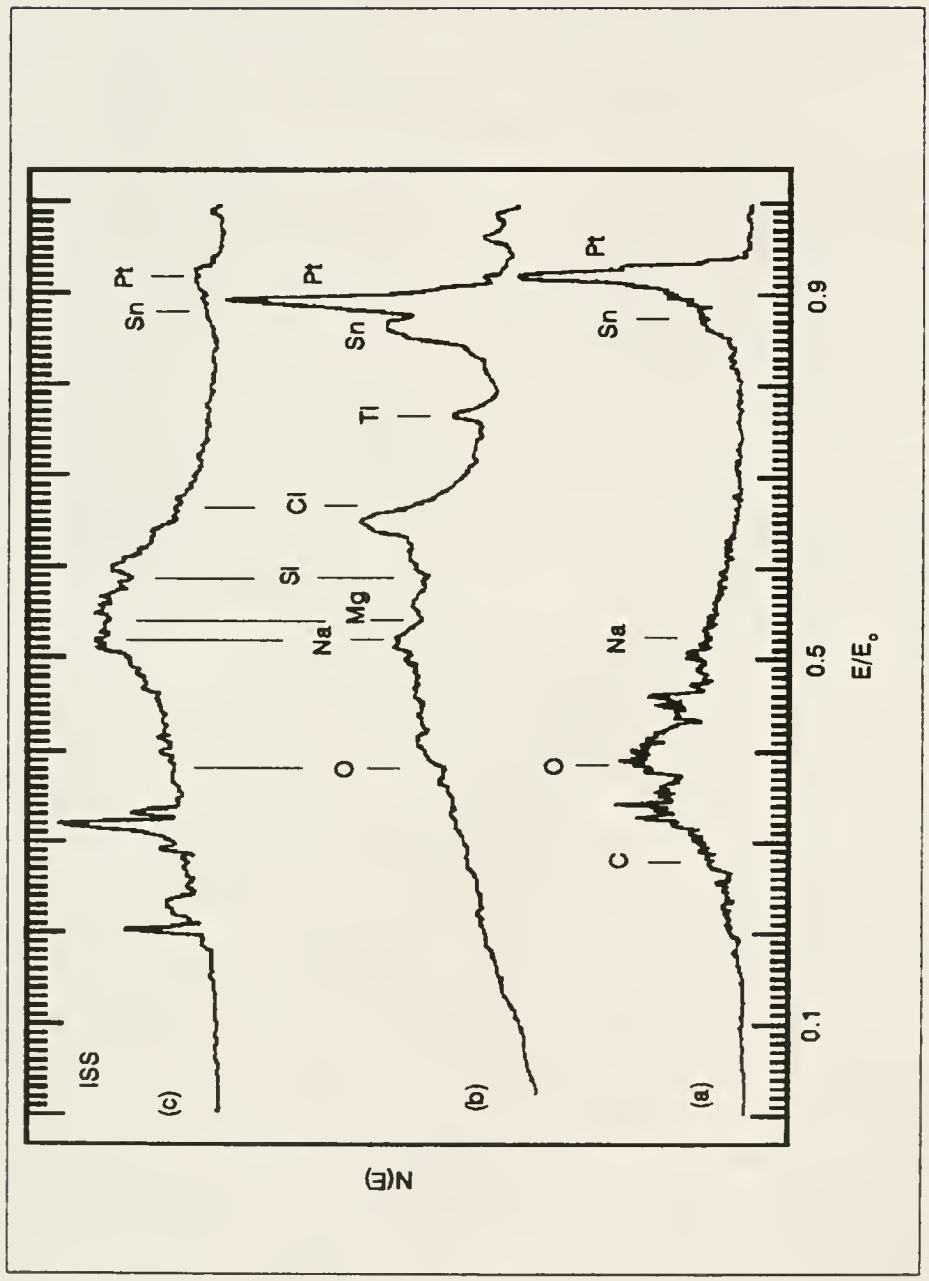

Figure 5-3. The ISS spectra taken (a) from the as-prepared sample, (b) after reduction at 125 °C and (c) after reduction at 250 °C.

has become more prominent and well defined in size with respect to the Pt. As shown in Chapter 1, this behavior is characteristic of Pt/Sn alloy formation. A few peaks due to migration of substrate impurities such as Na and Mg also appear after the reduction as does a Ti peak from the sample holder. After reduction at 250 °C the Sn and Pt peaks are greatly reduced in size due to coverage by contaminants (primarily Na and Mg) in the silica which migrate to the surface during reduction. Due to the stability of silica at these fairly low reduction temperatures, silica-containing species most likely do not migrate over the Pt and Sn. Since ISS is essentially sensitive to the outermost layer of surface atoms, the data in Figure 5-3 suggest that the 250 °C reduction results in physical coverage (encapsulation) of most of the surface Pt and Sn. This encapsulation hypothesis is confirmed by ISS data taken after the reduced surface was lightly sputtered. As shown in Figure 5-4, the sputtering process uncovered significant amounts of underlying Pt and Sn. Although peak energy shifts and surface charging features appear in these spectra, the peaks which correspond to Pt and Sn remain prominent and meaningful.

The data presented thus far suggest that reduction at both 125 and 250 °C promotes movement of O, Sn and subsurface impurities contained in the silica. The O

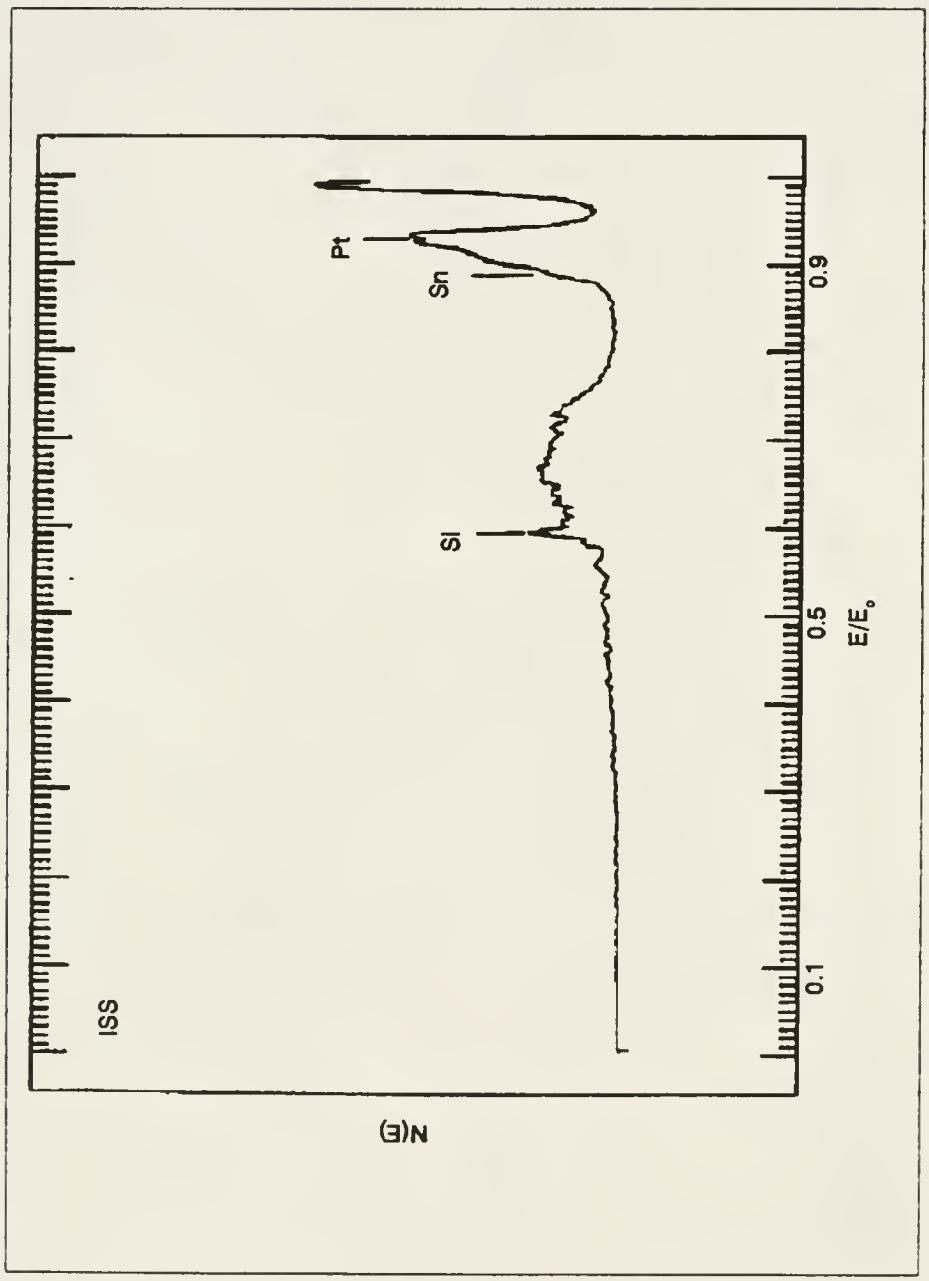

Figure 5-4. The ISS spectrum taken after reduction at 250 °C (Figure 5-3c) and subsequent sputtering with 2-keV $^4He^+$ ions for 5 minutes using a primary beam current of 10 μA over a 1-cm^2 area.

concentration in the near-surface region is probably determined by the rates of several mechanisms. One is migration of subsurface O to the near-surface region during the reduction at elevated temperature under the chemical potential produced by the presence of the reducing gas. Another is loss of surface O through reaction with the reducing gas and subsequent desorption as CO_2. As stated above, O loss may also occur through OH^- combination followed by desorption of H_2O. At 125 °C the rate of migration of subsurface O to the surface apparently is greater than the rate of O loss by reaction to form CO_2 and H_2O, which results in an increase in the near-surface O concentration as observed in the XPS data. Similar observations have been made during the reduction of a TiO_2(001) surface [84]. However, at 250 °C the rate of O loss through reaction is greater than the rate of O migration to the surface, resulting in a decrease in the O concentration in the near-surface region.

As shown in Figure 5-5, the Pt 4f XPS spectra exhibit broad features suggesting that multiple Pt oxidation states are present both before and after reduction. According to a standard reference [80] and previous studies from this laboratory [32,89], Figure 5-5(a) indicates that a mixture of primarily PtO_2 and PtO with smaller amounts of $Pt(OH)_2$ and metallic Pt is present on the air-exposed surfaces.

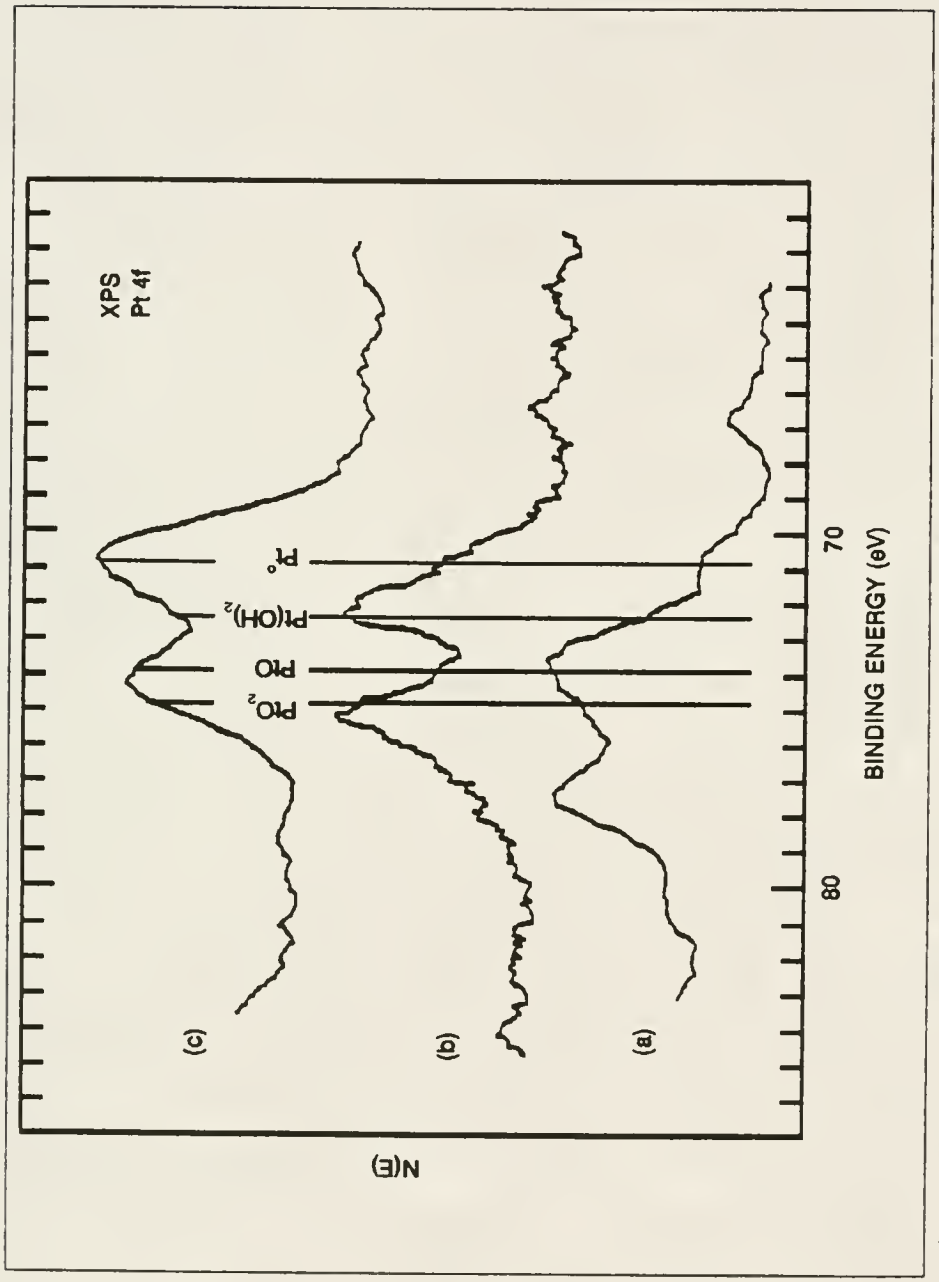

Figure 5-5. The Pt 4f XPS spectra taken (a) from the as-prepared, silica-supported Pt/SnO_x surface, (b) after CO reduction at 125 °C and (c) after CO reduction at 250 °C.

After reduction, peak positions shift toward lower binding energies as the surface Pt species are partially reduced. After reduction at 125 °C the predominant species present is $Pt(OH)_2$ with an increased amount of metallic Pt. However, only very small amounts of PtO and PtO_2 remain after the 125 °C reduction. The extent of reduction is much greater after the 250 °C reduction. The Pt is primarily in metallic form with a relatively small amount of $Pt(OH)_2$. Little or no PtO or PtO_2 is present. There has been some debate concerning the stability of PtO, but its existence is well substantiated in numerous studies [32,80,89-94].

Tin can be present in several forms which include SnO_2, SnO, Sn hydroxides, Sn suboxides, Sn-O-Pt species [32,89], metallic Sn and Sn alloyed with Pt. Using XPS, it is not difficult to distinguish between metallic Sn and Sn oxides because their Sn 3d binding energies differ by about 1.8 eV, and Asbury and Hoflund have observed XPS features due to suboxides [60]. However, it is difficult to distinguish between SnO_2 and SnO using XPS, but this can be done using valence-band XPS [50,95] or electron energy-loss spectroscopy (ELS) [56,96]. Paparazzo and co-workers [97] claim that there is a 0.18 eV difference in the Sn 3d binding energies of SnO and SnO_2. Valence-band XPS [50,95] and electron-stimulated desorption (ESD) [50] can be used to

identify Sn hydroxides. These species also yield a high-binding-energy shoulder on the O 1s XPS peak [50,81], but no studies have reported any influence on the Sn 3d XPS peaks. Studies of Pt/Sn alloys [55,58] suggest that the Sn 3d XPS alloy features differ from those of metallic Sn, but a systematic study of Sn 3d shifts due to alloying has not been reported.

The Sn 3d XPS spectrum taken before reduction is shown in Figure 5-6(a), and spectra taken after reduction in CO at 125 and 250 °C are shown in Figures 5-6(b) and 5-6(c), respectively. Small changes in the Sn 3d peak shapes occur during annealing in CO. Since a large number of Sn species may be present and their contributions to the Sn 3d XPS features are not well understood, it is only possible to analyze these peaks in a qualitative manner. Before reduction, the Sn 3d XPS peaks are due predominantly to SnO_2. However, they are not symmetrical, and the symmetry on the low-binding-energy side indicates that some of the Sn on the as-prepared catalyst may be present as suboxides and SnO and possibly as metal. The Sn 3d peaks become slightly wider with increasing reduction temperature as indicated in Figure 5-6. Based on the data of Paparazzo and co-workers [97], this is probably due to partial conversion of SnO_2 to SnO. After reduction at 250 °C it appears that the low-binding-energy shoulder near the baseline increases

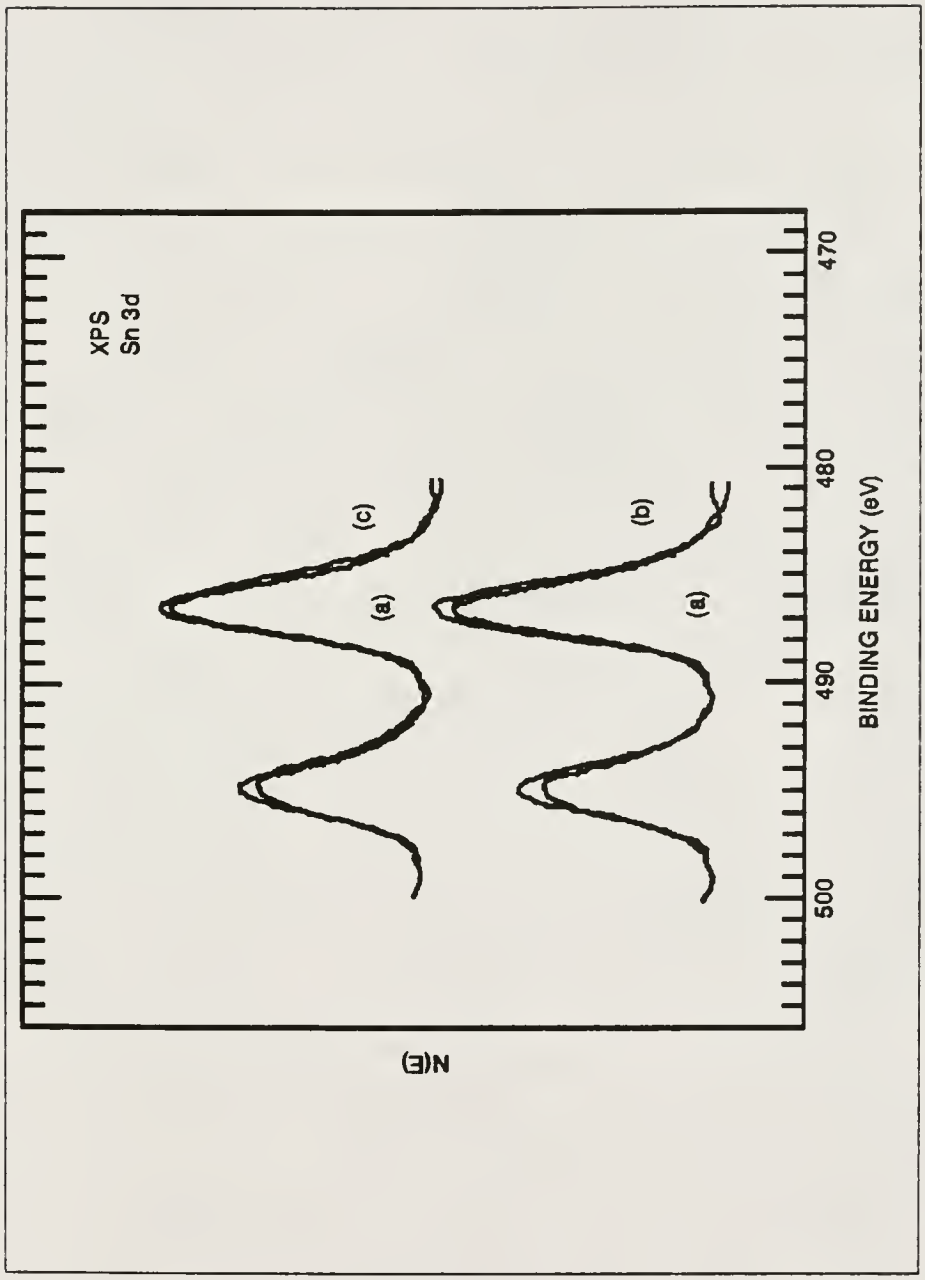

Figure 5-6. The Sn 3d XPS spectra taken from the silica-supported Pt/SnO_x surface (a) before and (b) after CO reduction at 125 °C and (c) after CO reduction at 250 °C.

as well suggesting that some of the Sn oxides are reduced to metallic Sn. Metallic Sn probably forms during reduction at 125 °C, but the amount is so small that it is not detected by XPS. Recall that similar changes in the Sn 3d peak shape were observed during reduction of platinized tin oxide surfaces in Chapters 1 and 3. Some, but probably not all, of the metallic Sn formed alloys with Pt. Paffett and Windham [55] have found that Pt/Sn alloy formation occurs at temperatures as low as 175 °C in their study of Sn deposited on Pt(111). Recently, tin oxide films (no Pt) have been reduced in CO under conditions similar to those used in this study [98]. The XPS data indicate that metallic Sn does not form in this case. Thus, it appears that Pt promotes the formation of metallic Sn during reduction in CO. The XPS data in Figure 5-6 also indicate that the extent of reduction is greater at 250 °C than at 125 °C.

It is interesting to relate the results of this characterization study with those obtained from the commercial Pt/SnO_x catalyst (not supported on silica) investigated in Chapter 4. Both catalysts require a reductive pretreatment for optimization of catalytic performance, but increasing the reduction temperature affects the two catalysts differently. The silica-supported catalyst examined in this study yields an optimum CO oxidation activity after a 125 °C pretreatment. The commercial Pt/SnO_x

catalyst exhibits the same activity over a broad range of pretreatment temperatures (125 to 225 °C) [26]. The XPS data in this study and the characterization study in Chapter 4 agree that Pt is present predominantly as hydroxides after a pretreatment which yields high activity. This fact is consistent with the observation that the catalytic activity of the commercial Pt/SnO_x catalyst is enhanced by the presence of water vapor in the reaction gas mixture [26]. Another similarity is that the data obtained from both catalysts indicate that a Pt/Sn alloy forms during reduction. This fact apparently explains why Pt supported on tin oxide is greatly superior as a catalyst for CO oxidation at low temperatures compared to Pt supported on alumina or other nonreducible oxides.

Another factor relating to catalytic activity which must be considered is encapsulation of the active Pt and Sn species. This process does not occur when reducing the commercial Pt/SnO_x catalyst at temperatures up to 175 °C. The impurities in the silica-supported Pt/SnO_x catalyst which cover the Pt and Sn species during the 250 °C reduction may be responsible for the loss in catalytic activity since the encapsulation does not occur during the 125 °C reduction after which the catalytic activity remains high.

The catalyst surface produced during the reduction step is not the same surface responsible for the long-term

catalytic behavior. Significant changes occur at the catalyst surface during the initial reaction period. Based on activity data [26], transient behavior may occur for hours after which time the activity goes through a maximum and then slowly decays. The changing activity must correlate with changes in composition and chemical states of species at the surface, but this relationship has not been determined yet.

Summary

The changes induced at an optimized, silica-supported platinized tin oxide surface by annealing at 125 and 250 °C in 10 Torr of CO for 2 hours have been determined using ISS and XPS. The reduction at 125 °C results in enrichment of the near-surface region in O, reduction of Pt oxides with the formation of Pt hydroxide, and the reduction of SnO_2 to SnO and metallic Sn which mostly alloys with Pt. Different results are obtained from the surface reduced at 250 °C in that the extent of the Sn oxide reduction is greater, the predominant form of the Pt is metallic, impurities in the silica migrate over the active Pt and Sn species, and the O content of the near-surface region is reduced. The differences found after reduction at the two temperatures may explain the fact that a 125 °C pretreatment results in a surface which is active for CO oxidation at low temperature

whereas a 250 °C pretreatment results in a catalytically inactive surface.

CHAPTER 6
CATALYTIC BEHAVIOR OF NOBLE METAL/REDUCIBLE OXIDE MATERIALS FOR LOW-TEMPERATURE CO OXIDATION: COMPARISON OF CATALYST PERFORMANCE

Introduction

The catalytic oxidation of CO near ambient temperatures has many important applications. As described previously, closed-cycle CO_2 lasers produce CO and O_2 in the laser discharge resulting in a rapid loss of output power. This problem can be overcome by incorporating a low-temperature CO oxidation catalyst into the laser system which converts the dissociated products back into CO_2 [7,8,22,23]. Also, air purification devices often contain catalysts to oxidize dangerous levels of toxic CO [17,99-101]. Such devices are utilized in fire safety equipment and in underground mines as respiratory aids.

Consequently, the development of low-temperature CO oxidation catalysts has received considerable attention [7-17]. Although significant progress has been made with regard to understanding the reaction mechanism, there remains a need for the development of catalysts which exhibit higher activities for prolonged periods at low temperatures (typically less than 100 °C) and in the diverse

range of oxidation environments which are encountered. Factors which determine oxygen availability and gaseous impurities often have a pronounced effect on catalyst performance. CO oxidation in ambient air has the advantages of excess O_2 and low CO_2 concentrations which facilitate the reaction considerably. Consequently, numerous materials are known to oxidize CO in excess O_2 at low temperatures [9-11,13,14], but complications due to the presence of humidity and/or air pollutants are often detrimental to their activity. In CO_2 lasers, CO and O_2 are present in small stoichiometric quantities in a large amount of CO_2. Although the catalytic reaction benefits from the fact that the lasers usually operate at temperatures somewhat above ambient (25-100 °C), catalytic CO oxidation is difficult under these conditions.

Recently, Haruta and co-workers [15,16] prepared supported-gold catalysts on various base-metal oxides including MnO_x, Fe_2O_3, Co_3O_4, NiO and CuO and determined their catalytic activities toward the oxidation of H_2 and/or CO. Most of the CO oxidation tests were performed using 1 vol% CO in dry air. At 0 °C, Au/Fe_2O_3 and Au/NiO maintain essentially 100% CO conversion under the flow conditions used over a 7-day test period. Similar performance was also observed for Au/Fe_2O_3 and Au/Co_3O_4 at 30 °C in 76% relative humidity. Therefore, these catalysts appear to be

quite useful in air purification devices, but activities in the presence of air contaminants were not determined. These catalysts may be useful in CO_2 lasers even though the reaction conditions are quite different as described above. It is interesting to note that Haruta and co-workers [15,16] apparently did not examine the behavior of Au/MnO_x toward CO oxidation.

Catalysts consisting of Pt and/or Pd supported on tin oxide have been researched extensively for use in CO_2 lasers [7,8,22-26]. Although these materials can exhibit considerable CO oxidation activity in this application, there are complications which must be overcome. Acceptable activity is observed only after the catalyst undergoes a reductive pretreatment. Unfortunately, such pretreatments may lead to considerable induction periods often lasting several days during which the observed activity declines before reaching a maximum [26]. Even after acceptable activity is recovered these materials exhibit a steady decay in performance over time.

The purpose of the present study is to explore the behavior of materials other than platinized tin oxide as catalysts for low-temperature CO oxidation, particularly with regard to CO_2 laser applications. Several materials were synthesized and screened for CO oxidation activity using small concentrations of stoichiometric CO and O_2 in

He and temperatures between 30 and 75 °C. The tests were run for periods as long as 18000 minutes in order to observe the induction and decay characteristics of the catalysts.

Catalysts Preparation

A review of the literature provided a basis for selection of support materials examined in this study which include iron oxide (Fe_2O_3), nonstoichiometric manganese oxides (MnO_x), and ceria (CeO_x) where x is between 1 and 2. The materials investigated were synthesized using established impregnation and coprecipitation techniques [102]. The samples prepared include MnO_x, Pt/MnO_x, Ag/MnO_x, Pd/MnO_x, Cu/MnO_x, Au/MnO_x, Ru/MnO_x, Au/CeO_x and Au/Fe_2O_3.

The MnO_x was used as-received from the Kerr-McGee Company, USA. It was prepared by the electrolytic oxidation of manganous sulfate and has BET surface area of 74 m^2/gram. The MnO_x served as a sample itself as well as an impregnation support for other materials.

Two Pt/MnO_x samples (0.2 wt% Pt) were prepared by impregnation of MnO_x using an aqueous solution of $Na_2Pt(OH)_6$. Sample #1 was dried in air at 280 °C for 4.5 hours whereas sample #2 was dried in air at 75 °C for 3 hours. A Pd/MnO_x catalyst (0.2 wt% Pd) was prepared by impregnating MnO_x with an aqueous solution of $PdCl_2$. The product was dried in air at 280 °C for 4.5 hours.

Two Ag/MnO_x samples were prepared, one containing 0.2 wt% Ag and another containing 1.0 wt% Ag. Impregnation of MnO_x with Ag was accomplished using a solution prepared by dissolving AgO in NH_4OH. The products were dried in air at 280 °C for 4.5 hours.

A sample which contained admixtures of CuO and MnO_x was prepared from the products of several procedures. Procedure A involved coprecipitation from aqueous solutions of $CuSO_4$ + sucrose and $KMnO_4$. The precipitate was washed with water and dried in air at 105 °C for 15 hours. The Cu:Mn molar ratio was approximately 1.4. In procedure B, a portion of the former product was dried in air at 280 °C for 2 hours. In procedure C, MnO_x was precipitated from aqueous solutions of sucrose and $KMnO_4$. The precipitate was washed and dried as outlined in procedure A. The final product consisted of an admixture of 0.4 grams from procedure A, 0.7 grams from procedure B, 0.3 grams from procedure C and 0.2 grams of commercial CuO powder.

A technique in which $Mn(OH)_2$ was precipitated in the presence of fine Ru powder was utilized to prepare a 2 wt% Ru/MnO_x sample. An aqueous solution of $Mn(NO_3)_2$ was added dropwise to a stirred mixture of Ru powder in NH_4OH. The resulting product was dried and calcined at 400 °C for 2 hours.

Three supported Au samples were synthesized via coprecipitation from aqueous $HAuCl_4$ and the nitrate of the corresponding support metal. The composition of the materials is approximately 5 at% Au/MnO_x, 20 at% Au/CeO_x and 5 at% Au/Fe_2O_3 on a Au/metal basis. In each case the appropriate precursor solutions were added dropwise to a stirred solution of Na_2CO_3 at room temperature. After washing with hot water (80 °C) and drying, the precipitates were calcined in air at 400 °C for 4 hours. Two Au/Fe_2O_3 samples were prepared which differed only in the temperature of the wash water utilized (25 °C and 80 °C).

Experimental

The reactor used to test the CO oxidation activity of the catalysts is located at NASA Langley Research Center in Hampton, VA, and has been described previously [27,103]. Screening of catalysts for CO oxidation has typically been performed using a test gas consisting of a few percent CO in air (excess O_2), and the catalytic behavior under stoichiometric CO and O_2 and in the presence of CO_2 has often not been determined. Since the catalytic behavior can vary considerably under different environments as described above, it is necessary to perform such experiments. All tests were conducted using 0.15 grams of catalyst and a reaction gas mixture consisting of 1 vol% CO, 0.5 vol% O_2 and 2 vol% Ne in He at a total pressure of 1 atmosphere

flowing at 10 standard cm^3 per minute (sccm). The reaction temperatures investigated were 75, 50 and 30 °C as noted. The conversions are quite high under these conditions which corresponds to operating the reactor in an integral mode.

In most cases the catalysts were tested as prepared without additional pretreatments. Unless noted otherwise, each catalyst was loaded into the reactor and exposed to flowing He for about 1 hour as the reaction temperature stabilized. Then the He flow was changed to the reaction gas mixture and product sampling was begun. At predetermined time intervals, an automated sampling valve directed a small fraction of the reaction products to a gas chromatograph (GC) for analysis of $\%CO_2$ yield, %CO loss and $\%O_2$ loss, and the results were plotted versus time.

Results and Discussion

During these initial activity screening experiments, emphasis is placed upon characteristics of the overall CO oxidation activity curves with respect to temperature and time. An appropriate catalyst for use in CO_2 lasers must not only exhibit high activity at low temperatures (25-100 °C) but also maintain acceptable activity over a lifetime of up to 3 years [6]. Since a catalyst cannot be practically tested for a 3-year lifetime, its activity profile must be extrapolated with reasonable confidence. Nevertheless, it is necessary to exercise caution when

evaluating potential catalysts for CO_2 lasers because a catalyst which exhibits the best activity initially might succumb to decay mechanisms which render it inferior after extended use. Consequently, a catalyst exhibiting only marginal activity initially may become the optimal choice if the corresponding activity decay remains negligible.

Carbon monoxide oxidation activity curves for several MnO_x-based catalysts appear in Figure 6-1. Initially, MnO_x and Cu/MnO_x exhibit the highest CO oxidation activities although their performance rapidly deteriorates. However, after about 2000 minutes the reaction curve for Cu/MnO_x appears to approach a steady-state conversion with negligible activity decay. The MnO_x sample may approach a more active steady-state conversion but more extensive testing is required to be certain. Even though the Pt/MnO_x #1 and Ag/MnO_x samples display superior activity throughout most of the test period, extrapolation of the data in Figure 6-1 indicates that Cu/MnO_x may be the optimal catalyst in a long-term test.

The data in Figure 6-1 also depict an interesting comparison between the catalytic activities of Pt/MnO_x #1 (dried for 4.5 hours at 280 °C) and Pt/MnO_x #2 (dried for 3 hours at 75 °C). The poor activity exhibited by Pt/MnO_x #2 may be the result of incomplete removal of surface impurities (such as Na, Cl or OH^-) associated with

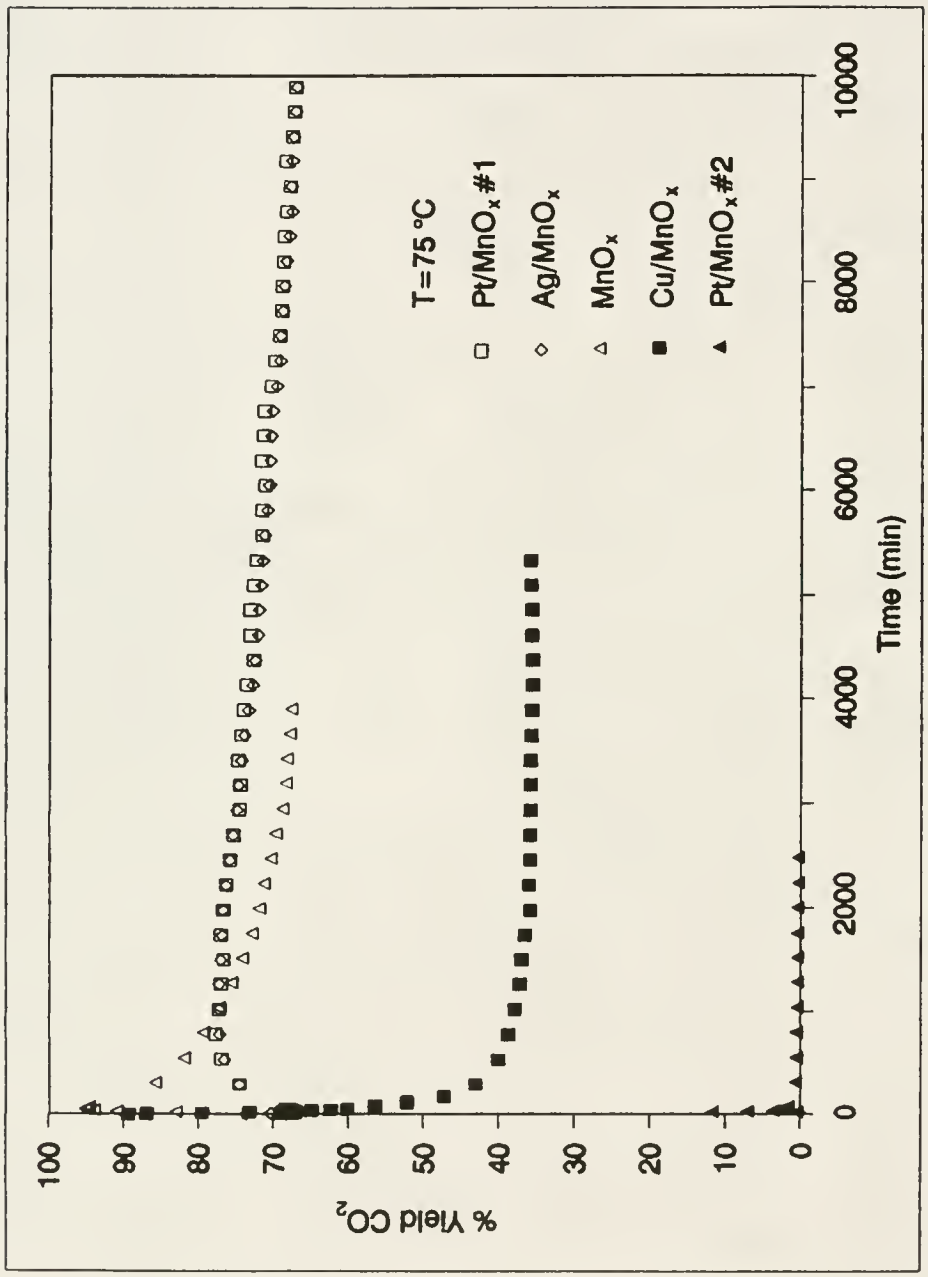

Figure 6-1. The CO oxidation activity of 0.2 wt% Pt/MnO_x #1, 0.2 wt% Ag/MnO_x, MnO_x, 60 at% Cu/MnO_x and 0.2 wt% Pt/MnO_x #2 at 75 °C as a function of time.

the impregnation step. However, as found in previous studies of MnO_2 and MnO_2-CuO catalysts [104-106], the inactivity is most likely the result of incomplete surface activation. Many MnO_x-based catalysts usually require heating between 100-200 °C in air or O_2 to produce an active surface. The heat treatments apparently activate the surface through the creation of reactive sites via partial surface reduction, depletion of adsorbed water or surface hydroxyl groups, and/or concurrent micropore generation.

An interesting observation is that the reaction profiles of Pt/MnO_x #1 and Ag/MnO_x are remarkably similar. This is unexpected based on the different catalytic properties of Pt and Ag. It is possible that this behavior results primarily from exposure of MnO_x to similar basic solutions followed by drying in air at 280 °C for 4.5 hours. The activity curve for pure MnO_x (as-received and common to both samples) is quite different in character, which is consistent with this hypothesis. Nevertheless, both materials performed well during the 10000-minute test period oxidizing 70-80% of available CO at 75 °C.

As mentioned above, Pt/SnO_x catalysts have received considerable attention for use in CO_2 lasers. A comparison of CO oxidation performance between Pt/MnO_x #1 (see Figure 6-1) and a commercial Pt/SnO_x catalyst manufactured by Engelhard Industries (see Chapter 4) is shown in Figure

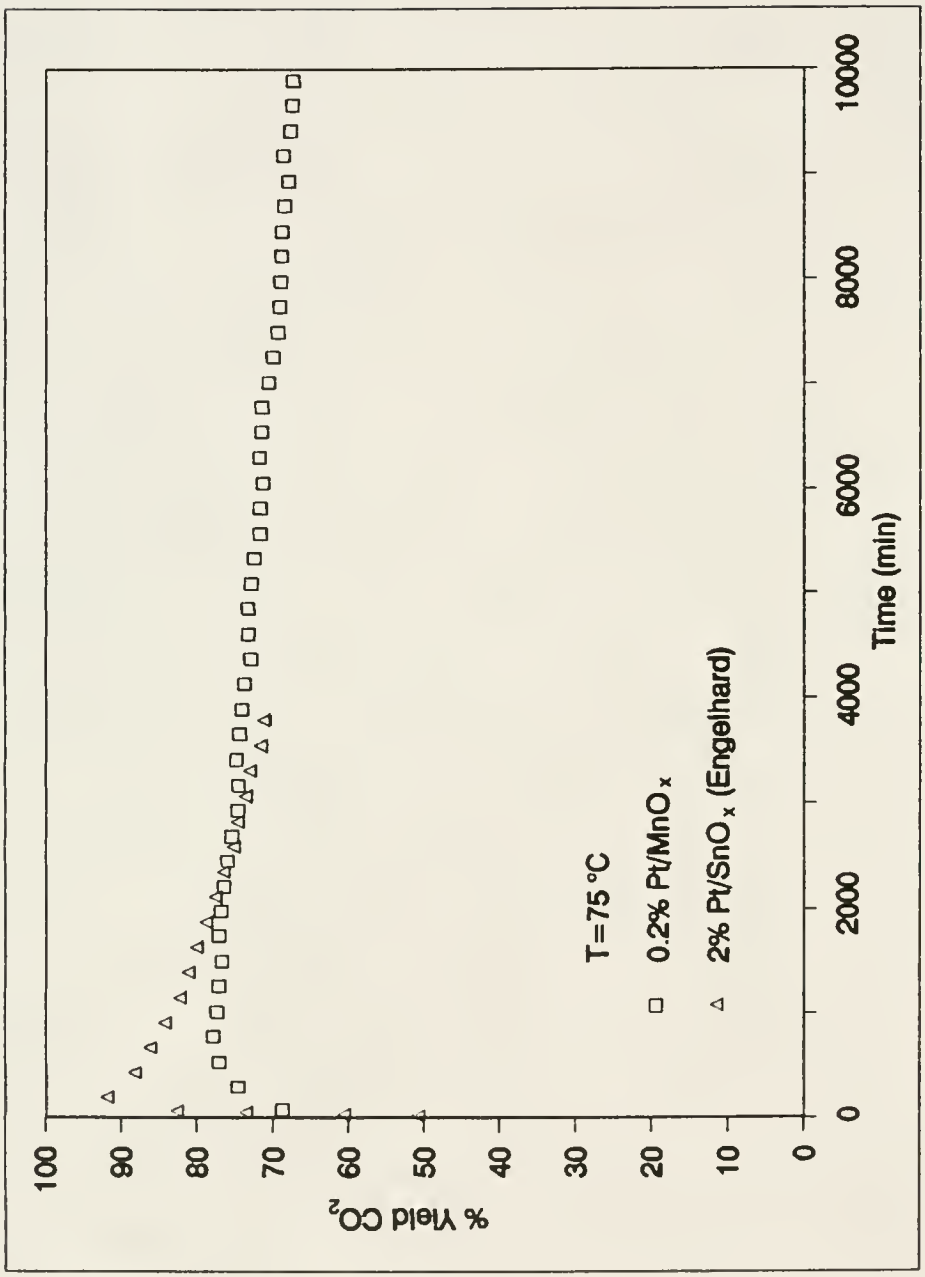

Figure 6-2. Comparison of CO oxidation activity between 0.2 wt% Pt/MnO_x #1 and a commercial Pt/SnO_x catalyst at 75 °C.

6-2. At 75 °C, the Pt/MnO_x #1 sample exhibits superior activity after approximately 2500 minutes of reaction. Due to the limited reaction data for the Pt/SnO_x sample, further comparisons require data extrapolation. Assuming that the indicated trends continue, Pt/MnO_x #1 represents the optimal catalyst over an extended time period. This also is true for Ag/MnO_x which behaves identically to Pt/MnO_x #1.

Figure 6-2 represents a valid comparison because the sample size and experimental parameters used were identical in both tests. It should be noted, however, that the Pt/SnO_x was pretreated in a 5% CO/He stream at 225 °C for 1 hour prior to activity testing. As discussed in previous chapters of this research, such reductive pretreatments significantly enhance the performance of Pt/SnO_x catalysts [26]. The fact that no pretreatments were used for the MnO_x-based catalysts is an advantage. Furthermore, since the precious metal loading for the Pt/MnO_x #1 and Ag/MnO_x samples is only 0.2 wt% (compared with 2 wt% for the Pt/SnO_x catalyst), there also appears to be an economic advantage over the Engelhard Pt/SnO_x catalyst. Of course, the Ag/MnO_x catalyst is the least costly.

The fact that reductive pretreatments activate Pt/SnO_x catalysts provided motivation to investigate the effects of similar pretreatments on Pt/MnO_x catalysts. Two

pretreatment conditions were used in which the Pt/MnO_x #1 sample was exposed to 5% CO/He for 1 hour at 125 and 225 °C. The effects on catalytic performance are shown in Figure 6-3. It is clear that the pretreatments are detrimental to the CO oxidation activity of Pt/MnO_x. In fact, the observed activity of Pt/MnO_x decreases with increasing pretreatment temperature, a trend opposite to that which is observed for Pt/SnO_x catalysts [26]. A possible explanation may involve the reducibility of the MnO_x and SnO_x supports. It appears that catalysts based on these materials require a certain degree of surface reduction for optimal activity. There is evidence that a completely dehydroxylated or an entirely oxygenated MnO_x surface is not active toward low-temperature CO oxidation [104,105]. Similarly, surface hydroxyl groups are believed to be instrumental in the CO oxidation mechanism over Pt/SnO_x [26]. Given the relative instability of MnO_x with respect to SnO_x, such an optimum degree of surface reduction most likely results from milder pretreatments than those used to generate the data shown in Figure 6-3. In fact, heat treatments in air or O_2 appear to be more beneficial for MnO_x CO oxidation catalysts [12,104,105,107,108]. Although the CO reductive pretreatments at 125 and 225 °C are appropriate for Pt/SnO_x, they apparently are too severe for Pt/MnO_x.

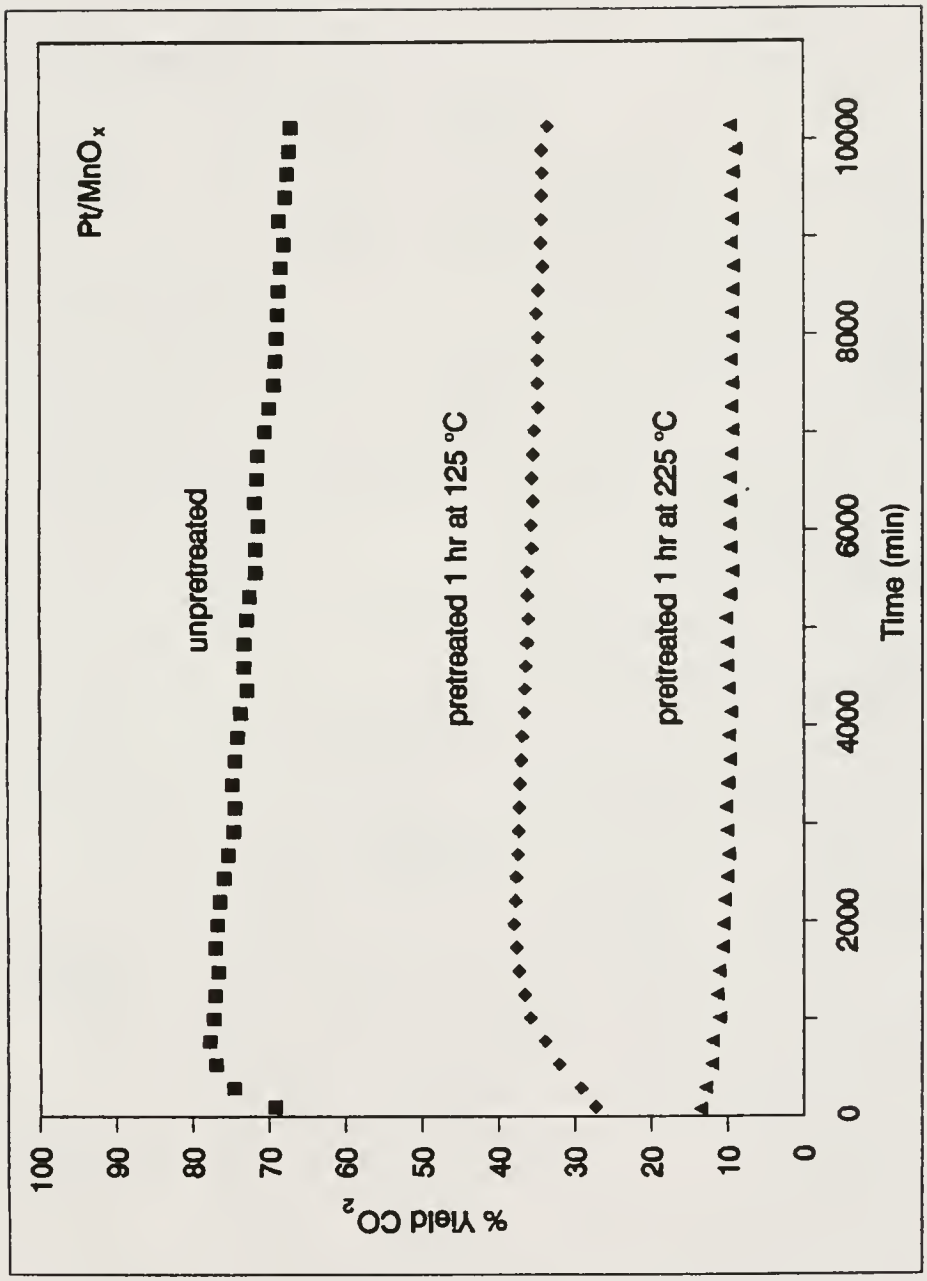

Figure 6-3. The CO oxidation activity of 0.2 wt% Pt/MnO_x #1 at 75 °C as a function of pretreatment in 5 vol% CO/He at 125 and 225 °C.

Additional insight on the pretreatment effects may be gained by considering the initial reaction characteristics with regard to CO_2 production, CO consumption and O_2 consumption (determined by GC analysis). These data are shown in Figures 6-4, 6-5 and 6-6 for Pt/MnO_x catalysts which were not pretreated, pretreated at 125 °C and pretreated at 225 °C, respectively. For unpretreated Pt/MnO_x #1, Figure 6-4 shows that a considerable amount of catalyst surface O_2 is utilized in CO_2 formation during the early stages of reaction because the O_2 loss is much lower than the CO_2 production. The participation of catalyst O_2 during CO oxidation has been observed for MnO_x catalysts previously [11,12,19,108]. After a 125 °C pretreatment, the catalyst activity is decreased, and this decrease is accompanied by a decrease in the utilization of catalyst O_2 as shown in Figure 6-5. Since the curves now nearly coincide, the early stages of CO oxidation on this pretreated surface appear catalytic in nature with only gas-phase O_2 being utilized. The data of Figure 6-6 obtained after pretreating in CO at 225 °C indicate essentially opposite behavior to that shown in Figure 6-4. That is, the surface appears to have been reduced to a point where gas-phase O_2 is utilized not only in CO_2 formation but in catalyst regeneration as well. Even though the catalyst surface acquires O_2 from the gas phase, this fresh surface O_2 does not appear to participate

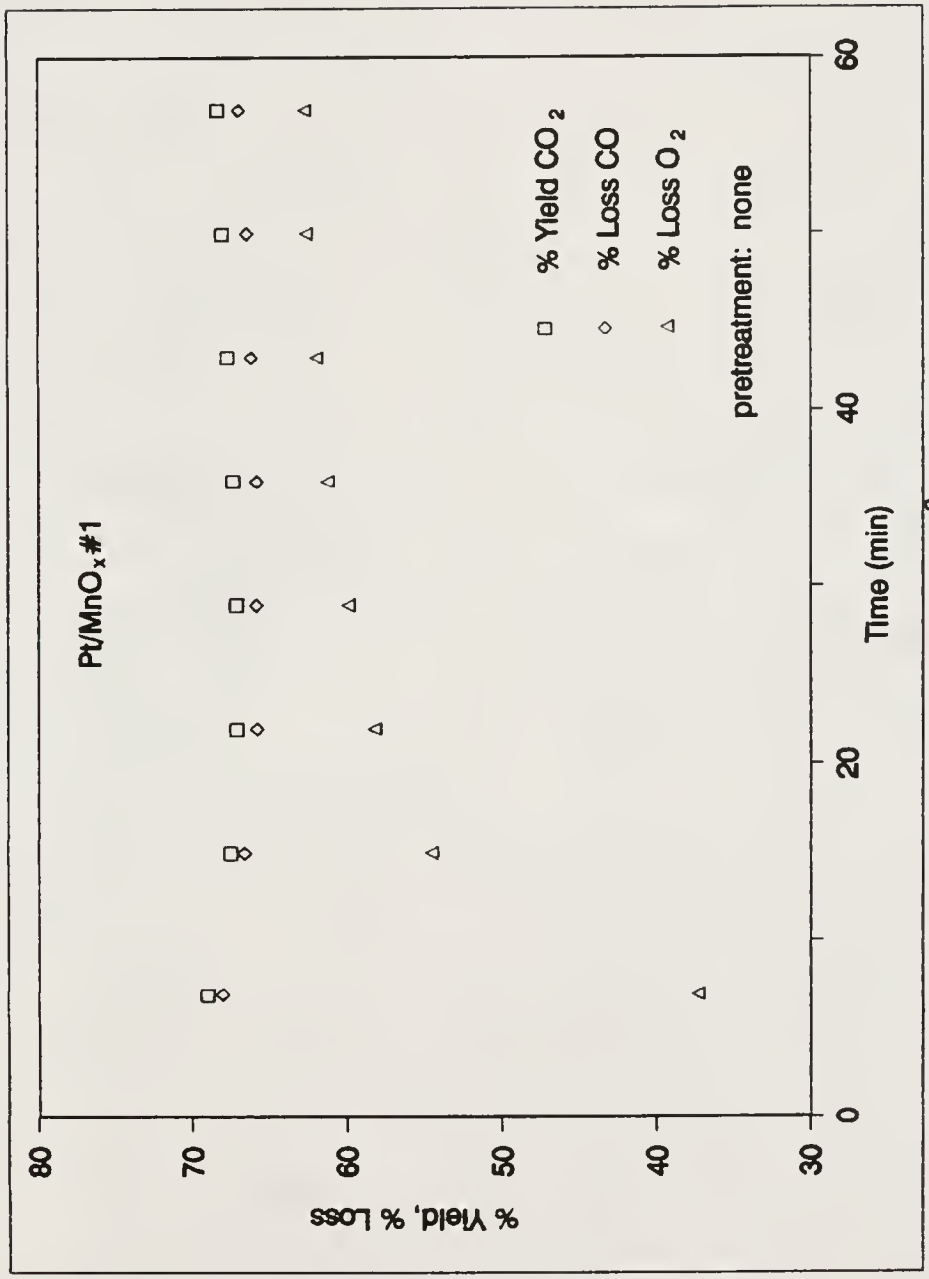

Figure 6-4. The % CO_2 yield at 75 °C with corresponding % loss CO and O_2 for unpretreated 0.2 wt% Pt/MnO_x #1.

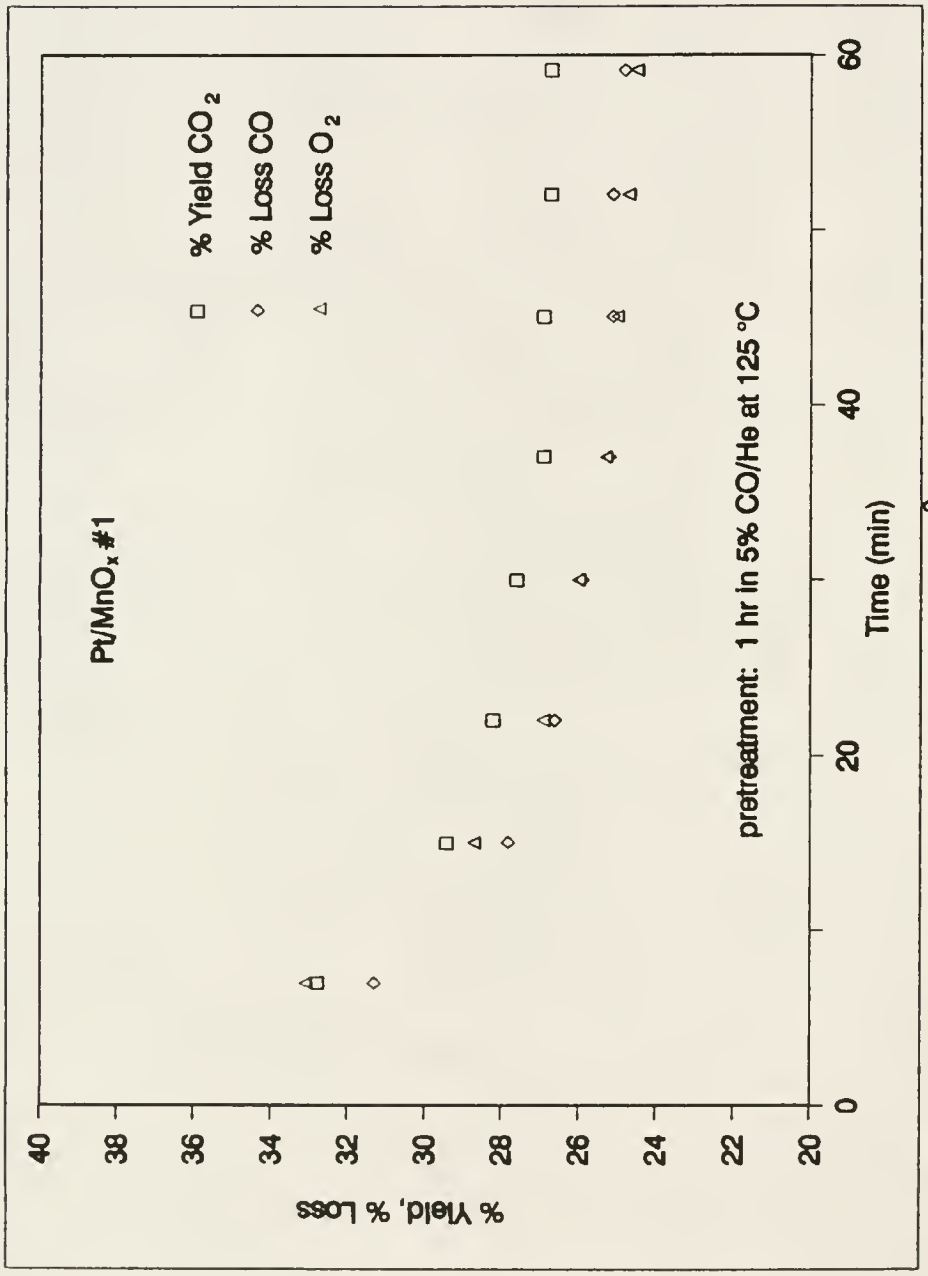

Figure 6-5. The % CO_2 yield at 75 °C with corresponding % loss CO and O_2 for 0.2 wt% Pt/MnO_x #1 pretreated in 5 vol% CO/He for 1 hour at 125 °C.

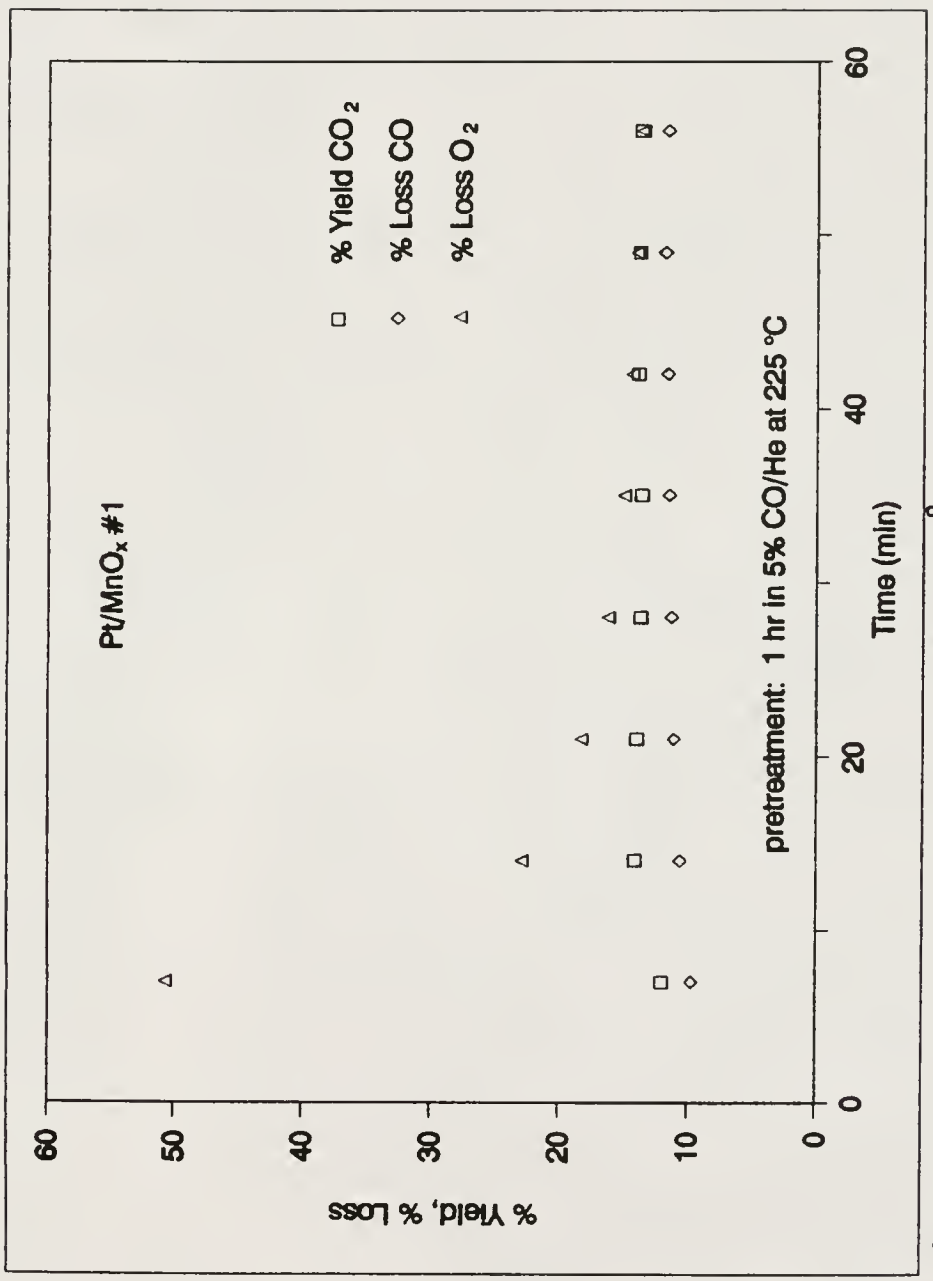

Figure 6-6. The % CO_2 yield at 75 °C with corresponding % loss CO and O_2 for 0.2 wt% Pt/MnO_x #1 pretreated in 5 vol% CO/He for 1 hour at 225 °C.

in the reaction or restore the catalytic activity which was lost during the pretreatment.

A consistent interpretation of the data in Figures 6-4 through 6-6 may be realized by invoking a REDOX (reduction-oxidation) mechanism for CO oxidation. The active surface in Figure 6-4 appears to reach a situation wherein both surface and gas-phase O_2 participate in the reaction. The active surface is partially reduced after the first 30 minutes of reaction, and the extent of reduction depends upon the relative rates of surface reduction by CO and reoxidation by gas-phase O_2. During the CO pretreatments, the surface can be reduced to such an extent that catalyst O_2 is not available for reaction. Therefore, the resulting surfaces are not as active toward CO oxidation. These data suggest that it might be possible to determine optimal pretreatment conditions and that these optimal conditions would be less severe than the ones used in this study. The exact form(s) of the active surface oxygen species remains to be determined.

Figure 6-7 shows the CO oxidation performance of Au/CeO_x, Au/Fe_2O_3 #1 and Au/Fe_2O_3 #2 at 75, 50 and 30 °C. Several important features appear in these activity curves. The Au/CeO_x exhibits very high activity at 75 °C oxidizing greater than 80% of the available CO. Also, the reaction profile exhibits negligible decay over 10000 minutes. This

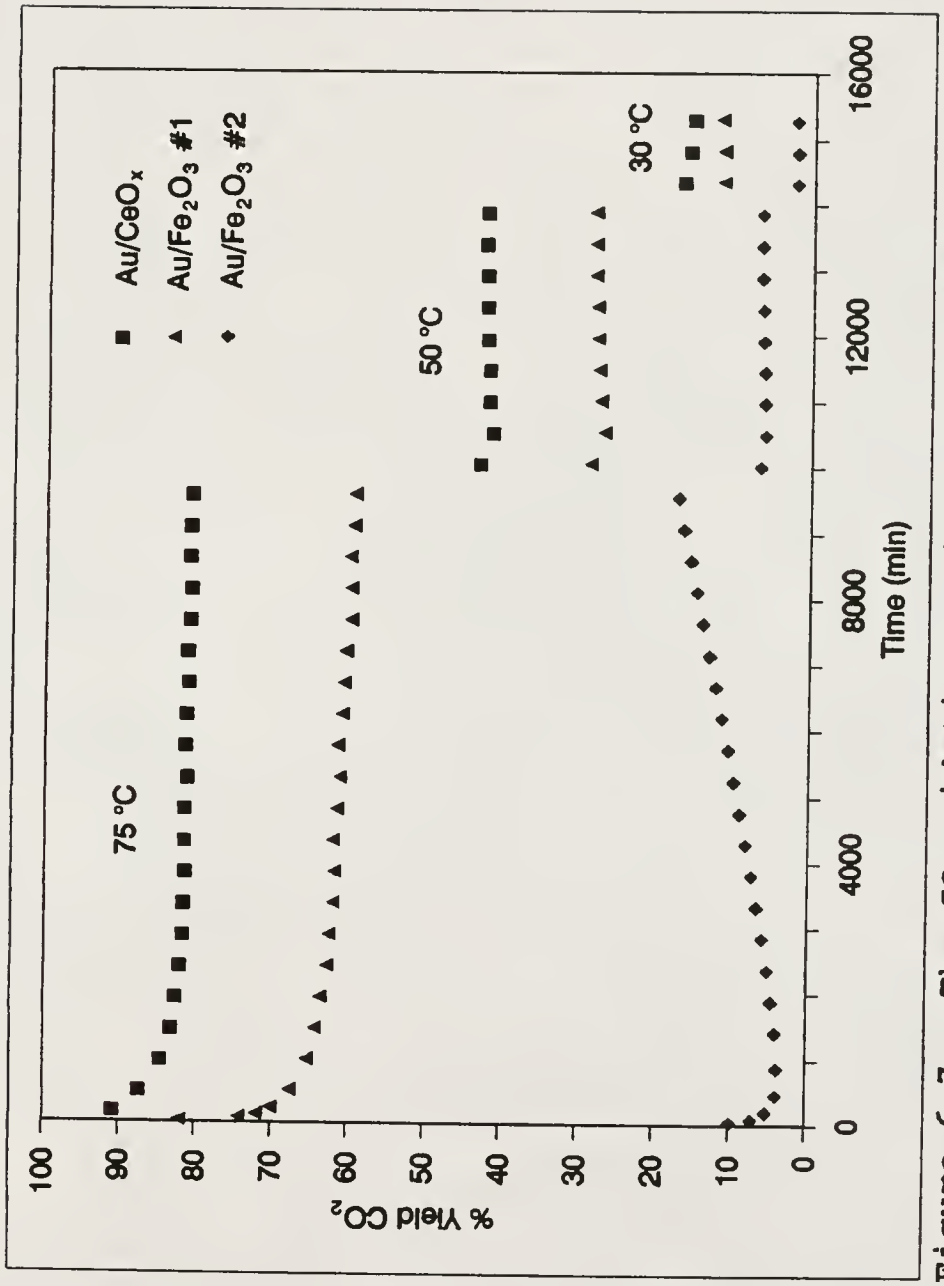

Figure 6-7. The CO oxidation activity of 20 at% Au/CeO_x, 5 at% Au/Fe_2O_3 #1 and 5 at% Au/Fe_2O_3 #2 at 75, 50 and 30 °C as a function of time.

represents a significant improvement over the performance of Pt/MnO_x #1 and Ag/MnO_x shown in Figure 6-1. At 50 °C, Au/CeO_x continues to perform well maintaining a CO_2 yield near 43%.

Figure 6-7 also provides an interesting comparison between Au/Fe_2O_3 #1 (washed with hot water) and Au/Fe_2O_3 #2 (washed with cold water). The activity of Au/Fe_2O_3 #1 is clearly superior although some decay in performance is evident. Surface Cl is generally believed to inhibit low-temperature CO oxidation [28]. Therefore, the difference in activity of the two samples may be attributable to poisoning by surface Cl (originating from the gold precursor $HAuCl_4$) which is not as effectively removed by washing with cold water compared to hot water. Nevertheless, it is interesting to note that the activity of Au/Fe_2O_3 #2 steadily increases with time (negative or inverse decay). This behavior may be a consequence of some surface process which removes the surface Cl as the reaction proceeds.

It is interesting to compare the performance of Au/Fe_2O_3 #1 with that of a Au/Fe_2O_3 catalyst investigated by Haruta and co-workers [15,16]. They observed that Au/Fe_2O_3 is essentially 100% efficient in oxidizing 1 vol% CO in air even below 0 °C. The lower activities found in this study apparently are due to the difficulties involved

in oxidizing CO in a stoichiometric mixture as described above.

Carbon monoxide oxidation activity curves for a second set of MnO_x-based materials appear in Figure 6-8. The data indicate that Au/MnO_x is clearly the most active catalyst examined in this study. At 75 °C, Au/MnO_x sustains nearly 100% CO_2 yield over a 10000-minute period, and excellent activity is also observed at 50 and 30 °C. At all temperatures the activity profiles are exceptional in that they exhibit negligible decay over the entire test period.

Figure 6-8 also shows the activity curves for two Ag/MnO_x samples (0.2 wt% Ag and 1.0 wt% Ag). As stated above, the two samples were prepared in a similar manner differing only in Ag content. The data indicate that small Ag loadings result in better catalytic behavior. Both reaction profiles are similar up to 1000 minutes of reaction after which the 1 wt% Ag/MnO_x sample exhibits accelerated decay in activity.

Although Pt/MnO_x and Ru/MnO_x are the least active catalysts according to the data in Figure 6-8, significant conversions are nevertheless observed. However, both of these materials and the others used in this study probably would be improved by optimizing preparation and pretreatment techniques.

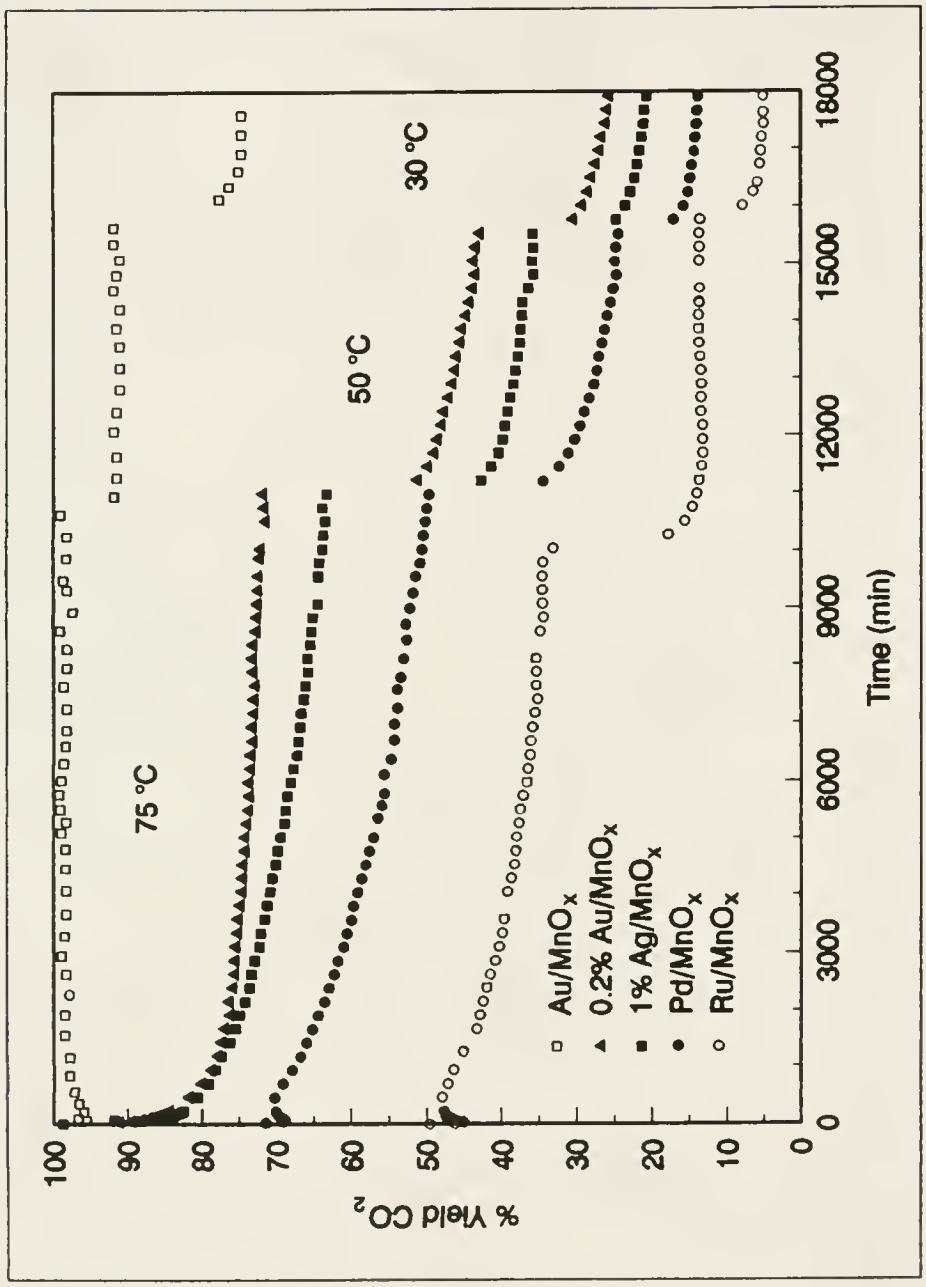

Figure 6-8. The CO oxidation activity of 5 at% Au/MnO_x, 0.2 wt% Pd/MnO_x, 2 wt% Ru/MnO_x, 0.2 wt% Ag/MnO_x and 1 wt% Ag/MnO_x at 75, 50 and 30 °C as a function of time.

Summary

Selected materials have been prepared and tested as low-temperature CO oxidation catalysts for long-term use in CO_2 lasers. These materials were prepared utilizing impregnation and coprecipitation techniques and include MnO_x, Pt/MnO_x, Ag/MnO_x, Pd/MnO_x, Cu/MnO_x, Ru/MnO_x, Au/MnO_x, Au/CeO_x and Au/Fe_2O_3. Each was tested for CO oxidation activity in low concentrations of stoichiometric CO and O_2 at temperatures between 30 and 75 °C. Although most of the materials exhibit significant CO oxidation activity, Au/MnO_x and Au/CeO_x are exceptionally active. At 75 °C, Au/MnO_x sustains nearly 100% CO_2 yield for 10000 minutes with no evidence of activity decay under the test conditions used. Exceptional activities are also observed at 50 and 30 °C. Many of the catalysts tested perform better than a platinized tin oxide catalyst either with regard to activity, decay characteristics or both. For example, Cu/MnO_x has a lower activity than several of the catalysts tested, but it shows negligible decay making it a potential candidate for long-term applications. A Pt/MnO_x catalyst and a Ag/MnO_x catalyst both exhibit similar and higher activities but decay more rapidly than Cu/MnO_x and less rapidly than the commercially available platinized tin oxide. Pretreatment in CO at 125 and 225 °C decreases the activity of Pt/MnO_x. Optimization studies of preparative

and pretreatment variables need to be performed in order to further increase the performance of low-temperature CO oxidation catalysts.

CHAPTER 7
COMPARISON OF THE PERFORMANCE CHARACTERISTICS OF Pt/SnO_x AND Au/MnO_x CATALYSTS FOR LOW-TEMPERATURE CO OXIDATION

Introduction

Long used as a research tool to study heterogeneous catalysis, the catalytic oxidation of CO is being utilized in an increasing number of practical applications. Carbon monoxide oxidation catalysts are often an integral component of pollution control devices designed to reduce industrial and automotive emissions. Air purification devices (for respiratory protection) [17,99-101] and CO gas sensors [85,101,109-112] commonly employ CO oxidation catalysis. Soon the catalytic oxidation of CO will be utilized in orbiting closed-cycle CO_2 lasers [5-8] used for weather monitoring or in other remote sensing applications. Sealed CO_2 lasers must incorporate a CO oxidation catalyst to recombine stoichiometric concentrations of CO and O_2 which are produced during the lasing process because both CO_2 loss and O_2 build-up can degrade the performance of the laser.

Therefore, there is a growing demand for CO oxidation catalysts which are more effective and versatile. Research directed toward the development of long-life, sealed CO_2

lasers [7-8] has produced several new materials which actively catalyze CO oxidation near ambient temperatures. In 1983 Stark and co-workers [23] identified platinized tin oxide (Pt/SnO_x) as a good catalyst for this application. However, the data given in the previous chapter indicate that gold supported on manganese oxide (Au/MnO_x) may perform even better than Pt/SnO_x. The purpose of this study is to compare the long-term CO oxidation performance of several Pt/SnO_x and Au/MnO_x catalysts and evaluate their potential utility in the former applications.

Experimental

Details regarding sample preparation and the CO oxidation reactor have been described elsewhere [27,103] and in the previous chapters of this research. The samples prepared for this study include 19.5 wt% Pt/SnO_x (15.8 at% Pt based on Pt and Sn content), 14.5 wt% $Pt/SnO_x/SiO_2$ (11.4 at% Pt based on Pt and Sn content) and 10 at% Au/MnO_x (based on Au and Mn content). The SnO_x support was prepared by dissolving Sn powder in nitric acid and heating to dryness at 150 °C. For the sample containing SiO_2, this was done in the presence of deaerated SiO_2 particles. Deposition of Pt was accomplished by reducing tetraaminoplatinum (II) hydroxide with formic acid in the presence of the deaerated SnO_x and SnO_x/SiO_2 supports. The resulting slurry was dried in air at 150 °C. The Au/MnO_x

sample was prepared via coprecipitation from aqueous tetrachloroauric acid, manganese (II) nitrate and sodium carbonate. The precipitate was washed with hot water, dried in air at 110 °C, and calcined at 400 °C for 4 hours. Since the final Mn oxidation state is unknown at this point, the Au/MnO_x composition is based on the molar ratio of Au:Mn in the precursor solutions. A 2 wt% Pt/SnO_x (1.6 at% Pt based on Pt and Sn content) catalyst was obtained from Engelhard Industries. The experiments were conducted at 35 or 55 °C using 50-150 mg of catalyst in powdered form. Unless noted otherwise, the reactor feed contained 1 vol% CO, 0.5 vol% O_2 and 2 vol% Ne (for GC calibration) in helium flowing at 10 sccm and 1 atmosphere of total pressure. No CO_2 was present in the reactor feed.

The experimental procedures varied depending upon whether the catalysts were pretreated prior to the onset of reaction. The unpretreated samples were exposed to 10 sccm of helium for 1 hour as the reactor temperature stabilized. Pretreated samples were subjected to the following sequence of events: (1) heating to the desired pretreatment temperature in 10 sccm of helium for 1 hour, (2) exposure to the pretreatment gas mixture (10 sccm) for 2 hours and (3) cooling to the reaction temperature in 10 sccm of helium for 1 hour. In each case the helium flow was subsequently replaced with the reaction gas mixture and product sampling

was initiated. At predetermined time intervals an automated sampling valve directed a 1-milliliter portion of the reaction products to a gas chromatograph (GC) for quantitative analysis of moles of CO_2 formed (referenced to 0 °C and 1 atmosphere) per second per gram of catalyst (moles CO_2/s/g). The results were plotted versus time to yield the CO oxidation activity curves for each catalyst.

Results and Discussion

Air purification and CO detection commonly involve the oxidation of small concentrations of CO in air (excess O_2) which may contain substantial amounts of water and/or other pollutants. Temperature extremes range from near ambient for respiratory aids to above 150 °C for CO gas sensors [110]. Carbon monoxide oxidation in CO_2 lasers is characterized by small, stoichiometric concentrations of CO and O_2 with a large partial pressure of CO_2 at temperatures near 50 °C. Such diverse environments can have a dramatic effect on the performance of low-temperature CO oxidation catalysts. For example, a Au/Fe_2O_3 catalyst has recently been shown to exhibit excellent CO oxidation activity in air (both wet and dry) near ambient temperature [15,16]. However, the research presented in Chapter 6 indicates that its performance is unacceptable in a CO_2 laser environment.

Apparently, CO oxidation on these supported catalysts is much more difficult when excess O_2 is not available.

The CO oxidation activities of the 10% Au/MnO_x, 19.5% Pt/SnO_x and 2% Pt/SnO_x samples are shown in Figure 7-1 as a function of time for unpretreated surfaces (open symbols) and surfaces pretreated with a 5 vol% CO/He mixture at 50 °C (solid symbols). The unpretreated Pt/SnO_x catalysts exhibit similar overall reaction profiles which are maximum at the onset of reaction but steadily decay over time. The data are consistent with previous experiments which indicate that maximum Pt/SnO_x activity occurs near 15 to 20 wt% Pt under similar experimental conditions [27]. The unpretreated Au/MnO_x catalyst exhibits remarkable CO oxidation activity which is approximately an order of magnitude greater than that of the 19.5% Pt/SnO_x sample after 6000 minutes of reaction. The fact that Au/MnO_x exhibits superior CO oxidation activity without the need for pretreatment is critical in many applications including respiratory protection.

It has previously been shown that CO pretreatments enhance the activity of Pt/SnO_x surfaces toward low-temperature CO oxidation [26]. This fact is clearly illustrated by the data in Figure 7-1. Furthermore, a CO pretreatment at 50 °C significantly enhances the activity of Au/MnO_x as well, and the effect is most dramatic for

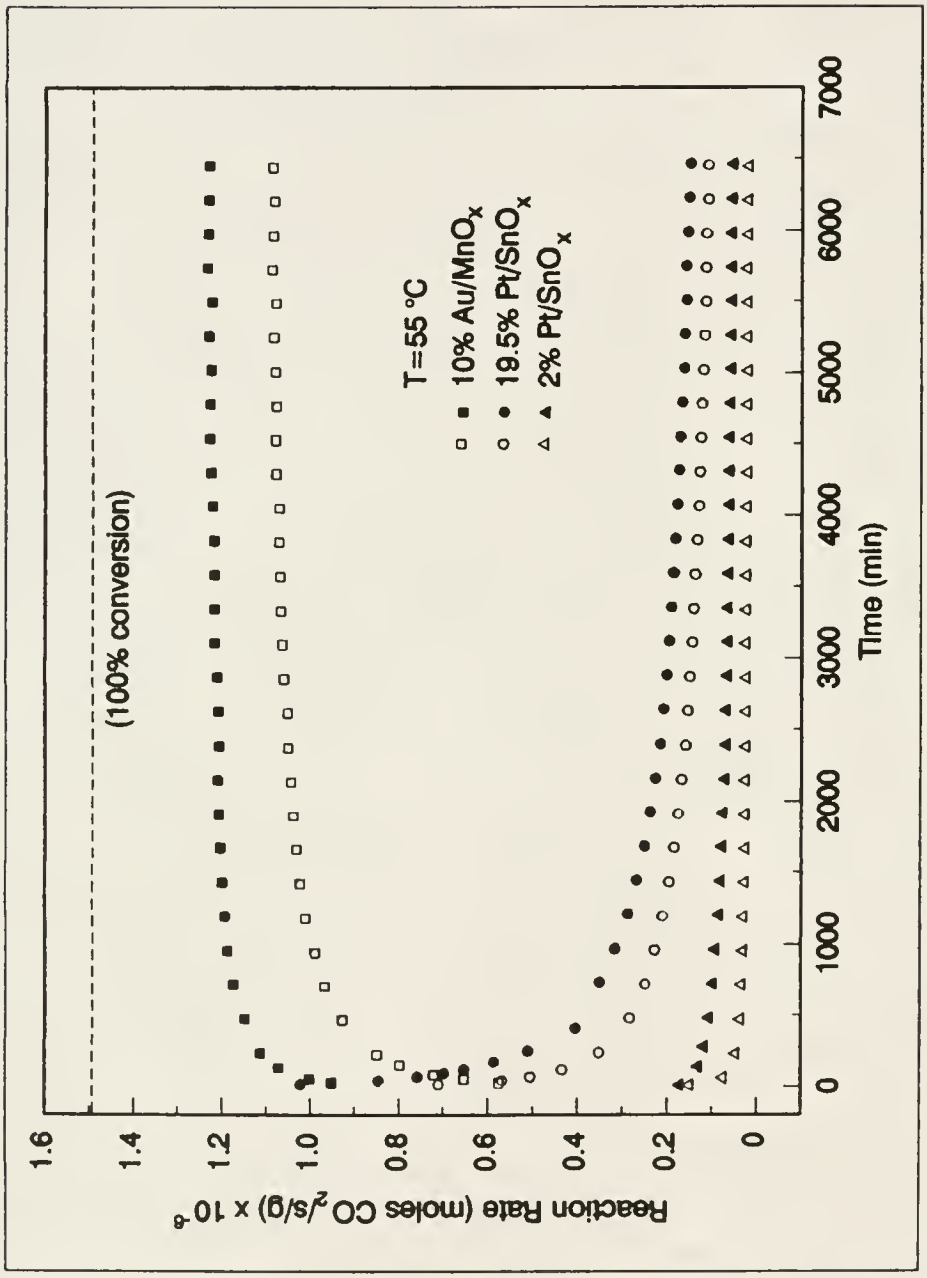

Figure 7-1. The CO oxidation activity of 10 at% Au/MnO_x, 19.5 wt% Pt/SnO_x and 2 wt% Pt/SnO_x at 55 °C without pre-treatment (open symbols) and pretreatment in 5 vol% CO/He at 50 °C (solid symbols).

Au/MnO_x where the CO conversion increases by approximately 10%. It is interesting to note that while the activity of each sample is enhanced as a result of the CO pretreatment, the overall character of the activity profiles remains unaffected.

As indicated in Figure 7-2, increasing the CO pretreatment temperature from 50 °C (open symbols) to 125 °C (solid symbols) further enhances the long-term activity of these catalysts. The activity profile of the 19.5% Pt/SnO_x catalyst is affected most by the increased pretreatment temperature. However, characteristics of an induction phenomenon (initial steep decline in activity followed by an increase and then a slow decline) soon become apparent in the activity profiles of both 2% Pt/SnO_x and 19.5% Pt/SnO_x. Although similar induction phenomena have been observed in a previous study of Pt/SnO_x [26], identical CO pretreatments at 125 °C did not result in any significant induction period during reaction at 75 or 85 °C. The fact that an induction period ensues during reaction at 55 °C is consistent with the hypothesis that the induction results from temporary surface dehydration caused by the reductive pretreatment [26] because replenishment of catalyst surface moisture via bulk diffusion would be less facile at 55 °C relative to 75 or 85 °C. Although the induction period exhibited by 19.5% Pt/SnO_x is

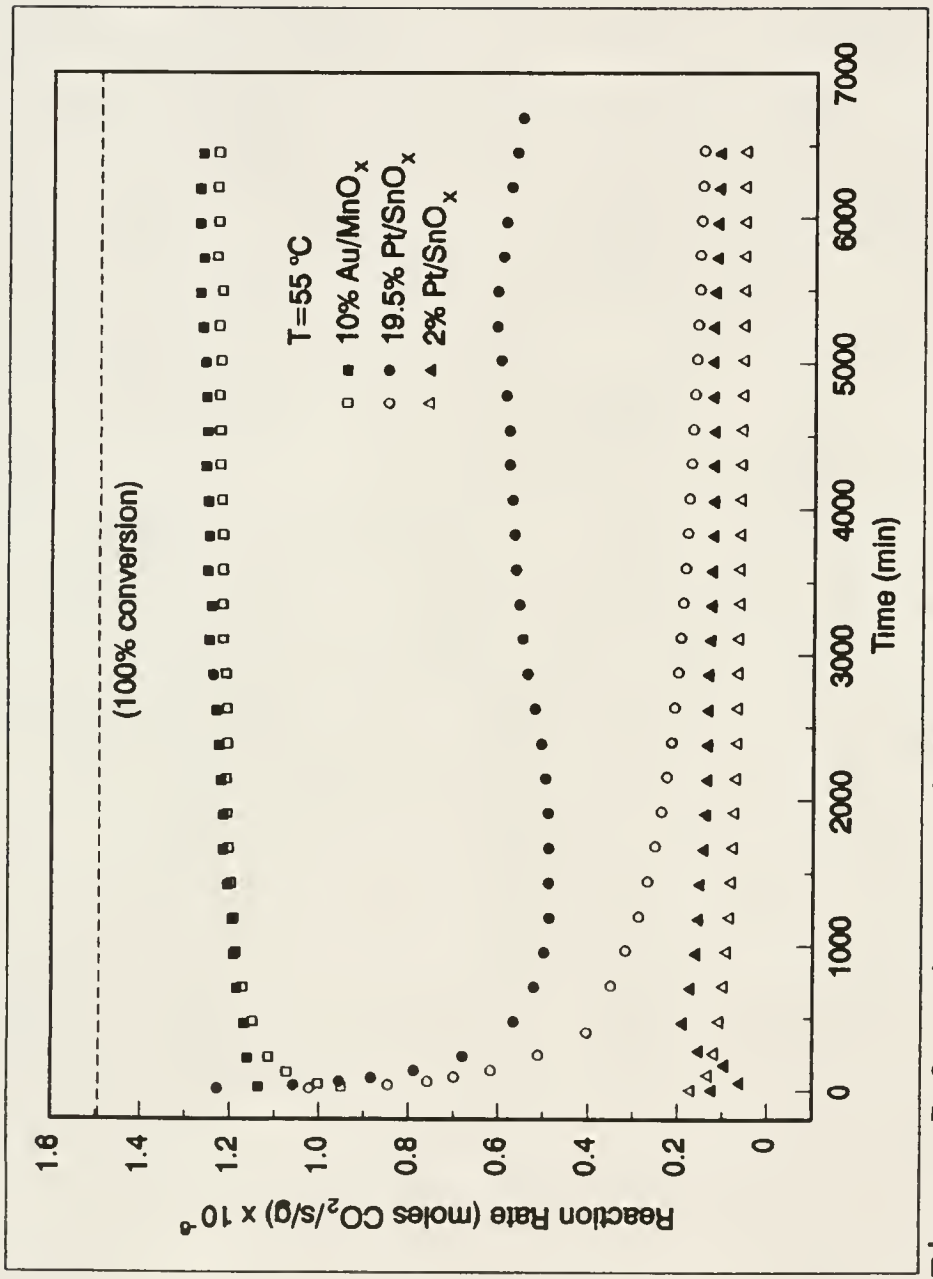

Figure 7-2. The CO oxidation activity of 10 at% Au/MnO_x, 19.5 wt% Pt/SnO_x and 2 wt% Pt/SnO_x at 55 °C after pre-treatment in 5 vol% CO/He at 50 °C (open symbols) and 125 °C (solid symbols).

the least severe, it spans a much greater time period (approximately 5300 minutes) relative to the 2% Pt/SnO_x sample. Nevertheless, beyond the induction period the CO oxidation activity of both Pt/SnO_x samples steadily decays with time. On the other hand, subsequent to CO pretreatment at 125 °C, the Au/MnO_x catalyst continues to exhibit its characteristic reaction profile exhibiting negligible activity decay. While reductive pretreatments are beneficial with regard to the low-temperature CO oxidation activity of Au/MnO_x, they have been shown to be detrimental to the CO oxidation performance of Pt/MnO_x under similar conditions (see Chapter 6).

In addition to reductive pretreatments, pretreatments in an oxidizing atmosphere were also investigated. As shown in Figure 7-3, a pretreatment in 5 vol% O_2/He at 50 °C (solid symbols) decreases the CO oxidation activity of all the samples relative to no pretreatment (open symbols). The effects of oxygen pretreatment on Au/MnO_x are the most significant; however, the characteristics of the overall activity profile are retained and activity decay remains negligible. The results for 2% Pt/SnO_x are once again consistent with a previous study which was performed using considerably different experimental conditions [26]. However, the relative degree of activity decline is much less under the conditions of this study. The effects

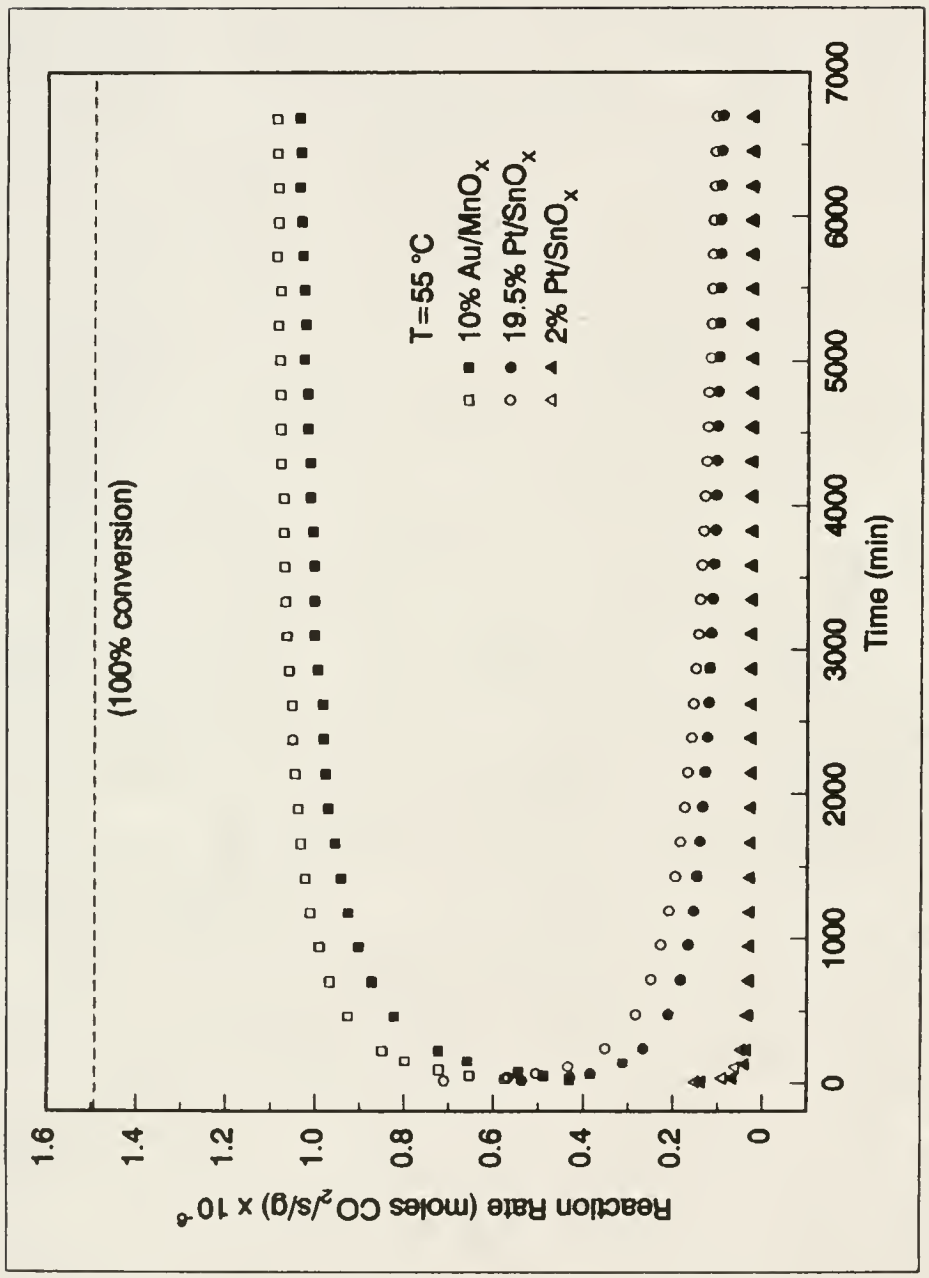

Figure 7-3. The CO oxidation activity of 10 at% Au/MnO_x, 19.5 wt% Pt/SnO_x and 2 wt% Pt/SnO_x at 55 °C without pre-treatment (open symbols) and pretreatment in 5 vol% O_2/He at 50 °C (solid symbols).

of the oxygen pretreatment are noticeable only during the first 500 minutes of reaction after which the unpretreated and pretreated curves essentially coincide. Similar behavior is also evident for 19.5% Pt/SnO_x where the majority of the activity decrease occurs during the initial stages of reaction. After 6500 minutes of reaction, the effect of the oxygen pretreatment is much less apparent.

Although the performance criteria of low-temperature CO oxidation catalysts may vary considerably among different applications, there is a common need for catalysts which maintain high activity over extended time periods without experiencing a significant decay in performance. The operational lifetime of catalysts utilized in respiratory aids is of course a critical factor to be considered. Catalysts for CO_2 lasers should be expected to perform well for at least 3 years [6-8]. In CO gas sensor applications, low-temperature operation is desirable without the need for periodic flash heating in order to restore catalyst activity [110]. Considering these important performance criteria, the data in Figure 7-4 indicate that Au/MnO_x is a promising candidate for all these applications. Even after 70 days near ambient temperature, Au/MnO_x continues to exhibit excellent CO oxidation performance with negligible activity decay. The optimized 14.5% $Pt/SnO_x/SiO_2$ catalyst does not perform nearly so well. It

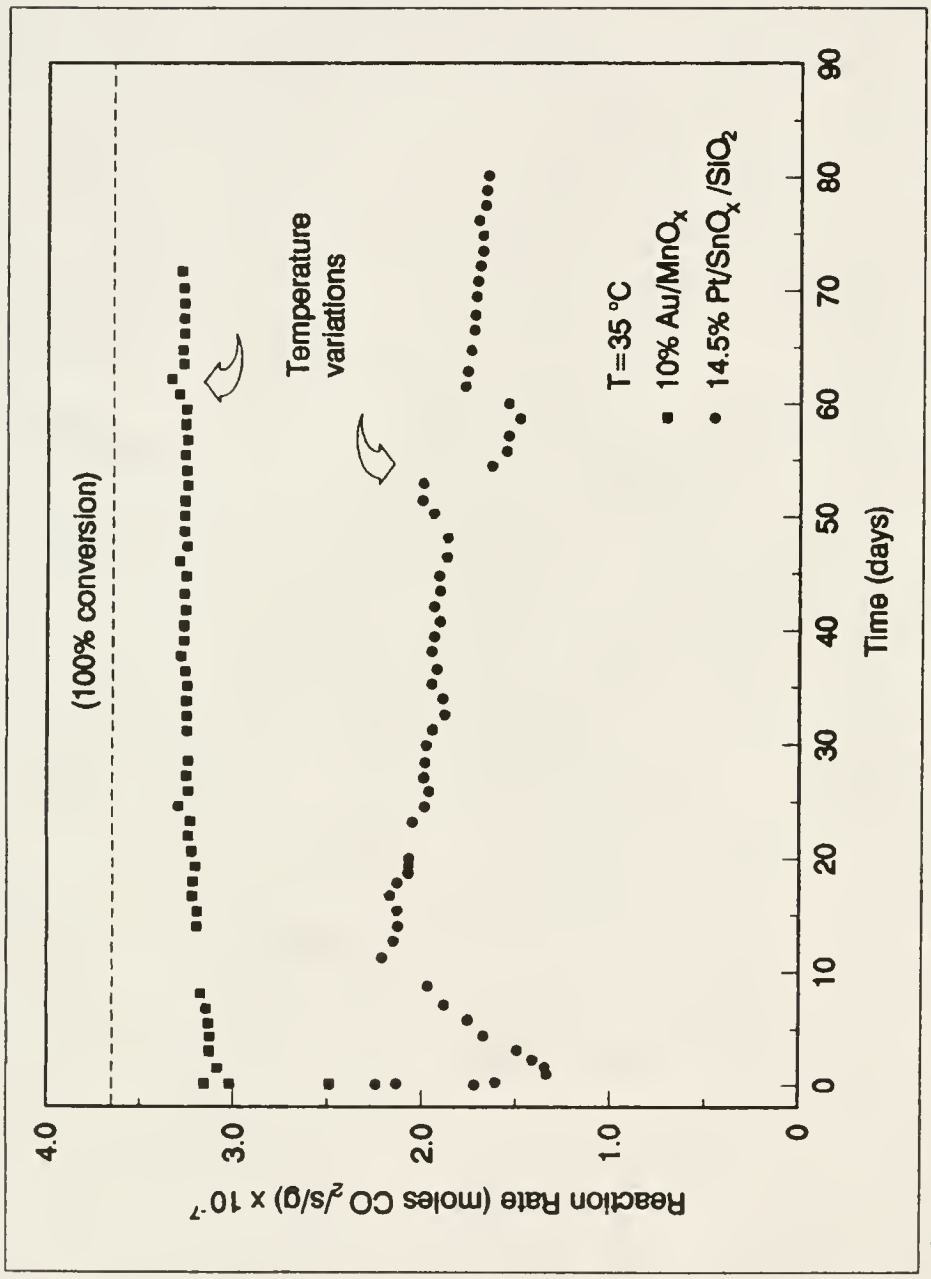

Figure 7-4. The CO oxidation activity of 10 at% Au/MnO_x (unpretreated) and 14.5 wt% $Pt/SnO_x/SiO_2$ (pretreated in 5 vol% CO/He at 125 °C) at 35 °C.

experiences a significant induction period which lasts approximately 1 week followed by considerable activity decay which precludes its use in long-term applications.

Further understanding of the Au/MnO_x catalyst can be gained by varying the CO/O_2 concentration ratio in the reaction gas mixture. As shown by the data in Figure 7-5, the composition of the test gas has a marked effect on the activity profile of Au/MnO_x. Overall performance is significantly enhanced in an oxygen-rich atmosphere whereas activity in a CO-rich reaction mixture is diminished considerably. Similar results have been witnessed for Pt/SnO_x catalysts as well [27]. The data in Figure 7-5 are important with regard to understanding the variations in catalyst performance with respect to compositional variations and indicate that excess CO should be avoided if possible. However, in the majority of low-temperature CO oxidation applications oxygen is present in at least stoichiometric concentrations relative to CO. Therefore, Au/MnO_x should continue to perform well in many applications. The mechanism responsible for the activity decay in a CO-rich reaction mixture is not fully understood at this time. During CO pretreatment of these catalysts, GC analysis suggests that the surfaces are progressively reduced with corresponding CO_2 formation. It is possible that excess CO in the reaction gas acts to further reduce

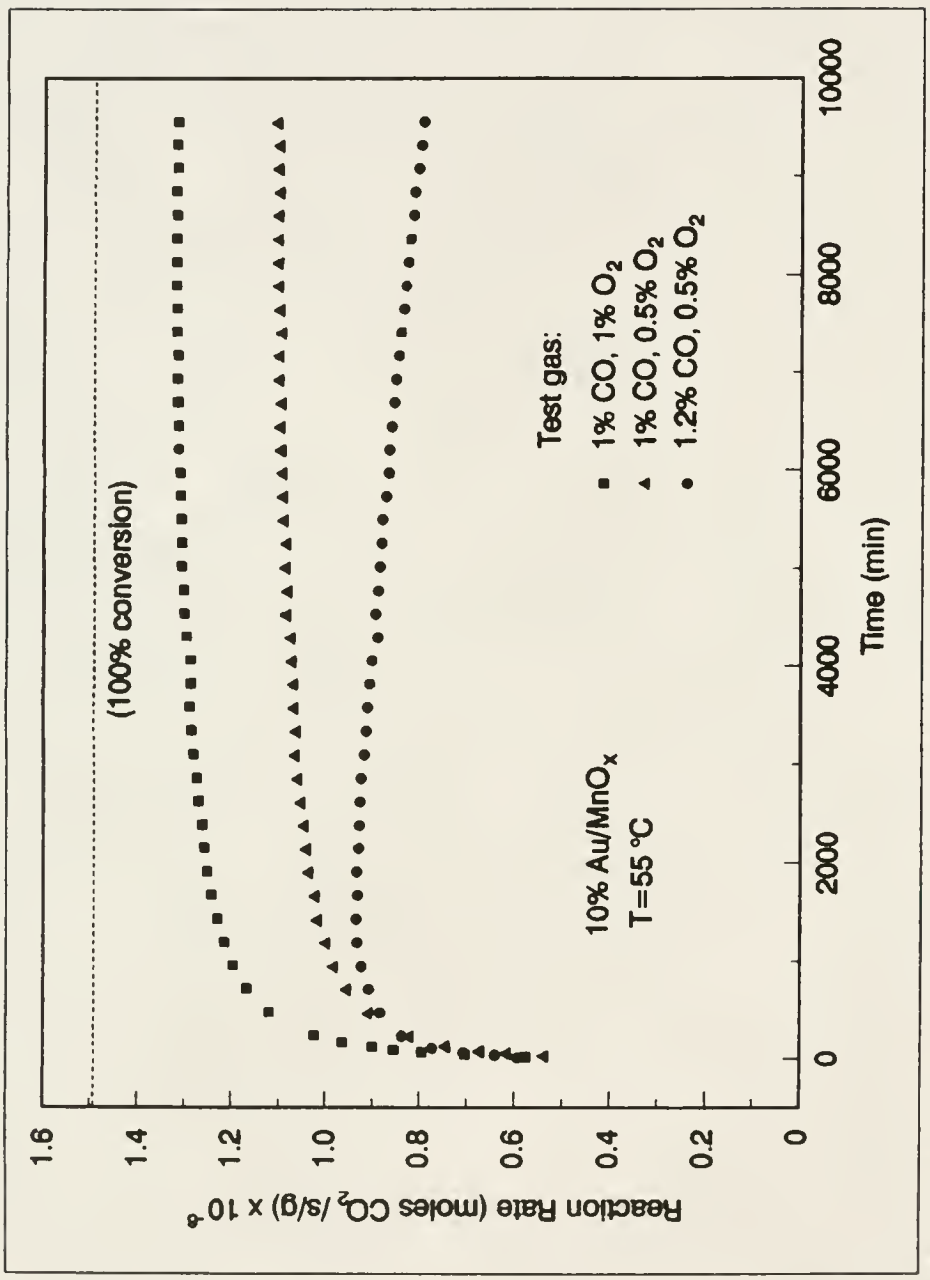

Figure 7-5. The CO oxidation activity of 10 at% Au/MnO_x (unpretreated) at 55 °C as a function of test gas composition (balance He).

the surface resulting in the subsequent loss of CO oxidation activity.

Under similar experimental conditions the performance data obtained in this study compare favorably with activity data for other low-temperature CO oxidation catalysts. All of the Pt/SnO_x catalysts prepared for this study have previously been shown to be superior to proprietary catalysts manufactured by General Motors and Teledyne [27]. Furthermore, the activity of 19.5 wt% Pt/SnO_x and 14.5 wt% $Pt/SnO_x/SiO_2$ appears to be comparable to numerous other Pt/SnO_x, Pd/SnO_x and $Pt-Pd/SnO_x$ catalysts for similar reaction times [27,28,113]. However, long-term activity decay continues to be a problem for all of the SnO_x-based materials. Consequently, Au/MnO_x remains the optimum catalyst under the test conditions used in this study.

Summary

This comparison study reveals that a 10 at% Au/MnO_x catalyst exhibits superior low-temperature CO oxidation performance relative to several Pt/SnO_x catalysts under similar conditions of stoichiometric CO and O_2 near ambient temperatures. The activity of both Au/MnO_x and Pt/SnO_x is enhanced subsequent to CO pretreatments at 50 and 125 °C whereas an O_2 pretreatment at 50 °C results in an activity decrease. Au/MnO_x exhibited a remarkable activity profile wherein the activity decay remained essentially negligible

for reaction times up to 70 days. The versatility of Au/MnO_x has been demonstrated further with respect to reaction mixtures containing excess oxygen. As a result, this study implies that Au/MnO_x is a promising catalyst for many practical applications of low-temperature CO oxidation including CO_2 lasers, air purification and CO gas sensing.

CHAPTER 8
CATALYTIC BEHAVIOR OF NOBLE METAL/REDUCIBLE OXIDE MATERIALS FOR LOW-TEMPERATURE CO OXIDATION: SURFACE CHARACTERIZATION OF Au/MnO_x

Introduction

The two previous studies (see Chapters 6 and 7) of low-temperature CO oxidation on noble metal/reducible oxide (NMRO) materials have identified several promising catalysts for use in CO_2 lasers, chemical sensors and air purification devices. By far the most active materials examined in these studies consist of gold supported on manganese oxide (Au/MnO_x). The reaction data indicate that Au and MnO_x interact synergistically exhibiting remarkable long-term CO oxidation activity near ambient temperatures with negligible activity decay. However, little is understood about the nature of the $Au-MnO_x$ synergism and the corresponding CO oxidation mechanism on these seemingly complex surfaces.

It is well documented that the catalytic properties of Au can be significantly altered in the presence of support materials. Reviews of gold in catalysis [114,115] cite numerous investigations of Au particles dispersed on supports such as MgO, Al_2O_3 and SiO_2. Relative to more massive forms of Au [116], supported Au particles often

exhibit a marked increase in surface reactivity, particularly toward oxygen-bearing molecules. It has been postulated that this enhanced reactivity results from an interaction between the Au and the support material. For example, in studies utilizing extended X-ray absorption fine structure spectroscopy (EXAFS), interatomic distances assigned to Au-O species have been measured on Au/MgO and Au/Al_2O_3 surfaces [117,118]. Infrared spectroscopy of Au/MgO has indicated CO adsorption bands which appear at significantly lower wavenumbers than those previously observed on Au/SiO_2 and Au films [119]. Reaction experiments have revealed that Au/SiO_2 and Au/MgO undergo extensive isotopic oxygen exchange whereas under comparable conditions metallic Au, SiO_2 and MgO do not [120]. Data from Mössbauer spectroscopy and X-ray photoelectron spectroscopy are consistent with Au-support interactions as well [121-123]. While the exact nature of the Au-support interaction (if it indeed occurs) remains somewhat speculative, it appears to be a unique property which is dependent upon the choice of support. In fact, a recent study has indicated that characteristics of strong metal-support interactions (SMSI) which are often observed for Group (VIII) metals supported on TiO_2, V_2O_3 and Nb_2O_5 are absent on Au/TiO_2 surfaces [124]. Nevertheless, the possibility of SMSI

remains for Au supported on metal oxides which are perhaps more readily reducible [125].

Although postulations of a "support effect" appear to be well substantiated on a considerable number of Au catalysts, there is evidence that the Au particle size may also affect the reactivity of these surfaces. Experiments with numerous Au catalysts including Au/Fe_2O_3, Au/Co_2O_3, Au/NiO, Au/Al_2O_3 and Au/SiO_2 [16] have revealed an overall trend wherein CO oxidation activity increases with decreasing Au particle size. These results are consistent with the observation that small Au particles exhibit an increased affinity for O_2 [126]. However, some exceptions to the former trend were observed which would appear to signify the importance of the support material as well. It is possible that ultrafine Au particles are a prerequisite for Au-support interaction [127]. Under this assumption the reactivity of supported Au may ultimately be traced to the method of preparation. Indeed, relative to preparation via impregnation, precipitation techniques yield smaller Au particles and more active catalytic surfaces [16,126].

It is evident that the increased reactivity of supported Au particles has prompted renewed interest in Au as a major catalyst constituent. While there has been considerable research on the interaction of Au with relatively inactive supports, it is apparent that Au supported on

reducible oxides has received little attention. This is probably due to the fact that the catalytic activity of these materials has only recently been discovered [16,110]. This chapter describes a detailed surface characterization study which has been undertaken to elucidate the mechanism of low-temperature CO oxidation on Au/MnO_x. Auger electron spectroscopy (AES), ion scattering spectroscopy (ISS) and X-ray photoelectron spectroscopy (XPS) were utilized to investigate Au/MnO_x surfaces in order to examine the chemical states of the surface species and the nature of their interaction. It is anticipated that these studies will aid in improving the performance of Au/MnO_x while yielding important information which may be applied to other NMRO catalytic surfaces as well.

Experimental

The catalytic surfaces investigated in this study were 10 at% Au/MnO_x (on a Au:Mn basis) and a bare MnO_x support. Details regarding their preparation have been described in the previous two chapters. Briefly, the samples were prepared via coprecipitation from $HAuCl_4$ and/or $Mn(NO_3)_2$. The appropriate precursor solutions were added dropwise to a stirred solution of Na_2CO_3 at room temperature. After washing and drying the crushed precipitates were calcined in air at 400 °C for 4 hours.

The as-prepared samples were pressed into tin specimen cups and inserted into an ultrahigh vacuum (UHV) system (base pressure of 10^{-11} Torr) for initial surface characterization (see Appendix). In order to correlate the surface characterization data to the CO oxidation activity curves (see Chapters 6 and 7), the samples were subsequently transferred to a preparation chamber connected to the UHV system and pretreated in 760 Torr of He for 1 hour at 55 °C. The samples were heated on a custom platform heating element [75]. After pretreatment the samples were returned to the UHV analytical chamber without air exposure for further characterization.

Energy analysis for the ISS, AES and XPS experiments was accomplished using a Perkin-Elmer PHI Model 25-270AR double-pass cylindrical mirror analyzer (CMA). The CMA utilized an internal, movable aperture which varied the polar acceptance angle for incoming particles. The ISS spectra were collected in the nonretarding mode using a 147°-scattering angle (fixed by the experimental geometry) and pulse counting detection [51]. A 100-nA, 1-keV $^4He^+$ primary ion beam was defocused over a 1-cm^2 area to minimize sputter damage. The AES experiments were performed in the nonretarding mode using a 3-keV, 10-μA primary electron beam with a 0.2-mm spot diameter. Survey and high-resolution XPS spectra were recorded with Mg Kα excitation

in the retarding mode using 50- and 25-eV pass energies, respectively. The XPS binding energies were referenced to SnO_2 (486.4 eV) which was always present on the surface of the tin specimen cups. The amount of Sn contribution to the XPS spectra was kept small to ensure that the oxygen present was not due to significant amounts of SnO_x.

Results and Discussion

The ISS spectra taken from the Au/MnO_x and MnO_x samples appear in Figures 8-1 and 8-2, respectively. The spectra yield interesting information regarding the composition of the outermost atomic layers of (a) the air-exposed surfaces and (b) the surfaces pretreated in He at 55 °C. Both figures reveal prominent spectral features due to the constituent atoms of Au, Mn and O. However, a significant surface concentration of Na is also indicated. The Na originates from aqueous Na_2CO_3 which was used in the preparation of both samples. Given the significant presence of Na on these surfaces, it is interesting that Figure 8-1 indicates essentially a negligible concentration of Cl (originating from the $HAuCl_4$ precursor solution) on Au/MnO_x. Chlorine features, if present, would appear near 0.66 E/E_o. It has not been determined if Cl was present on Au/MnO_x prior to washing, though it is possible that washing with hot water is more effective in removing Cl from these surfaces relative to Na. It has been suggested that

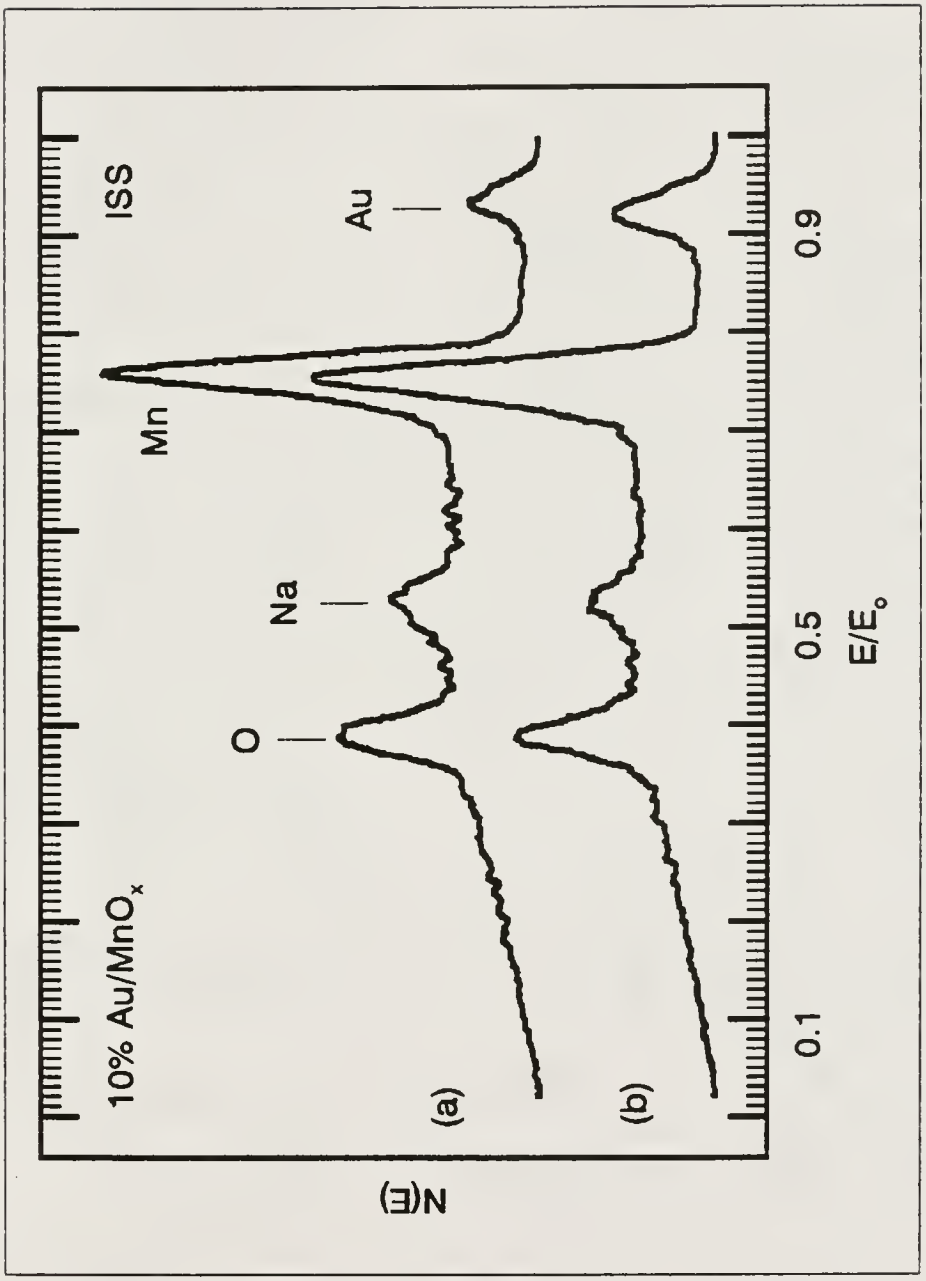

Figure 8-1. The ISS spectra of 10 at% Au/MnO_x (a) before and (b) after He pretreatment at 55 °C for 1 hour.

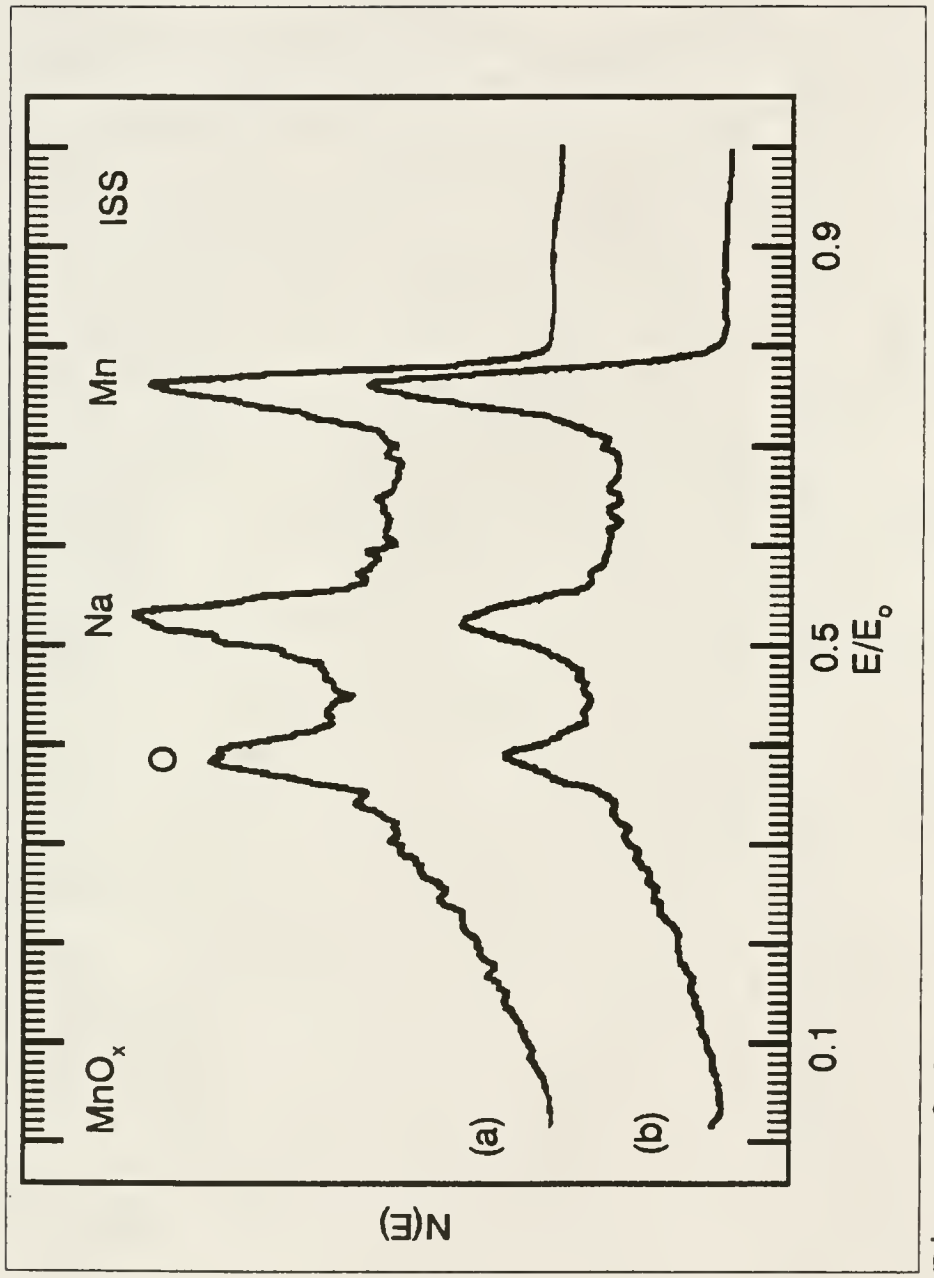

Figure 8-2. The ISS spectra of MnO_x (a) before and (b) after He pretreatment at 55 °C for 1 hour.

Cl should be avoided in the preparation of Pt/SnO_x low-temperature CO oxidation catalysts since the use of Cl-containing precursors decreases the observed activity [28]. Considering the ISS spectra in Figure 8-1 as well as the Au/MnO_x reaction data in Chapters 6 and 7, the preparation method used in this study appears to avoid significant complications due to Cl contamination from $HAuCl_4$. The relationship between surface Na and the low-temperature CO oxidation activity of Au/MnO_x has not yet been investigated.

Figures 8-1 and 8-2 also indicate that the surface composition of Au/MnO_x and MnO_x changes significantly as a result of the He pretreatment at 55 °C. The relative amounts of Na on both catalysts are subsequently reduced. However, the spectra indicate an opposite trend with respect to surface O concentration. That is, after He pretreatment the O/Mn concentration ratio on Au/MnO_x slightly increases whereas the O/Mn concentration ratio decreases considerably on MnO_x. Furthermore, as shown in Figure 8-1, there is a concurrent increase in surface Au concentration on Au/MnO_x. While these ISS data are consistent with an increased interaction between Au and MnO_x, additional information from AES and XPS experiments is helpful in determining the characteristics of these surfaces.

The AES spectra of Au/MnO_x and MnO_x both before (a) and after (b) He pretreatment appear in Figures 8-3 and 8-4, respectively. Distinct Mn and O features appear whereas features due to Au, Cl and Na are present but somewhat less discernible. The AES spectra are in many ways consistent with the ISS data. Firstly, the spectra indicate that the Na concentration is greater on the MnO_x surface and that the amounts on both samples decrease subsequent to He pretreatment. The previous trends concerning the surface O and Au concentrations are observed also. After He pretreatment, Figure 8-3 indicates that the concentration of Au and O on the Au/MnO_x surface increases relative to Mn whereas Figure 8-4 indicates that the relative surface concentration of O decreases on MnO_x. In addition, Figure 8-3 depicts an increase in Au concentration after the Au/MnO_x has been pretreated. Contrary to the ISS data in Figure 8-1, however, the AES spectra in Figure 8-3 reveal visible features due to Cl. These AES spectra indicate that the amount of Cl remains small relative to Na (the AES cross section for Cl is nearly 5 times that of Na [128]) and that the Cl is essentially confined to a region slightly beneath the Au/MnO_x surface. This is due to the fact that AES probes a region which consists of approximately the top 20 angstroms of the surface whereas ISS is essentially sensitive to the outermost one or two atomic

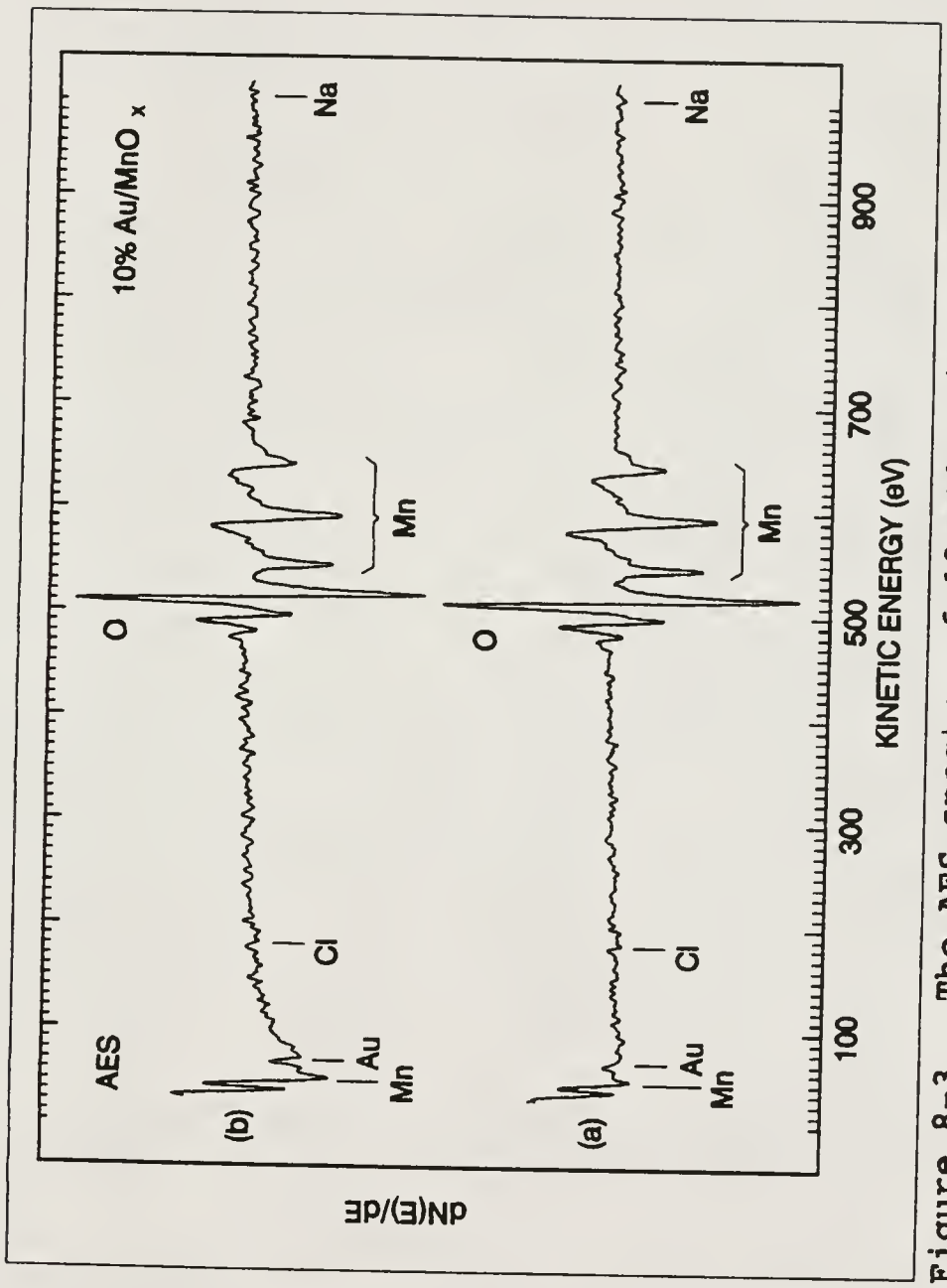

Figure 8-3. The AES spectra of 10 at% Au/MnO_x (a) before and (b) after He pretreatment at 55 °C for 1 hour.

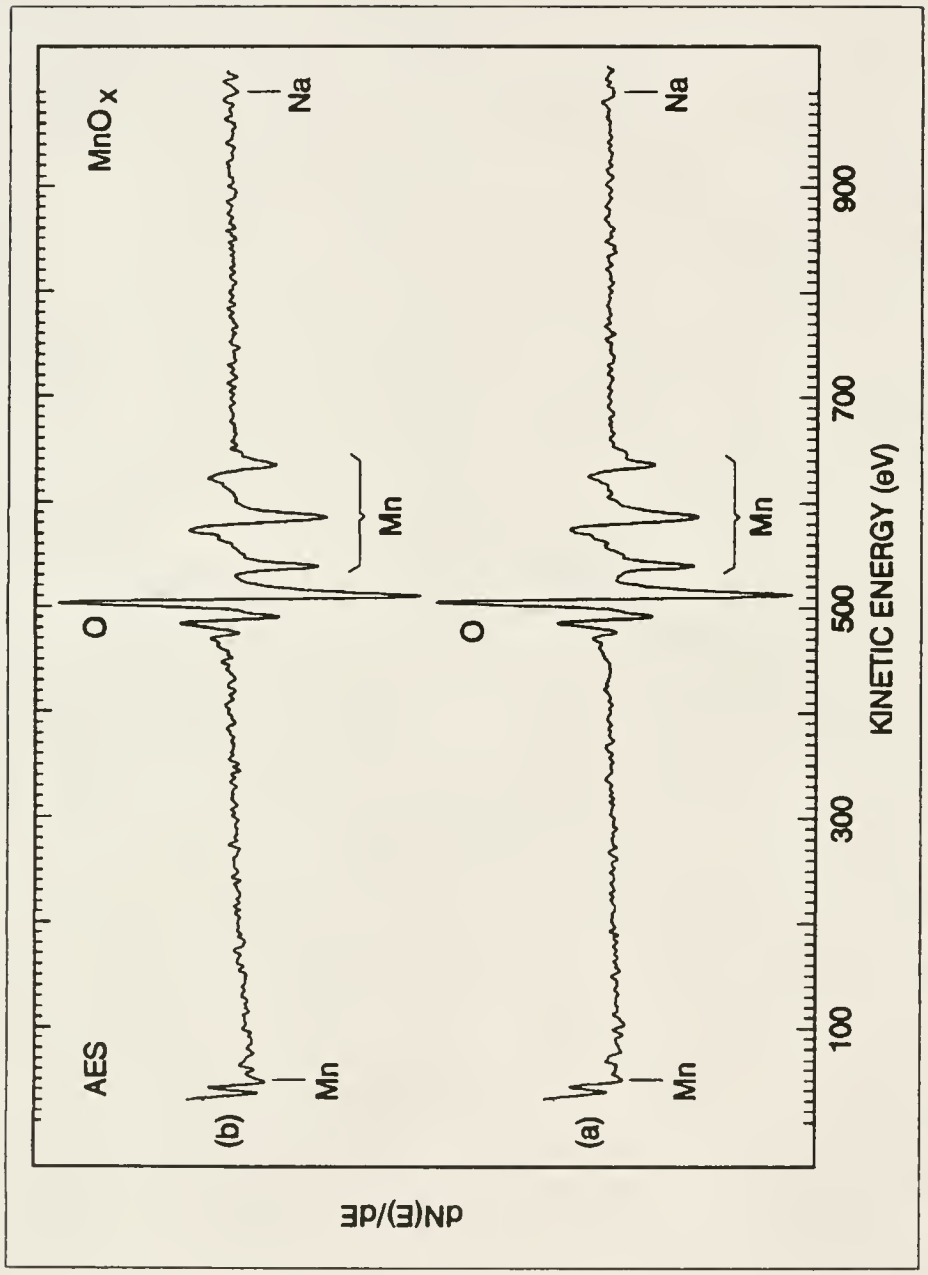

Figure 8-4. The AES spectra of MnO_x (a) before and (b) after He pretreatment at 55 °C for 1 hour.

layers. In a manner similar to that observed for Na, the amount of Cl decreases after He pretreatment. Considering the AES spectra in Figures 8-3(b) and 8-4(b), an estimate of elemental cross sections [128] and surface composition suggests an O/Mn concentration ratio which corresponds approximately to Mn_3O_4. Similarly, the data in Figure 8-3(b) indicate a gold concentration near 11 at% based upon Au and Mn only. This compares favorably with a Au concentration of 10 at% based upon Au and Mn contained in the preparation solutions.

In order to understand the CO oxidation mechanism on Au/MnO_x, it is necessary to determine not only the surface composition but also the chemical states of the surface species. In addition, knowledge of the Au and Mn chemical states with respect to both Au/MnO_x and MnO_x should provide insight into the synergistic interaction between Au and MnO_x. X-ray photoelectron spectroscopy is a particularly useful technique for obtaining chemical state information and it complements the data which is available from ISS and AES experiments. Thus far the ISS and AES data have indicated that Au/MnO_x and MnO_x each respond differently to a pretreatment in He at 55 °C. The surface of MnO_x becomes depleted of O whereas the surface of Au/MnO_x is enriched not only with O but with Au as well. It is important to determine whether the O enrichment is due to a genuine

change in the Mn and/or Au oxidation state(s) or simply the result of an increased surface concentration of Au which is present in an oxidized state.

Manganese-oxygen systems have previously been studied using XPS techniques [129-133]. Unfortunately, XPS peak binding energies alone are not sufficient to accurately determine the chemical state of Mn in manganese oxides. That is, the Mn 2p features are relatively broad for MnO_x compounds and consequently, shifts in binding energy generally occur within experimental error of the XPS instrument. This problem is compounded by the fact that manganese oxides are often complex and may contain Mn which is present in several chemical states together with considerable amounts of water [134]. As a result, the reported Mn $2p_{3/2}$ binding energies for manganese oxides have been largely inconsistent [129-133]. However, additional information is available from XPS which has proven useful in determining the Mn oxidation state. This information is obtained from the location of Mn 2p shake-up lines, the extent of Mn 3s multiplet splitting, XPS valence-band structure and XPS O 1s spectra [129-133].

The Mn 2p XPS spectra of Au/MnO_x and MnO_x taken (a) before and (b) after pretreatment in He at 55 °C appear in Figures 8-5 and 8-6, respectively. Although the spectra for both samples appear similar in overall character there

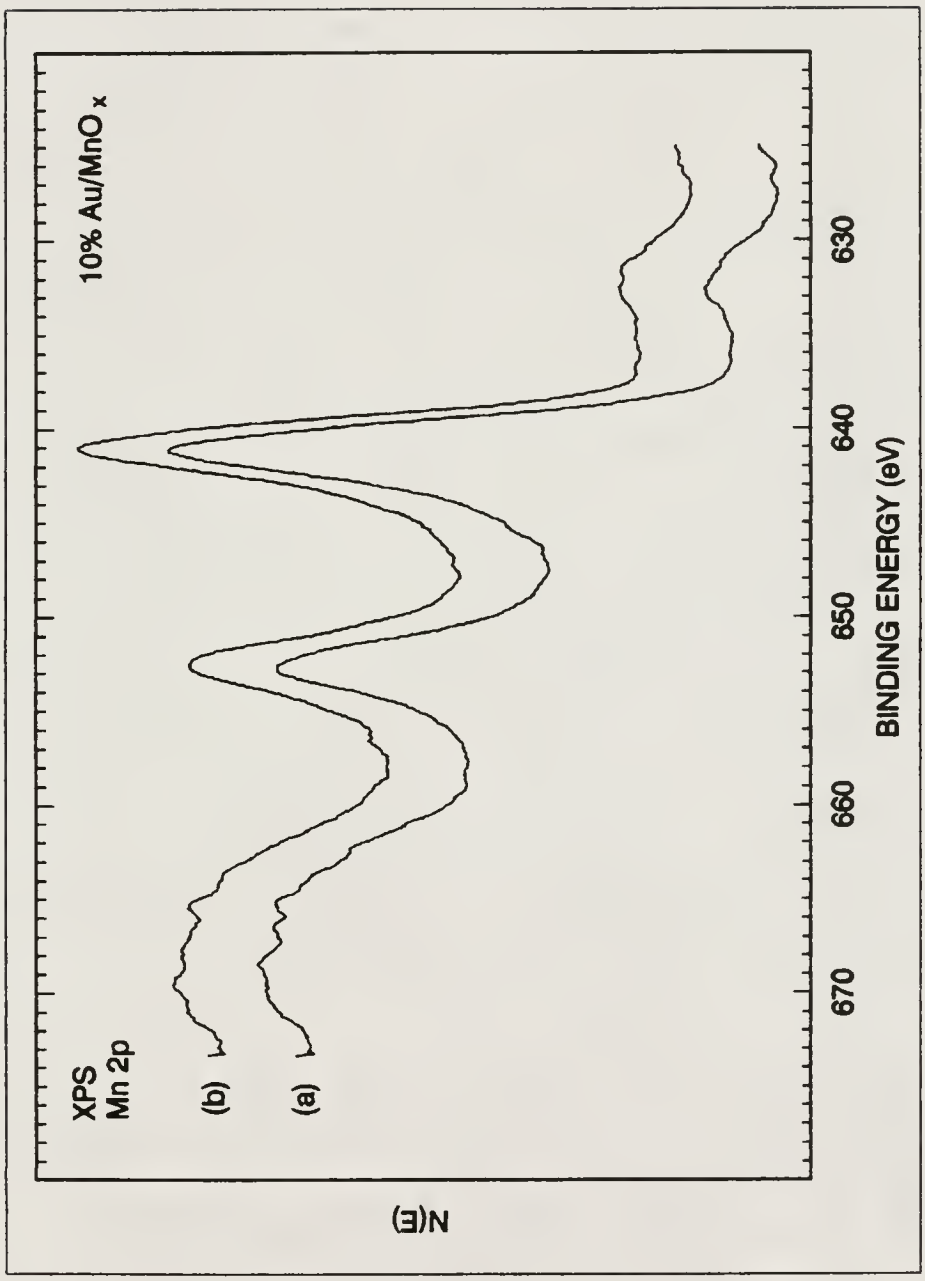

Figure 8-5. The XPS Mn 2p spectra of 10 at% Au/MnO_x (a) before and (b) after He pretreatment at 55 °C for 1 hour.

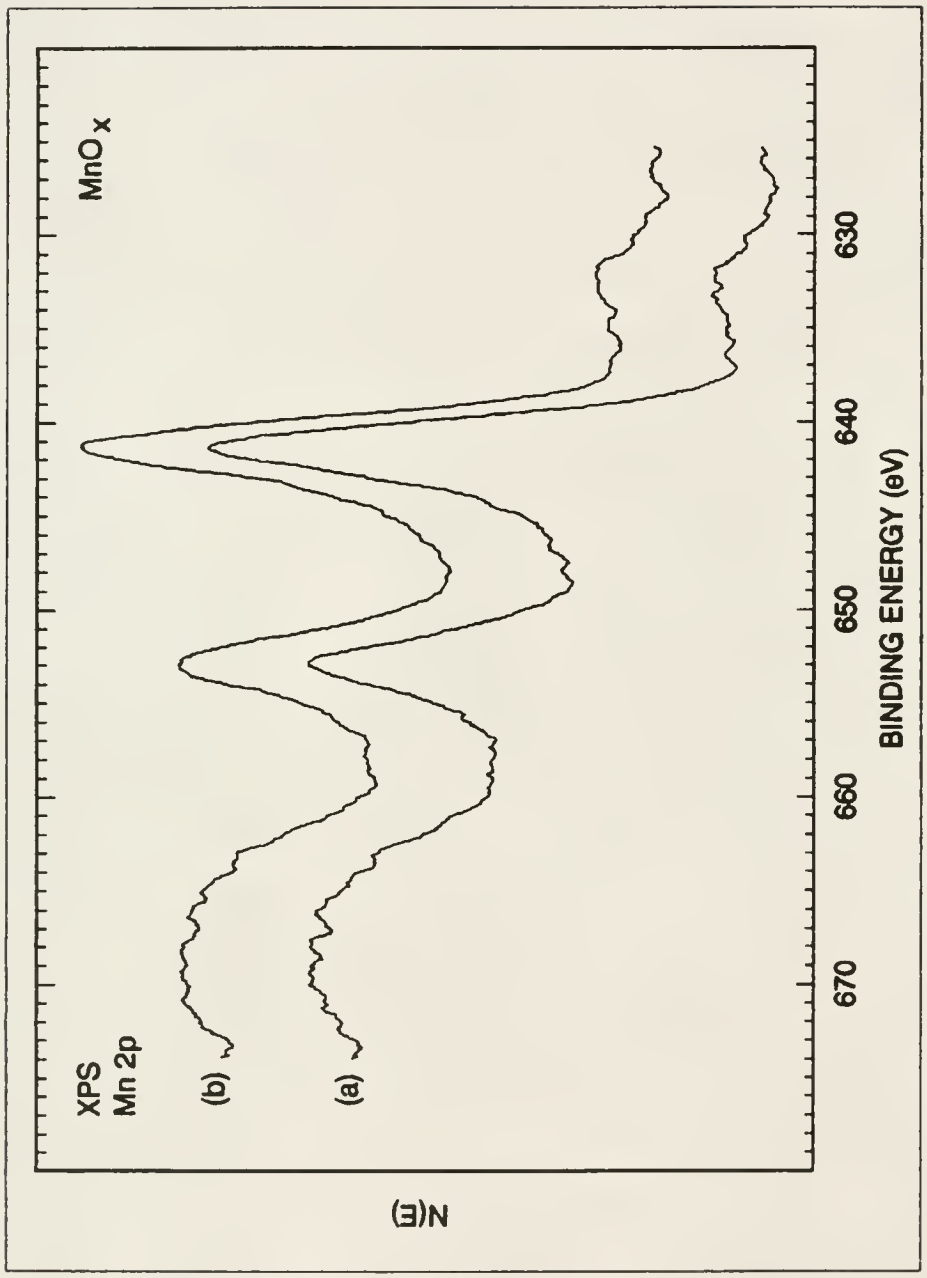

Figure 8-6. The XPS Mn 2p spectra of MnO_x (a) before and (b) after He pretreatment at 55 °C for 1 hour.

are visible differences between them. Figure 8-5 indicates that the Mn $2p_{3/2}$ peaks of Au/MnO_x remain essentially stationary after pretreatment with a binding energy near 641.1 eV. In addition, several features appear on the high binding energy side of the 2p peaks. In Figure 8-5(a), a small shoulder is indicated approximately 4.4 eV from the Mn $2p_{3/2}$ peak and two small shake-up peaks appear which are shifted about 5.5 eV from their respective 2p peaks. Subsequent to the He pretreatment, Figure 8-5(b) suggests that the two shake-up peaks remain whereas the $2p_{3/2}$ shoulder becomes more apparent on the $2p_{1/2}$ peak. Unlike many of the Mn 2p spectra reported in the literature [129,130,132,133], the Mn 2p spectra recorded in this work exhibited a high background signal above 660 eV binding energy. As a result it is difficult to identify shake-up structures which might correspond to Mn_2O_3, Mn_3O_4 or MnO_2. These structures, if present, would be located near 664 eV binding energy [133]. Although several features resembling shake-up structures appear in this proximity, it is speculated that such features are artifacts of the high-intensity background given their number and randomness. The small shake-up structures appearing about 5.5 eV from the 2p peaks are consistent with MnO presence. However, the position of the shoulders on the 2p peaks themselves does not correspond to previously measured Mn 2p binding

energies or shake-up peak separations [129-133]. Although these features are not fully understood, they may be an indication of the complexity of these MnO_x surfaces. This assumption is consistent with the small magnitude of the shake-up peaks. It has been suggested that strong shake-up lines are observed on these types of surfaces only when stoichiometric oxides are present [131]. Accordingly the spectra in Figure 8-5 (and 8-6) would appear to indicate multiple Mn oxidation states. Indeed, spectra similar to those in Figures 8-5 and 8-6 exhibiting numerous shoulders on the Mn 2p peaks have been observed for discontinuous films consisting of mixtures of Mn metal and MnO [132].

As indicated in Figure 8-6, relative to Au/MnO_x, the Mn 2p peaks of MnO_x appear at slightly higher binding energy (about 641.4 eV) and they too remain essentially stationary as a result of the He pretreatment. Furthermore, the shoulders on the high binding energy side of the 2p peaks appear more distinct and numerous, again perhaps an indication of several Mn chemical states. Small shake-up structures are visible approximately 5 eV from the 2p peaks which within experimental error are consistent with MnO presence. Similar to the Mn 2p lines of Au/MnO_x, the Mn 2p spectra in Figure 8-6 exhibit a high-intensity background above 660 eV which hinders the identification of potential shake-up lines in this region.

The XPS Mn 2p binding energies measured for Au/MnO_x and MnO_x are near those which have been reported for both MnO and Mn_3O_4 [133]. Therefore, the existence of multiple Mn oxidation states in Figures 8-5 and 8-6 is further substantiated. However, a shake-up structure approximately 10-11 eV above the Mn $2p_{1/2}$ peak has been shown to be indicative of Mn_3O_4 presence [129-133]. Given the data in Figures 8-5 and 8-6, the appearance of such a feature cannot be confirmed. Observation of XPS Mn 2p spectra of Mn_3O_4 [129] reveals that the magnitude of the shake-up structures are such that they could become insignificant against a high-intensity background. The shake-up structures should be further attenuated if additional forms of Mn are present on a complex surface [131,133]. Therefore, it is possible that the shake-up features are present yet too small to be resolved in this work.

It has been demonstrated that information regarding the Mn oxidation state may be realized from the extent of Mn 3s multiplet splitting [129,131-133]. Unfortunately, XPS Mn 3s spectra may only be obtained for MnO_x because the Mn 3s peaks of Au/MnO_x are obscured by the Au 4f peaks. In order to compensate for excessive surface charging in the region of 0-100 eV binding energy, the Mn 3s spectra were referenced to the valence band of Mn at approximately 4 eV below the Fermi level [132,133]. The surface charging is

not a severe limitation in this case since the magnitude of the Mn 3s splitting is measured relative to the Mn 3s signal itself. The Mn 3s spectra of MnO_x (a) before and (b) after He pretreatment appear in Figure 8-7. The broad appearance of the spectra, particularly after He pretreatment, is consistent with the presence of multiple Mn chemical states. In addition, it appears that the multiplet splitting features also contain contributions from different oxidation states of Mn. As a result, it is difficult to determine a representative value of the extent of Mn 3s multiplet splitting. The spectrum in Figure 8-7(a), which is the most easily resolved, indicates two significant features which are separated by approximately 5 eV. This value is close to that which has been measured for Mn_3O_4 and Mn_2O_3 [129].

Figures 8-8 and 8-9 show valence-band XPS spectra for Au/MnO_x and MnO_x (a) before and (b) after He pretreatment at 55 °C, respectively. The spectra indicate at least two major peaks which are located near 4 and 7 eV binding energy. The former is attributed to the localized 3d states of Mn and the latter is due to O 2p electrons [130,132,133]. The shape and relative intensity of these two features yields insight into the nature of the Au/MnO_x and MnO_x surfaces. As indicated by Figures 8-8(a) and 8-9(a), the XPS valence-band spectra of the air-exposed

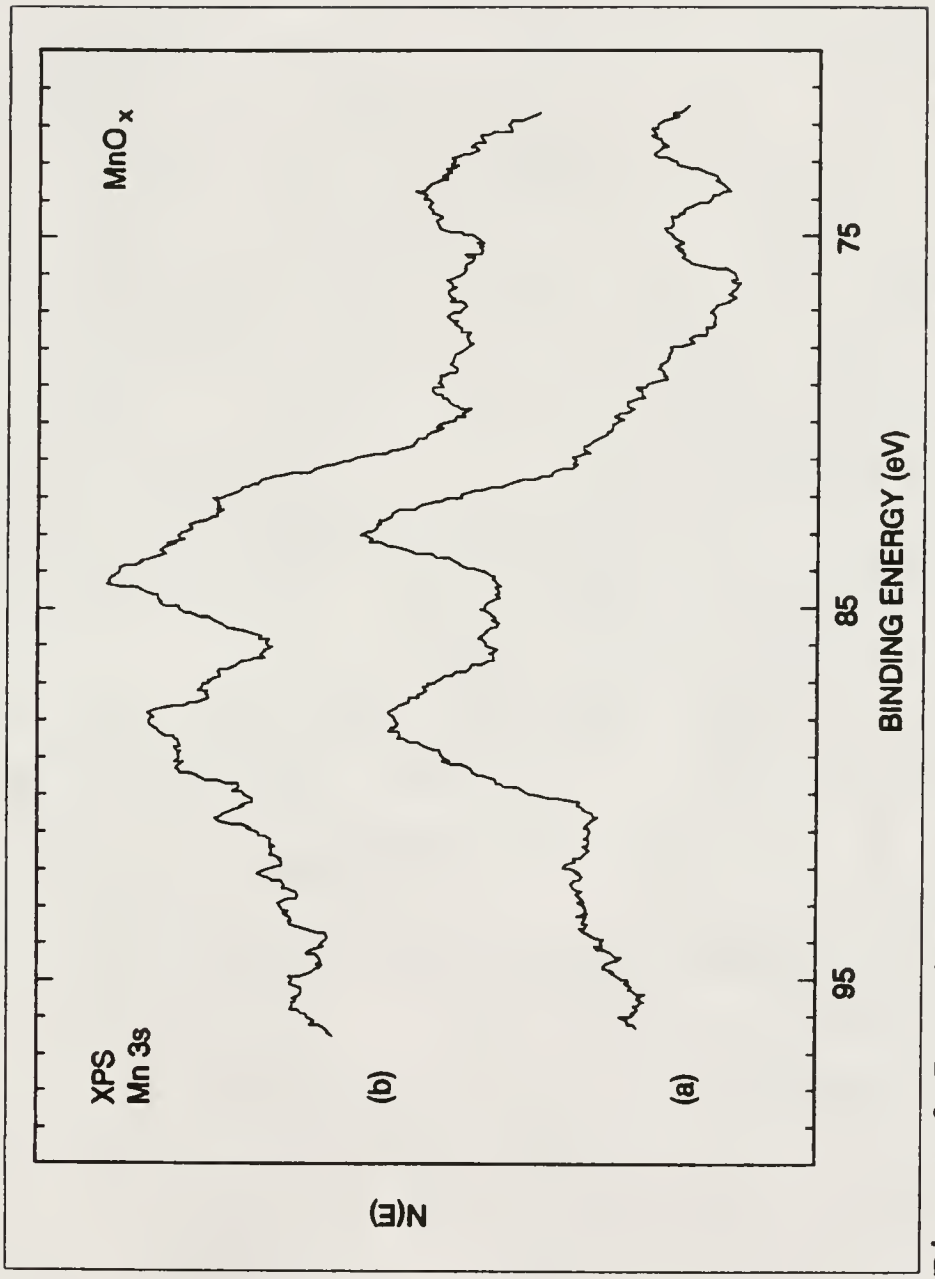

Figure 8-7. The XPS Mn 3s spectra of MnO_x (a) before and (b) after He pretreatment at 55 °C for 1 hour.

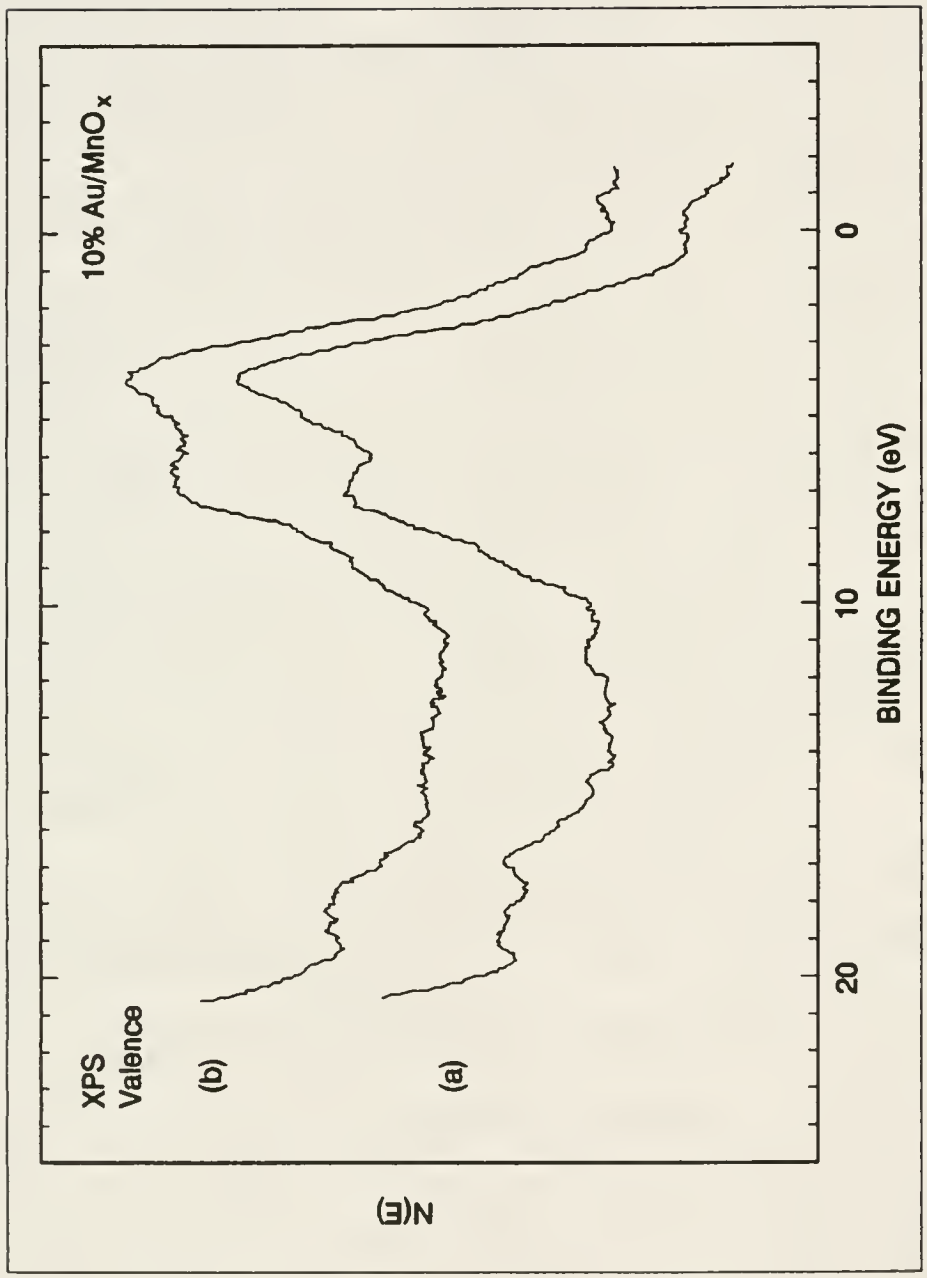

Figure 8-8. The valence-band XPS spectra of 10 at% Au/MnO_x (a) before and (b) after He pretreatment at 55 °C for 1 hour.

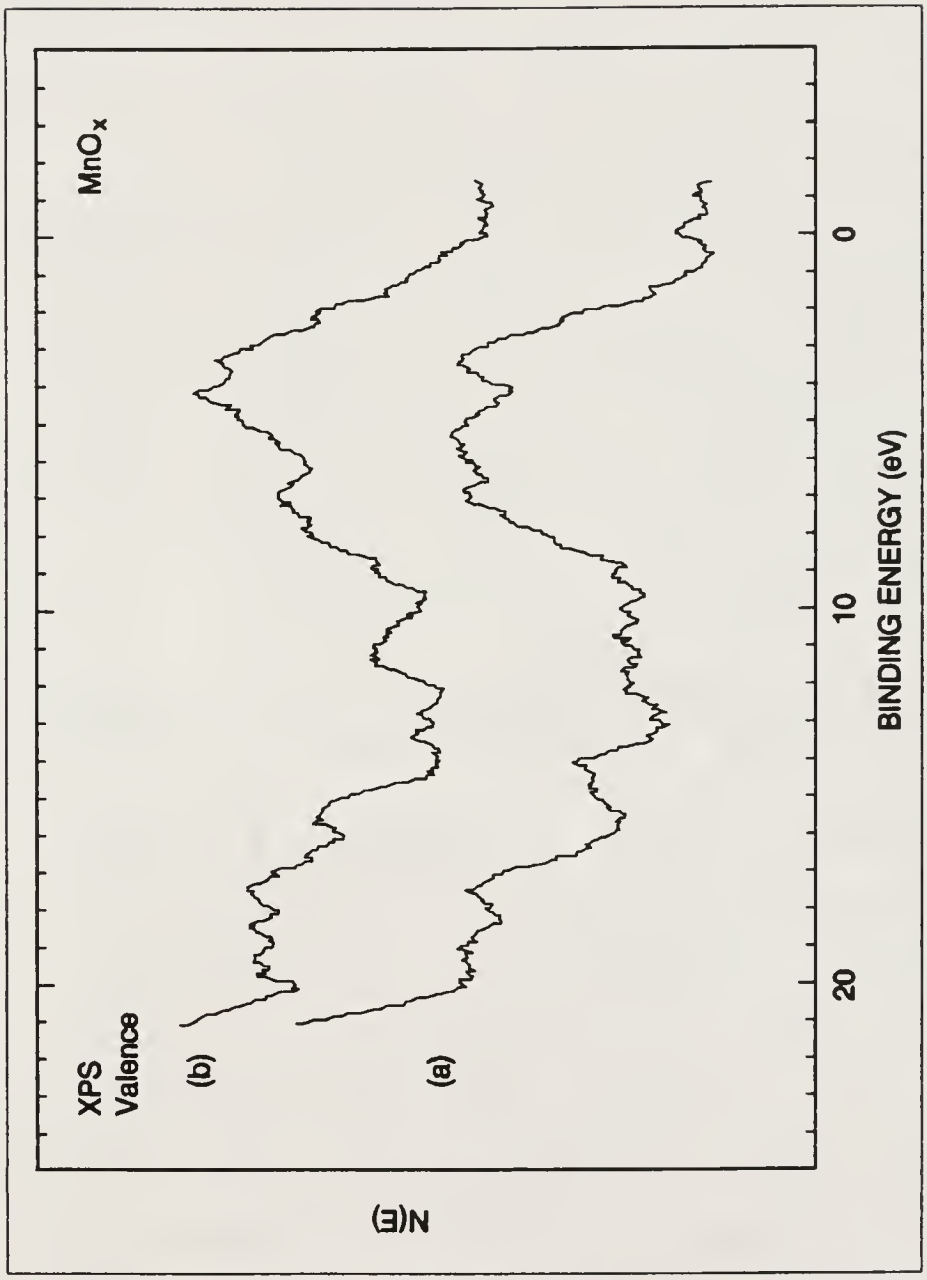

Figure 8-9. The valence-band XPS spectra of MnO_x (a) before and (b) after He pretreatment at 55 °C for 1 hour.

Au/MnO_x and MnO_x surfaces exhibit different characteristics. The spectrum for Au/MnO_x resembles spectra corresponding to the intermediate formation of Mn_2O_3 on MnO while the spectrum for MnO_x appears to be more indicative of Mn_2O_3 [132,133]. Figures 8-8(b) and 8-9(b) suggest that significant changes occur in the surface composition of Au/MnO_x and MnO_x as a result of the He pretreatment. Relative to the Mn 3d peak, the intensity of the O 2p peak increases on Au/MnO_x and decreases on MnO_x. This is consistent with the ISS and AES data which indicate that the surface of Au/MnO_x becomes oxygen-enriched whereas the MnO_x surface becomes depleted of oxygen. The spectrum in Figure 8-8(b) is similar to that of Mn_2O_3 while the spectrum in Figure 8-9(b) resembles that of MnO [132,133].

It is apparent that the assignment of a single Mn oxidation state on the Au/MnO_x and MnO_x surfaces would not be consistent with the data obtained in this study thus far. That is, with respect to previous investigations of MnO_x systems [129-133] the XPS data in the present study have indicated characteristics which correspond to MnO, Mn_3O_4 as well as Mn_2O_3. If Mn is indeed present as several phases of manganese oxide, perhaps evidence of different Mn oxidation states may be realized from the XPS O 1s spectra. The O 1s XPS spectra of Au/MnO_x and MnO_x (a) before and (b) after He pretreatment at 55 °C are shown in Figures 8-10

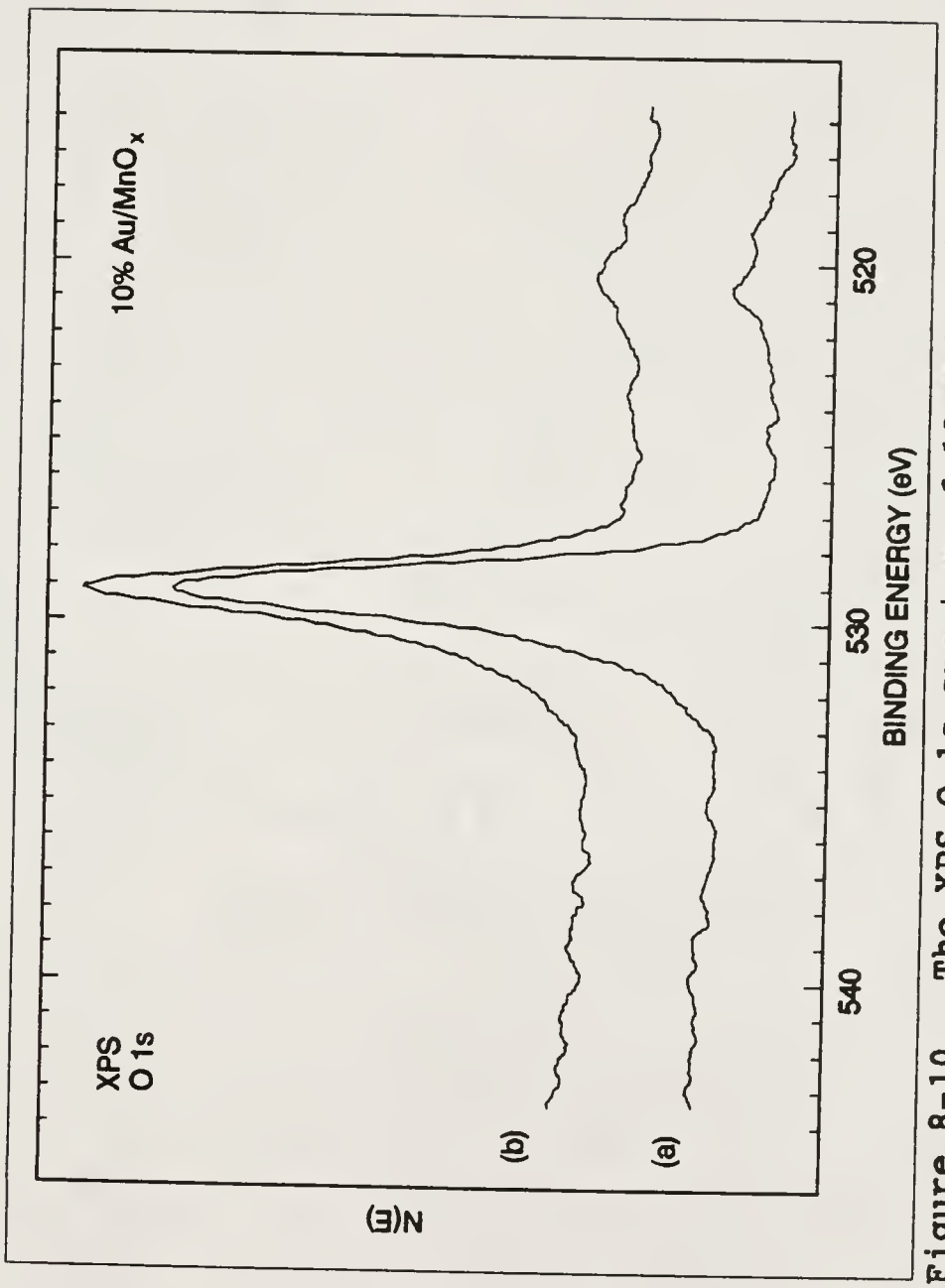

Figure 8-10. The XPS O 1s spectra of 10 at% Au/MnO_x (a) before and (b) after He pretreatment at 55 °C for 1 hour.

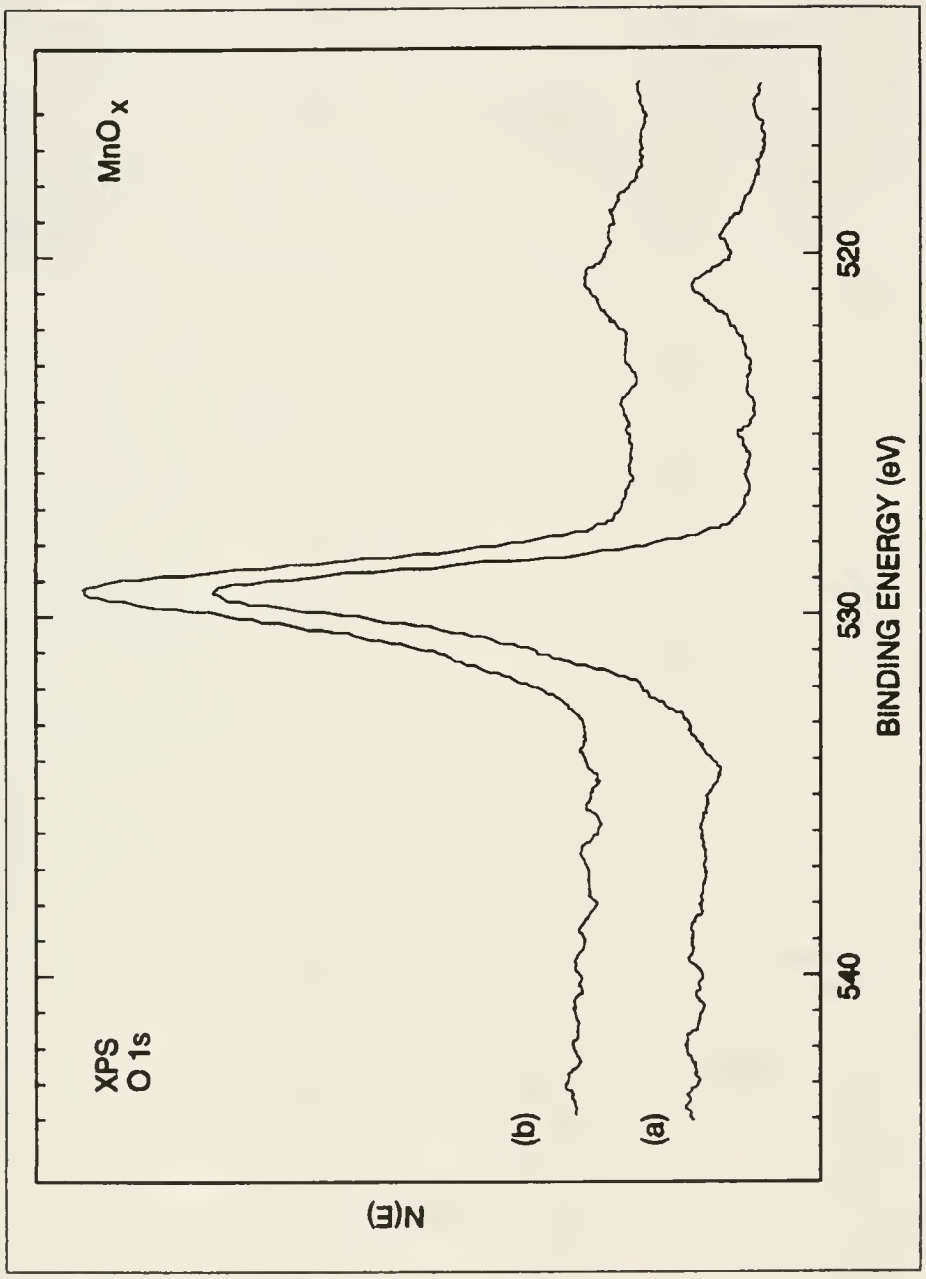

Figure 8-11. The XPS O 1s spectra of MnO_x (a) before and (b) after He pretreatment at 55 °C for 1 hour.

and 8-11, respectively. The binding energies are near 529.1 eV for Au/MnO_x and approximately 529.3 eV for MnO_x and they remain essentially constant. The spectral binding energies and peak shapes are similar to O 1s spectra recorded for Mn_3O_4 [129]. Subsequent to the He pretreatment, Figures 8-10(b) and 8-11(b) reveal that the high binding energy shoulder increases for Au/MnO_x and slightly decreases for MnO_x. Similar peak shoulders have been observed in XPS O 1s spectra of Pt/SnO_x surfaces and they are believed to be due to hydroxyl groups and adsorbed water as discussed in Chapter 4. Tin oxide, like MnO_x, is a reducible metal oxide whose surface composition is often quite complex [48,60]. Therefore, the data in Figures 8-10 and 8-11 may indicate that relative to pretreated MnO_x, the pretreated surface of Au/MnO_x contains a greater concentration of hydroxide species and adsorbed water. This assumption is consistent with the hypothesis that hydroxyl groups and surface moisture are important in the low-temperature CO oxidation mechanism on Pt/SnO_x and perhaps other NMRO surfaces [26]. Recall that the data in Chapters 4 and 5 for Pt/SnO_x surfaces indicated that optimum CO oxidation performance coincides with a maximum in surface $Pt(OH)_2$ concentration.

Given the data above it is possible that the increased O concentration on the surface of pretreated Au/MnO_x may be

due to Au which is present in an oxidized state, perhaps as Au hydroxide. Therefore, it was anticipated that information from the Au 4f spectra of Au/MnO_x might prove beneficial. The XPS Au 4f spectra of Au/MnO_x (a) before and (b) after He pretreatment appear in Figure 8-12. The Au $4f_{7/2}$ peak of the air-exposed Au/MnO_x surface is located near 85.3 eV binding energy whereas upon He pretreatment the peak shifts to approximately 85.7 eV. However, when the spectra are superimposed they appear essentially identical in overall peak shape and peak width. Such behavior is indicative of differential surface charging and as a result the binding energies of the spectra in Figure 8-12 may not be representative of the true chemical state of Au. Nevertheless, the binding energies are between those reported for metallic Au at 83.8 eV [80] and Au_2O_3 at 86.3 eV [16]. A literature search was unable to locate an established binding energy for Au hydroxide.

There is additional information to consider with respect to Figure 8-12 and its interpretation. Investigations of Au deposited on Al_2O_3 and SiO_2 [122,135] have reported XPS Au 4f peaks which are shifted to higher binding energy (as high as 85 eV) when small Au particles (or islands) with dimensions on the order of 30 angstroms or less are present. When the Au particle dimensions became larger, the Au 4f peaks were progressively shifted toward

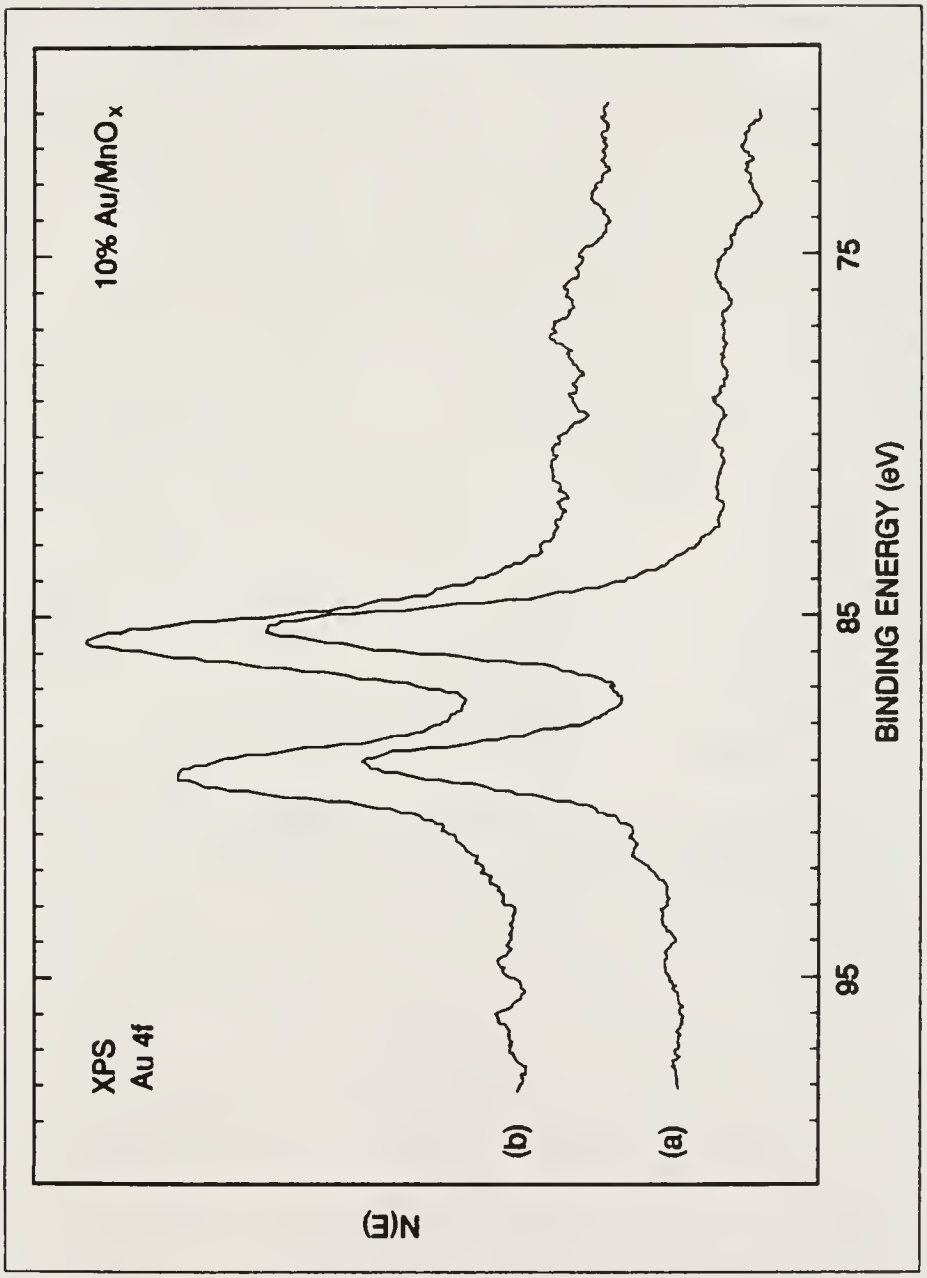

Figure 8-12. The XPS Au 4f spectra of 10 at% Au/MnO_x (a) before and (b) after He pretreatment at 55 °C for 1 hour.

the binding energy of bulk metallic gold. These observations have been attributed to matrix effects of the support material and perhaps real differences in the electronic structure of small Au particles relative to bulk Au. The latter is consistent with the increased reactivity of small Au particles. Since the Au particle size distribution has not been measured for the Au/MnO_x sample, relationships between the Au particle size and the Au 4f binding energy cannot be assessed in the present study. On the contrary, Haruta and co-workers [16] have studied a Au/Fe_2O_3 catalyst which was prepared by a coprecipitation technique similar to the one used in this study. The surface was characterized by ultrafine Au particles (mean diameter of approximately 36 angstroms) and the measured Au $4f_{7/2}$ binding energy was 83.9 eV. Furthermore, no detectable differences were observed between the Fe 2p and O 1s spectra of the Au/Fe_2O_3 surface and the bare Fe_2O_3 support. The Mn 2p and O 1s spectra of Au/MnO_x and MnO_x in the present study, however, do exhibit significant differences and this may correlate with the increased binding energies observed in the Au 4f spectra of Figure 8-12. These differences are consistent with reaction data in Chapter 6 which indicate that Au/MnO_x is superior to Au/Fe_2O_3 with respect to measurements of low-temperature CO oxidation activity using stoichiometric CO and O_2.

Summary

Numerous Au/MnO_x and MnO_x surfaces used for low-temperature CO oxidation have been characterized before and after pretreatment in He at 55 °C using ion scattering spectroscopy (ISS), Auger electron spectroscopy (AES) and X-ray photoelectron spectroscopy (XPS). The surfaces are complex and appear to contain multiple phases of Mn with an average composition estimated near Mn_3O_4. Significant concentrations of Na with much smaller amounts of Cl remain on the surfaces as a result of the preparation. In addition, hydroxylated species and adsorbed water appear to be present. Subsequent to the He pretreatment, the surface of Au/MnO_x is enriched in O and Au whereas the surface of MnO_x becomes oxygen-depleted. Coincidentally, the XPS spectra before and after pretreatment exhibit significant differences which may be indicative of a $Au-MnO_x$ interaction. However, the extreme heterogeneous nature of the Au/MnO_x and MnO_x surfaces precludes an exact determination of the Mn and Au chemical states present. The relative surface concentrations observed for Au, Mn, O, Na and Cl must correlate with the exceptional low-temperature CO oxidation activity exhibited by Au/MnO_x but such a correlation has not been investigated in this study.

CHAPTER 9
SUMMARY

Research has been performed with the objective of developing novel catalysts for low-temperature CO oxidation in CO_2 lasers. Initial experiments were designed to learn more about the low-temperature CO oxidation mechanism on Pt/SnO_x, a catalyst previously known to exhibit significant activity in this application. The experiments utilized ion scattering spectroscopy (ISS), Auger electron spectroscopy (AES) and X-ray photoelectron spectroscopy (XPS) to examine the chemical species present on Pt/SnO_x surfaces as a function of numerous pretreatments, and the results were correlated to catalytic activity data. The results indicate that pretreatments which produce optimum CO oxidation activity alter the surface composition of Pt/SnO_x such that $Pt(OH)_2$ becomes the dominant Pt species. In addition, a measurable amount of Sn is reduced to metallic form which appears to alloy with Pt. Similar results were obtained for a $Pt/SnO_x/SiO_2$ catalyst, although pretreatment at an elevated temperature beyond the optimum promoted extensive encapsulation of surface Pt and Sn with impurities contained in the SiO_2 substrate.

These results provided motivation for investigating Pt/Sn alloy surfaces themselves. A Pt_3Sn alloy was characterized with ISS, XPS, AES and angle-resolved Auger electron spectroscopy (ARAES) before and after reduction in H_2 at 300 °C. The air-exposed surface consisted of a uniform layer of SnO_x and $Sn(OH)_x$ over a Pt-rich sublayer. The data suggest that during reduction in H_2, Pt diffuses to the surface through vacancies left in the matrix by O which reacted with the H_2 and desorbed. Furthermore, most of the Sn is reduced to metallic Sn which probably alloys with the Pt.

In another phase of the research, numerous materials were synthesized and screened for low-temperature CO oxidation activity in stoichiometric amounts of CO and O_2. The most active catalysts tested were Au/CeO_x and Au/MnO_x. In particular, the Au/MnO_x catalyst exhibited remarkable CO oxidation activity near ambient temperature, surpassing that of Pt/SnO_x by approximately one order of magnitude. The long-term activity of Au/MnO_x was sustained for periods greater than 70 days with negligible decay in performance. The experiments indicate that Au/MnO_x, and perhaps Au/CeO_x, are promising catalysts for use in CO_2 lasers as well as air purification and CO gas sensing applications. The activities need to be tested over a wider range of CO oxidation environments.

Using ISS, AES and XPS, Au/MnO_x and MnO_x surfaces were subsequently characterized in order to investigate the CO oxidation mechanism. The surfaces appeared to be extremely heterogeneous containing several chemical forms of Mn with substantial amounts of water or hydroxyl groups. The spectra were consistent with Mn_3O_4 identification whereas Au appeared to be present in very small dimensions, possibly in an oxidized state. The behavior of Au/MnO_x and MnO_x toward an inert pretreatment suggests the possibility of a $Au-MnO_x$ interaction.

Although Au/MnO_x was the most active catalyst discovered in the screening experiments, its performance has yet to be optimized. That is, significant increases in CO oxidation activity may be realized by pretreating the surface prior to reaction and/or optimizing the preparation procedures. Variables which should be considered include the overall Au content and the concentration of surface impurities. The Au/MnO_x samples prepared in this study always contained considerable amounts of Na originating from the preparation procedure. It is therefore important to determine if surface Na plays a key role in the CO oxidation mechanism on Au/MnO_x. In addition to Na, other elements should be screened as promoters for low-temperature CO oxidation on Au/MnO_x.

Finally, the experimental data from this research have established correlations between CO oxidation activity and the surface composition of Pt/SnO_x and Au/MnO_x which are valid only during the onset of reaction. However, data indicate that the surfaces of Pt/SnO_x and Au/MnO_x undergo considerable changes during long-term CO oxidation activity measurements. Therefore, future research should be oriented toward surface characterization studies which relate the surface composition to the activity data over a much broader time scale. Such information may provide insight into the exceptional decay properties of Au/MnO_x relative to Pt/SnO_x while providing further knowledge of the CO oxidation mechanism on these surfaces.

APPENDIX
DESCRIPTION OF THE ULTRAHIGH VACUUM SURFACE ANALYSIS SYSTEM

A schematic (top view) of the ultrahigh vacuum (UHV) system which was utilized in this research appears in Figure A-1. The apparatus is composed of several individual chambers each of which may be isolated to perform a specific function. A preparation chamber is available for numerous surface treatments including exposure to selected gaseous atmospheres (low and high pressure), sample heating and metal deposition. In addition, the system consists of two analytical chambers which are equipped to perform an extensive number of surface analytical techniques as listed in Table A-1. Two long-stroke manipulators provide an effective means of specimen transfer among the chambers without exposing the surfaces to air.

The UHV system itself utilizes turbo molecular pumping throughout in series with dual-stage, rotary-vane mechanical pumps. In addition, the analytical chambers employ Ti sublimation and ion pumping to attain ultimate pressures near 10^{-11} Torr. A PHI Model 25-270AR double-pass cylindrical mirror analyzer (CMA) is mounted vertically in

the main chamber as indicated in Figure A-1. A specimen manipulator provides accurate sample placement beneath the CMA while enabling heating and cooling via feedthroughs in its flange. Numerous chamber ports are available which may be used to direct various source beams to the CMA focal point. The UHV system main chamber is currently equipped with an ion gun, two electron guns (one mounted coaxially within the CMA and one mounted off-axis for angle-resolved Auger electron spectroscopy (ARAES)) and a Mg Kα X-ray source.

The UHV surface analytical system has proven to be very effective in studying catalytic surfaces of varying degrees of heterogeneity. The complimentary nature of the analytical techniques allows the determination of the composition and chemical states of elements in a region consisting of the outermost atomic layers to near 50 angstroms beneath the surface. In particular, the system has enabled the catalytic surfaces to be characterized as a function of numerous reductive and oxidative surface pretreatments (performed in the preparation chamber without intermittent exposure to air) which may then be correlated with catalytic activity data. Indeed, this type of information has been a powerful tool for the elucidation of the low-temperature CO oxidation mechanism on Pt/SnO_x and Au/MnO_x catalysts as indicated by the present research.

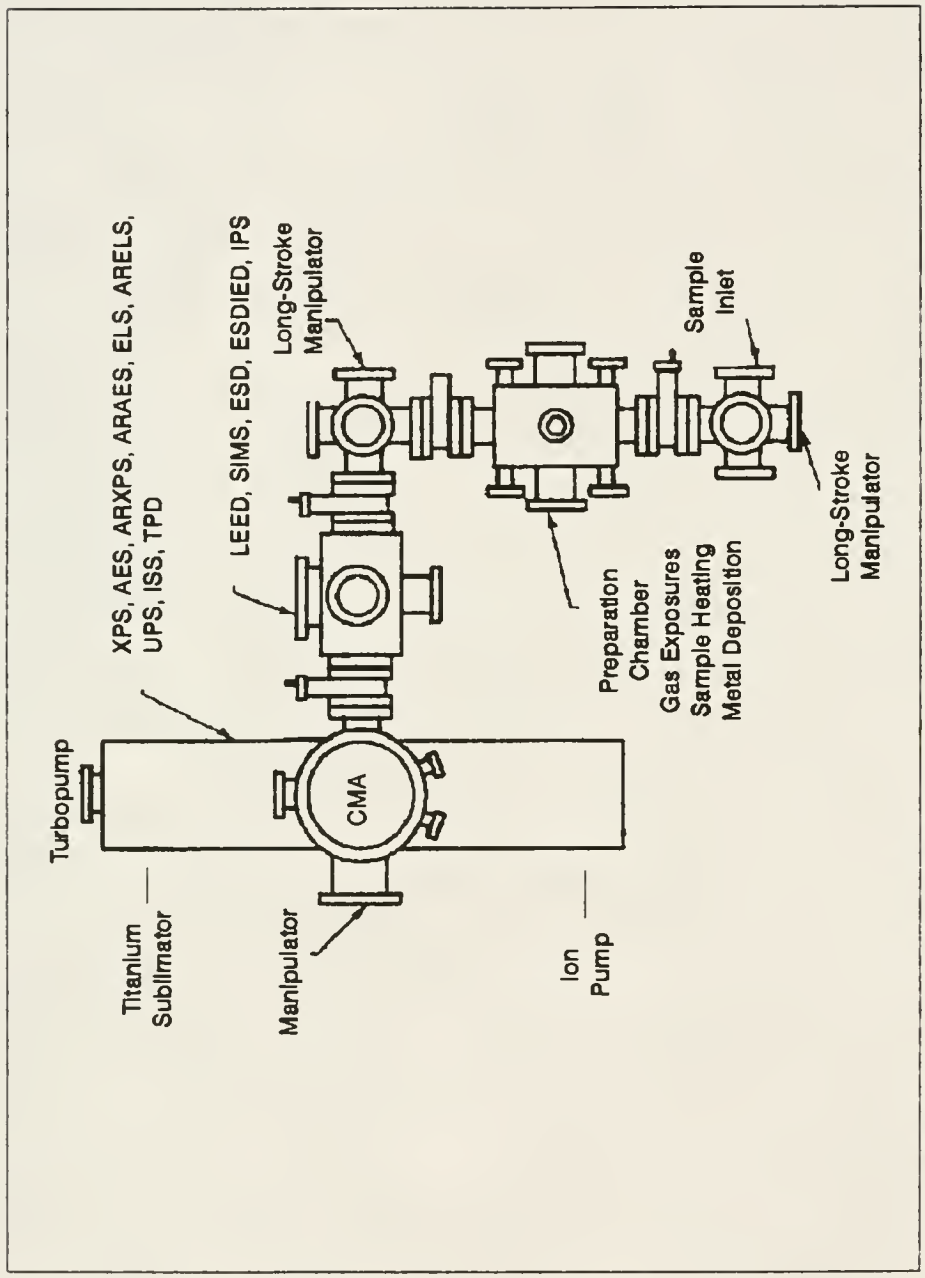

Figure A-1. A schematic of the UHV surface analysis system.

Table A-1. The experimental techniques available from the UHV surface analysis system.

Cylindrical Mirror Analyzer
[a] A. X-ray Photoelectron Spectroscopy
[a] B. Ultraviolet Photoelectron Spectroscopy (UPS)
[a] C. Auger Electron Spectroscopy (AES)
D. Scanning Auger Microscopy (SAM)
[a] E. Electron Energy-Loss Spectroscopy (EELS)
[a] F. Electron-Stimulated Desorption (ESD)
G. Ion Scattering Spectroscopy (ISS)
H. Depth Profiling
Others
A. Work Function Measurements
B. Temperature-Programmed Desorption (TPD)
C. Isotope Exchange Experiments
D. Secondary Ion Mass Spectroscopy (SIMS)
E. Gas dosing
F. Heating to 1800 K
G. Cooling to 10 K
H. Inverse Photoelectron Spectroscopy (IPS)
I. Metal Deposition
J. High-Pressure Treatment

[a] Can be performed in the angle-resolved mode

REFERENCES

1. R.M. Huffaker, Applied Optics 9(5)(1970)1026.

2. R.T.H. Collis, Applied Optics 9(8)(1970)1782.

3. V.E. Derr and C.G. Little, Applied Optics 9(9)(1970)1976.

4. W.W. Duley, CO_2 Lasers: Effects and Applications, Academic Press, New York, NY, 1976.

5. Laser Applications in Meteorology and Earth and Atmospheric Remote Sensing, proceedings of SPIE - The International Society for Optical Engineering, Vol. 1062, Ed. M.M. Sokoloski, SPIE, Bellingham, WA, 1989.

6. R.G. Beranek, J.W. Bilbro, D.E. Fitzjarrald, W.E. Jones, V.W. Keller and B.S. Perrine in Laser Applications in Meteorology and Earth and Atmospheric Remote Sensing, proceedings of SPIE - The International Society for Optical Engineering, Vol. 1062, p. 234, Ed. M.M. Sokoloski, SPIE, Bellingham, WA, 1989.

7. Closed-Cycle Frequency-Stable CO_2 laser technology, proceedings of workshop held at NASA Langley Research Center, Hampton, VA, 1986, Eds. C.E. Batten, I.M. Miller, G.M. Wood and D.V. Willetts, NASA Conference Publication 2456, 1987.

8. Low-Temperature CO Oxidation Catalysts for Long-Life CO_2 Lasers, proceedings of an international conference held at NASA Langley Research Center, Hampton, VA, 1989, Eds. D.R. Schryer and G.B. Hoflund, NASA Conference Publication 3076, 1990.

9. G. Croft and M.J. Fuller, Nature 269(1977)585.

10. G.C. Bond, L.R. Molloy and M.J. Fuller, J.C.S. Chem. Comm. (1975)796.

11. M. Katz in Advances in Catalysis and Related Subjects, Vol. 5, p. 177, Eds. W.G. Frankenburg, E.K. Rideal and V.I. Komarewsky, Academic Press, New York, NY, 1953.

12. E.C. Pitzer and J.C.W. Frazer, J. Phys. Chem. 45(1941)761.

13. S. Imamura, H. Sawada, K. Uemura and S. Ishida, J. Catal. 109(1988)198.

14. S. Imamura, S. Yoshie and Y. Ono, J. Catal. 115(1989)258.

15. M. Haruta, T. Kobayashi and N. Yamada, Chem. Lett. (1987)405.

16. M. Haruta, N. Yamada, T. Kobayashi and S. Iijima, J. Catal. 115(1989)301.

17. R.B. Jagow, R.A. Lamparter, T. Katan and C.D. Ray, Am. Soc. Mech. Eng., [pap.] 77-ENAs-28 (1977).

18. R.B. Gibson, A. Javan and K. Boyer, Appl. Phys. Lett. 32(11)(1978)726.

19. M.I. Brittan, H. Bliss and C.A. Walker, AIChE J. 16(2)(1970)305.

20. D.S. Stark, P.H. Cross and M.R. Harris, J. Phys. E: Sci. Instrum. 11(1978)311.

21. D.S. Stark and M.R. Harris, J. Phys. E: Sci. Instrum. 11(1978)316.

22. D.S. Stark, A. Crocker and G.J. Steward, J. Phys. E: Sci. Instrum. 16(1983)158.

23. D.S. Stark and M.R. Harris, J. Phys. E: Sci. Instrum. 16(1983)492.

24. K.G. Brown, B.D. Sidney, D.R. Schryer, B.T. Upchurch, I.M. Miller, G.M. Wood, R.V. Hess, C. Batten, L.G. Burney, P.A. Paulin, R. Hoyt and J. Schryer in Laser Radar Technology and Applications, proceedings of SPIE - The International Society for Optical Engineering, Vol. 663, p.136, Ed. M.M. Sokoloski, SPIE, Bellingham, WA, 1986.

25. B.D. Sidney, D.R. Schryer, B.T. Upchurch, R.V. Hess, G.M. Wood, I.M. Miller, L.G. Burney, K.G. Brown, J.D. Van Norman and J. Schryer in Laser Radar II, proceedings of SPIE - The International Society for Optical Engineering, Vol. 783, p. 162, Ed. M.M. Sokoloski, SPIE, Bellingham, WA, 1987.

26. D.R. Schryer, B.T. Upchurch, J.D. Van Norman, K.G. Brown and J. Schryer, J. Catal. 122(1990)193.

27. B.T. Upchurch, E.J. Kielin and I.M. Miller in Low-Temperature CO Oxidation Catalysts for Long-Life CO_2 Lasers, proceedings of an international conference held at NASA Langley Research Center, Hampton, VA, 1989, p. 69, Eds. D.R. Schryer and G.B. Hoflund, NASA Conference Publication 3076, 1990.

28. Catalysts For Long Range CO_2 Laser System, a progress report from a catalyst development program carried out be GEC Avionics, UK Atomic Energy Authority Harwell and UOP Ltd. under the auspices of the Royal Signals and Radar Establishment, November, 1988. Contract No. SDIO 84-87-C-0046.

29. D.R. Schryer, B.D. Sidney, I.M. Miller, R.V. Hess, G.M. Wood, C.E. Batten, L.G. Burney, R.F. Hoyt, P.A. Paulin, K.G. Brown, J. Schryer and B.T. Upchurch in Closed-Cycle, Frequency-Stable CO_2 Laser Technology, proceedings of a workshop held at NASA Langley Research Center, Hampton, VA, 1986, p. 113, Eds. C.E. Batten, I.M. Miller , G.M. Wood, and D.V. Willetts, NASA Conference Publication No. 2456, 1987.

30. B.T. Upchurch, G.M. Wood, D.R. Schryer, R.V. Hess, I.M. Miller and E.J. Kielin in Low-Temperature CO Oxidation Catalysts for Long-Life CO_2 Lasers, proceedings of an international conference held at NASA Langley Research Center, Hampton, VA, 1989, p. 193, Eds. D.R. Schryer and G.B. Hoflund, NASA Conference Publication 3076, 1990.

31. J.A. Macken, S.K. Yagnik and M.A. Samis, IEEE J. Quantum Electron. 25(7)(1989)1695.

32. G.B. Hoflund, D.A. Asbury and R.E. Gilbert, Thin Solid Films 129(1985)139.

33. F.M. Dautzenberg, J.N. Helle, P. Biloen and W.M.H. Sachtler, J. Catal. 63(1980)119.

34. J. Völter, G. Lietz, M. Uhlemann and M. Hermann, J. Catal. 68(1981)42.

35. H. Lieske and J. Völter, J. Catal. 90(1984)96.

36. R. Bacaud, P. Bussiere and F. Figueras, J. Catal. 69(1981)399.

37. R. Burch, J. Catal. 71(1981)348.

38. R. Burch and L.C. Garla, J. Catal. 71(1981)360.

39. R. Burch and A.J. Mitchell, Appl. Catal. 6(1983)121.

40. A.C. Muller, P.A. Engelhard and J.E. Weisang, J. Catal. 56(1979)65.

41. B.A. Sexton, A.E. Hughes and K. Foger, J. Catal. 88(1984)466.

42. S.R. Adkins and B.H. Davis, J. Catal. 89(1984)371.

43. J.M. Stencel, J. Goodman and B.H. Davis in Catalysis: Theory to Practice, Vol. 3, p. 1291, Eds. M.J. Phillips and M. Ternan, Chem. Inst. Can., Ottawa, Ontario, 1988.

44. Y.-X. Li, J.M. Stencel and B.H. Davis, in press.

45. G.B. Hoflund, D.F. Cox, G.L. Woodson and H.A. Laitinen, Thin Solid Films 78(1981)357.

46. G.B. Hoflund, D.F. Cox, F. Ohuchi, P.H. Holloway and H.A. Laitinen, Appl. Surf. Sci. 14(1982-1983)281.

47. G.B. Hoflund, P.H. Holloway and W.H. Hocking in Secondary Ion Mass Spectrometry SIMS IV, proceedings of the Fourth International Conference, Osaka, Japan, 1983, Vol. 36, p. 231, Eds. A. Benninghoven, J. Okano, R. Shimizu and H.W. Werner, Springer-Verlag, Berlin, 1984.

48. D.F. Cox, G.B. Hoflund and H.A. Laitinen, Appl. Surf. Sci. 20(1984)30.

49. G.B. Hoflund, Scanning Electron Microsc. IV, 1391(1985).

50. G.B. Hoflund, A.L. Grogan, D.A. Asbury and D.R. Schryer, Thin Solid Films 169(1989)69.

51. R.E. Gilbert, D.F. Cox and G.B. Hoflund, Rev. Sci. Instrum. 53(1982)1281.

52. V.Y. Young and G.B. Hoflund, Anal. Chem. 60(1988)269.

53. E.S. Parilis in Proceedings of the 7th International Conference on Phenomena in Ionized Gases, Belgrade, 1965, Vol. 1, p. 129, Eds. B. Perovic and D. Tosic, Gradevinska Knjiga Publishing House, Belgrade, 1966.

54. G.B. Hoflund, D.A. Asbury, P. Kirszensztejn and H.A. Laitinen, Surf. Int. Anal. 9(1986)169.

55. M.T. Paffett and R.G. Windham, Surf. Sci. 208(1989)34.

56. D.F. Cox and G.B. Hoflund, Surf. Sci. 151(1985)202.

57. D.A. Asbury and G.B. Hoflund, Surf. Sci. 199(1988)552.

58. T.T.P. Cheung, Surf. Sci. 177(1986)L887.

59. G.B. Hoflund, A.L. Grogan and D.A. Asbury, J. Catal. 109(1988)226.

60. D.A. Asbury and G.B. Hoflund, J. Vac. Sci. Technol. A 5(1987)1132.

61. H. Berndt, H. Mehner, J. Völter and W. Meisel, F. Anorg. Allg. Chem. 49(1977)47.

62. B.H. Davis, J. Catal. 46(1977)348.

63. Y.-X. Li and K.J. Klabunde, Langmuir 3(1987)558.

64. A. Palazov, Ch. Bonev, D. Shopov, G. Leitz, A. Sárkány and J. Völter, J. Catal. 103(1987)249.

65. B. Coq and F. Figueras, J. Catal. 85(1984)197.

66. B. Coq and F. Figueras, J. Mol. Catal. 25(1984)87.

67. R. Bouwman, L.H. Toneman and A.A. Holscher, Surf. Sci. 35(1973)8.

68. R. Bouwman and P. Biloen, Surf. Sci. 41(1974)348.

69. R. Bouwman and P. Biloen, Anal. Chem. 46(1974)136.

70. P. Biloen, R. Bouwman, R.A. Van Santen and H.H. Brongersma, Appl. Surf. Sci. 2(1979)532.

71. G.B. Hoflund, D.A. Asbury, P. Kirszensztejn and H.A. Laitinen, Surf. Sci. 161(1985)L583.

72. G.B. Hoflund and D.A. Asbury, Langmuir 2(1986)695.

73. G.B. Hoflund, D.A. Asbury, C.F. Corallo and G.R. Corallo, J. Vac. Sci. Technol. A 6(1988)70.

74. R.E. Gilbert, G.B. Hoflund, D.A. Asbury and M.R. Davidson, J. Vac. Sci. Technol. A 6(1988)2280.

75. G.B. Hoflund and G.R. Corallo, submitted for publication.

76. H.A. Laitinen, J.R. Waggoner, C.Y. Chan, P. Kirszensztejn, D.A. Asbury and G.B. Hoflund, J. Electrochem. Soc. 133(1986)1568.

77. E. Taglauer and W. Heiland, Appl. Phys. 9(1976)261.

78. H.H. Brongersma, M.J. Sparnaay and T.M. Buck, Surf. Sci. 71(1978)657.

79. D.F. Cox, G.B. Hoflund and W.H. Hocking, Appl. Surf. Sci. 26(1986)239.

80. Handbook of X-ray Photoelectron Spectroscopy, Eds. C.D. Wagner, W.M. Riggs, L.E. Davis, J.F. Moulder and G.E. Muilenberg, Perkin-Elmer Corporation, Eden Prairie, MN, 1979.

81. M.J. Tarlov and J.F. Evans, Chem. Mater. 2(1990)49.

82. E.W. Giesekke, H.S. Gutowsky, P. Kirkov and H.A. Laitinen, Inorg. Chem. 6(1967)1294.

83. M.P. Seah and W.A. Dench, Surf. Interface Anal. 1(1979)2.

84. G.B. Hoflund, H.-L. Yin, A.L. Grogan, D.A. Asbury, H. Yoneyama, O. Ikeda and H. Tamura, Langmuir 4(1988)346.

85. T. Fryberger and S. Semancik in Low-Temperature CO Oxidation Catalysts for Long-Life CO_2 Lasers, proceedings of an international conference held at NASA Langley Research Center, Hampton, Va, 1989, p. 277, Eds. D.R. Schryer and G.B. Hoflund, NASA Conference Publication 3076, 1990.

86. D.R. Schryer, B.T. Upchurch, R.V. Hess, G.M. Wood, B.D. Sidney, I.M. Miller, K.G. Brown, J.D. Van Norman, J. Schryer, G.B. Hoflund and R.K. Herz in Low-Temperature CO Oxidation Catalysts for Long-Life CO_2 Lasers, proceedings of an international conference held at NASA Langley Research Center, Hampton, VA, 1989, p. 41, Eds. D.R. Schryer and G.B. Hoflund, NASA Conference Publication 3076, 1990.

87. B.T. Upchurch, D.R. Schryer, G.M. Wood and R.V. Hess in Laser Applications in Meteorology and Earth and Atmospheric Remote Sensing, proceedings of SPIE - The International Society for Optical Engineering, Vol. 1062, p. 287, Ed. M.M. Sokoloski, SPIE, Bellingham, WA, 1989.

88. V.Y. Young, G.B. Hoflund and A.C. Miller, Surf. Sci. 235(1990)60.

89. D.F. Cox, G.B. Hoflund and H.A. Laitinen, Langmuir 1(1985)269.

90. W.D. Westwood and C.D. Bennewitz, J. Appl. Phys. 45(5)(1974)2313.

91. C.D. Bennewitz and W.D. Westwood, J. Appl. Phys. 46(2)(1975)558.

92. T.H. Fleisch, G.W. Zajac, J.O. Schreiner and G.J. Mains, Appl. Surf. Sci. 26(1986)488.

93. J. Kumar and R. Saxena, J. Less-Common Met. 147(1989)59.

94. M. Hecq, A. Hecq, J.P. Delrue and T. Robert, J. Less-Common Met. 64(1979)25.

95. C.L. Lau and G.K. Wertheim, J. Vac. Sci. Technol. 15(1978)622.

96. R.A. Powell, Appl. Surf. Sci. 2(1979)397.

97. E. Paparazzo, G. Fierro, G.M. Ingo and N. Zacchetti, Surf. Interface Anal. 12(1988)438.

98. J.E. Drawdy, G.B. Hoflund, M.R. Davidson and D.R. Schryer, submitted for publication.

99. M.F. Collins in Closed-Cycle, Frequency-Stable CO_2 Laser Technology, proceedings of a workshop held at NASA Langley Research Center, Hampton, VA, 1986, p. 153, Eds. C.E. Batten, I.M. Miller, G.M. Wood and D.V. Willetts, NASA Conference Publication 2456, 1987.

100. E. Nordally and J.R. Richmond in Low-Temperature CO Oxidation Catalysts for Long-Life CO_2 Lasers, proceedings of an international conference held at NASA Langley Research Center, Hampton, VA, 1989, p. 387, Eds. D.R. Schryer and G.B. Hoflund, NASA Conference Publication 3076, 1990.

101. E.J. Poziomek in Low-Temperature CO Oxidation Catalysts for Long-Life CO_2 Lasers, proceedings of an international conference held at NASA Langley Research Center, Hampton, VA, 1989, p. 403, Eds. D.R. Schryer and G.B. Hoflund, NASA Conference Publication 3076, 1990.

102. F.G. Ciapetta and C.J. Plank in Catalysis, Ed. P.H. Emmett, Vol. I, p. 315, Reinhold Publishing Corporation, New York, NY, 1954.

103. C.E. Batten, I.M. Miller, P.A. Paulin and J. Schryer in Closed-Cycle, Frequency-Stable CO_2 Laser Technology, proceedings of a workshop held at NASA Langley Research Center, Hampton, VA, 1986, p. 199, Eds. C.E. Batten, I.M. Miller, G.M. Wood and D.V. Willetts, NASA Conference Publication 2456, 1987.

104. V. Dondur, S. Lampa and D. Vucelic, J. Chem. Soc., Faraday Trans. 1, 79(1983)1633.

105. S. Kanungo, J. Catal. 58(1979)419.

106. J.A. Lee, C.E. Newnham, F.S. Stone and F.L. Tye, J. Colloid Interface Sci. 45(1973)289.

107. M. Kobayashi, H. Matsumto and H. Kobayashi, J. Catal. 21(1971)48.

108. M. Kobayashi and H. Kobayashi, J. Catal. 27(1972)100.

109. T. Kobayashi, M. Haruta, H. Sano and M. Nakane, Sensors and Actuators 13(1988)339.

110. T. Kobayashi, M. Haruta and H. Sano, Chem. Express 4(4)(1989)217.

111. C. Xu, J. Tamaki, N. Miura and N. Yamazoe, Chem. Lett. (1990)441.

112. P.G. Harrison and M.J. Willett, Nature 332(1988)337.

113. C.F. Sampson and N. Jorgensen in Low-Temperature CO Oxidation Catalysts for Long-Life CO_2 Lasers, proceedings of an international conference held at NASA Langley Research Center, Hampton, VA, 1989, p. 57, Eds. D.R. Schryer and G.B. Hoflund, NASA Conference Publication 3076, 1990.

114. J. Schwank, Gold Bull. 16(4)(1983)103.

115. I.E. Wachs, Gold Bull. 16(4)(1983)98.

116. D.A. Outka and R.J. Madix, Surf. Sci. 179(1987)351.

117. G. Cocco, S. Enzo, G. Fagherazzi, L. Schiffini, I.W. Bassi, G. Vlaic, S. Galvagno and G. Parravano, J. Phys. Chem. 83(19)(1979)2527.

118. I.W. Bassi, F.W. Lytle and G. Parravano, J. Catal. 42(1976)139.

119. J. Schwank, G. Parravano and H.L. Gruber, J. Catal. 61(1980)19.

120. J. Schwank, S. Galvangno and G. Parravano, J. Catal. 63(1980)415.

121. W.N. Delgass, M. Boudart and G. Parravano, J. Phys. Chem. 72(10)(1968)3563.

122. K.S. Liang, W.R. Salaneck and I.A. Aksay, Solid State Commun. 19(1976)329.

123. M. Batista-Leal, J.E. Lester and C.A. Lucchesi, J. Electron Spectrosc. Relat. Phenom. 11(1977)333.

124. A.G. Shastri, A.K. Datye and J. Schwank, J. Catal. 87(1984)265.

125. P.M. Ajayan and L.D. Marks, Nature 338(1989)139.

126. D.Y. Cha and G. Parravano, J. Catal. 18(1970)200.

127. G.C. Bond and P.A. Sermon, Gold Bulletin 6(1973)102.

128. Handbook of Auger Electron Spectroscopy, Eds. L.E. Davis, N.C. MacDonald, P.W. Palmberg, G.E. Riach and R.E. Weber, Perkin-Elmer Corporation, Eden Prairie, MN, 1972.

129. M. Oku, K. Hirokawa and S. Ikeda, J. Electron Spectrosc. Relat. Phenom. 7(1975)465.

130. H.K. Hu and J.W. Rabalais, Surf. Sci. 107(1981)376.

131. J.S. Foord, R.B. Jackman and G.C. Allen, Phil. Mag. A 49(5)(1984)657.

132. L.Z. Young and V. Young, J. Electron Spectrosc. Relat. Phenom. 34(1984)45.

133. V.D. Castro and G. Polzonetti, J. Electron Spectrosc. Relat. Phenom. 48(1989)117.

134. W. Levason and C.A. McAuliffe, Coord. Chem. Rev. 7(1972)353.

135. K.S. Kim and N. Winograd, Chem. Phys. Lett. 30(1)(1975)91.

BIOGRAPHICAL SKETCH

The author was born on December 19, 1961, in Gadsden, Alabama, to James H. and R.J. Gardner. He attended Anniston High School and graduated in May, 1980, with valedictorian honors. He subsequently enrolled at the University of Alabama in Huntsville (UAH) where he was awarded a B.S.E. degree in chemical engineering in June, 1985. The author chose to continue studying at UAH under the direction of Professor James E. Smith where he researched heterogeneous catalysis and CO hydrogenation. He was awarded an M.S.E. degree in chemical engineering in June, 1987. The following fall the author enrolled at the University of Florida where he continued his graduate studies in catalysis and surface science under the guidance of Professor Gar B. Hoflund. The author will receive his Ph.D. in chemical engineering during December, 1990, after which he will join the chemical engineering faculty at Mississippi State University as Assistant Professor.

I certify that I have read this study and that in my opinion it conforms to acceptable standards of scholarly presentation and is fully adequate, in scope and quality, as a dissertation for the degree of Doctor of Philosophy.

Gar B. Hoflund, Chairman
Professor of Chemical
Engineering

I certify that I have read this study and that in my opinion it conforms to acceptable standards of scholarly presentation and is fully adequate, in scope and quality, as a dissertation for the degree of Doctor of Philosophy.

Timothy J. Anderson
Professor of Chemical
Engineering

I certify that I have read this study and that in my opinion it conforms to acceptable standards of scholarly presentation and is fully adequate, in scope and quality, as a dissertation for the degree of Doctor of Philosophy.

Paul H. Holloway
Professor of Materials
Science and Engineering

I certify that I have read this study and that in my opinion it conforms to acceptable standards of scholarly presentation and is fully adequate, in scope and quality, as a dissertation for the degree of Doctor of Philosophy.

Herbert A. Laitinen
Graduate Research
Professor of Chemistry

I certify that I have read this study and that in my opinion it conforms to acceptable standards of scholarly presentation and is fully adequate, in scope and quality, as a dissertation for the degree of Doctor of Philosophy.

Vaneica Y. Young
Associate Professor of
Chemistry

This dissertation was submitted to the Graduate Faculty of the College of Engineering and to the Graduate School and was accepted as partial fulfillment of the requirements for the degree of Doctor of Philosophy.

December, 1990

for Winfred M. Phillips
Dean, College of Engineering

Madelyn M. Lockhart
Dean, Graduate School